SOME CONSIDERATIONS OF PERFORMANCE AND CAPACITY OF VOICE OVER IP HIGH BIT RATE WIRELESS REVERSE LINKS

by

RICHARD FRAMJEE

Presented to the Faculty of the Graduate School of
The University of Texas at Arlington in Partial Fulfillment
of the Requirements
for the Degree of

DOCTOR OF PHILOSOPHY

THE UNIVERSITY OF TEXAS AT ARLINGTON
December 2014

To my wife Barnali and daughters Rhea (God bless her soul), Eva and Sara.

ACKNOWLEDGEMENTS

I would like to thank Dr. Vasant Prabhu for all his mentoring and numerous reviews of my work for so many years. Dr. Prabhu, has helped me understand the importance of an academic approach and how it is useful for industry.

I would like to thank my supervising professor Dr. Jonathan Bredow for providing constant motivation, encouragement, guidance and reviews of my work.

I would like to thank my committee Dr. Alan Davis, Dr. Chien-Pai Han, Dr. Qilian Liang and Dr. Ioannis D. Schizas for the feedback and review comments they provided. I would also like to say thanks to Dr. Harold Sobol (God bless his soul) for all the knowledge he imparted.

I would like to thank my wife Barnali and my daughters Eva and Sara for backing me up and being patient with me as I spent time on my research.

I would like to thank my mom (Jeanne), dad (Murzban), sisters (Deborah and Jennifer) and brother (Zubin) for backing me up on numerous occasions.

I would also like to thank my UTA assigned host family Melanie and Bill Purcell and their family for their sincere friendship over the years.

November 14, 2014

ABSTRACT

SOME CONSIDERATIONS OF PERFORMANCE AND CAPACITY OF VOICE OVER IP HIGH BIT RATE WIRELESS REVERSE LINKS

RICHARD FRAMJEE, Ph.D.

The University of Texas at Arlington, 2014

Supervising Professor: Jonathan Bredow

Evaluation of the performance and capacity of the wireless reverse links, that support concurrent voice over IP and packet data services, is important for spectral efficiency considerations. For a given traffic mix, this capacity is the maximum Erlangs and data throughput at a given packet error rate, voice packet expected wait time and probability of wait time outage. The voice packet wait times are traffic induced and due to retransmissions caused by high packet error rate. In this dissertation the error rate of high bit rate DS-SS BPSK RAKE receivers and traffic induced expected packet wait time for voice over IP reverse links, that support one or two bursts at acceptable packet error rate, are determined.

In high bit rate DS-SS BPSK mobile radio reverse links with dual space diversity RAKE demodulators the frequency selective channel causes intersymbol interference. For many years the standard Gaussian approximation error rate has been used, and for high bit rates it's accuracy is not known. We compare the Gaussian approximation to the error rate derived from the total probability theorem, Chernoff and Prabhu bounds with true statistics of intersymbol interference. For signal-to-noise ratio's (SNR's)

greater than 6 dB(cases of interest), we show that the Gaussian approximation is a much looser upper bound than our bounds. The Prabhu bound which can be tailored to different intersymbol interference conditions is the tightest bound. We show that the RAKE receiver combats incoherent intersymbol interference while the immunity it offers decreases for SNR's greater than 10 dB. Finally, a dual space diversity RAKE provides an 8 dB space diversity gain.

We have also derived the bandwidth occupancy in a rigorous way for the first time by developing a method to compute the spectral density. This density is used to determine operating SNR by deriving received signal power and averaging it over the channel. The fractional containment bandwidth with two Gold codes is smaller than that with a PN sequence. The spectral density has no discrete lines; while it is a function of the signature coefficients and the chip Fourier transform. Within the bandwidth the spectral density of a set of frequencies is 15 dB greater than at other frequencies and this set varies from signature to signature. These methods can be used to select signatures that minimize adjacent and co-channel interference.

For voice over IP wireless reverse links with a G/D/1 (G/D/2)[1] queue, where the radio channel supports one (two)[2] radio burst(s) or server(s) at any time with acceptable packet error rate, traffic induced expected packet wait times are obtained by deriving the modified Little's-multinomial analytical approximation for the first time. For high utilization factors, which is the operating point of interest, correlation between interarrival times results in high wait times. For the G/D/1 queue our method provides a better estimate of expected packet times than the M/D/1 queue approximation at high utilization factors. For the G/D/2 queue our method provides

[1]General arrival time distribution / Transmission interval is D / Number of servers

[2]The radio channel supports at maximum two simultaneous high bit rate bursts at reasonably acceptable packet error rates $\approx 2.6\%$ with no coding or retransmission.

a much better estimate than the Kingman upper bound approximation at high utilization factors. An upper bound on the probability of outage derived for the first time using the Steffensen inequality is a better estimate than that obtained by the Markov inequality. The dual burst wireless reverse link provides a capacity gain of 2.16 over the single burst case at a given packet expected wait time threshold. Using our bound at a 2% probability of outage and 60 ms wait time threshold, the voice over IP users supported by the G/D/1 and G/D/2 queue is 26 and 59 respectively.

Methods presented here can be used to assess radio packet wait times that can be used for Erlang capacity determination and end-to-end delay budgets. The methods can be extended to G/D/K queues.

TABLE OF CONTENTS

LIST OF ILLUSTRATIONS

LIST OF TABLES

CHAPTER 1

INTRODUCTION

Wireless cellular systems shall soon support simultaneous voice over IP and packet data services. The radio channel can support a finite number of simultaneous high bit rate bursts or servers at a low packet error rate. Evaluation of the performance and capacity of the reverse link is important. Evaluation of spectral efficiency and capacity of transmission schemes that combat frequency selectivity are main challenges. This requires determination of error rate, operating SNR and bandwidth where the last two are obtained from the spectral density. Spectral density is also used to assess adjacent and co-channel interference impacts. For a given traffic mix this requires determination of capacity, which is the maximum Erlangs and data throughput at a given packet error rate, voice packet expected wait time and probability of wait time outage. The voice packet wait times are traffic induced and due to retransmissions caused by high packet error rate.

The main thrust of this dissertation is determination of the error rate of high bit rate Direct-Sequence Spread-Spectrum Binary Phase Shift Keyed (DS-SS BPSK) RAKE receivers and traffic induced expected packet wait time for voice over IP reverse links. Such performance and capacity methods can be used for packetized wireless cellular system design.

1.1 DS-SS BPSK Spectrum and Error Rate of High Bit Rate RAKE

For DS-SS BPSK over wideband channels, the delayed signal [1]-[2], original delayed signature and modified [3] delayed signature RAKE demodulator structures can

be used. The first RAKE mitigates intersymbol interference and the second retains coherent intersymbol interference in DS-SS FSK [1]. In addition a modified delayed signature RAKE demodulator [2], [3] with two horizontally separated antennas [4] can be used. The dual space diversity RAKE receiver combines the desired signal extracted from multiple delayed paths of each diversity channel. For one user, the desired symbol at the RAKE output is corrupted by correlated Gaussian noise and multipath [5] interference.

Over the years the standard Gaussian approximation error rate [6] was extended [7], [8] by assuming that multipath interference is Gaussian. The approximation is good [7] for a single branch receiver with a 31 rectangular chip signature. In the low data rate RAKE system [8] with a 127 rectangular chip signature, two intersymbol interference terms were considered. For high bit rates with up to 8 chip signatures, the error rate was determined by simulation [9], [10]. For a single branch receiver at 10^{-3} error rate, intersymbol interference degrades [9] the required SNR by 4 dB.

It is established [2], [11] that the spectral density of a linear digital modulated signal is obtained by the Fourier transform of its autocorrelation function. First the ensemble autocorrelation function is obtained assuming that the information sequence is wide sense stationary. Next the time variable of the periodic autocorrelation function, is eliminated by averaging over time. The spectral density is the product of the pulse Fourier transform magnitude square and the Fourier transform of the information autocorrelation sequence. Various methods have been developed for the spectral density of GMSK (Gaussian Minimum Shift Keyed) [12] and DS-SS signals [13], [14], [15]. The spectral density [13], of a periodic Pseudo random noise (PN) sequence with shaped chips was determined from the discrete Fourier transform of the signatures temporal autocorrelation sequence. In [14] the spectral density for a DS-SS BPSK signal, with discrete lines, was obtained by expressing it as a linear

digital modulated signal and direct use of its density [2]. It was assumed [14] that the product of information and signature sequences results in a wide sense stationary chip rate sequence. For DS-SS BPSK with Gold or PN sequences this assumption [14] of wide sense stationarity is not theoretically feasible. The spectral density of DS-SS BPSK signal with rectangular chips was determined [15] by assuming the information sequence has a random delay uniformly distributed over the baud. The PN sequence ensemble autocorrelation sequence is used by assuming [15] the signature has statistical properties like the information sequence and random pulse train. In CDMA (Code Division Multiple Access) [4] mobiles are synchronized to base stations that are synchronized to GPS, and the mobile signal has small delay shifts. A PN sequence is not truly random unless it has infinite length. The models used in references [14] and [15] are not consistent with real applications. Hence, there is no accurate analytical expression for spectral density of DS-SS BPSK with deterministic signatures and small spreading factors.

In this dissertation a high data rate DS-SS BPSK reverse link, with a 7 chip signature and chips with raised-cosine characteristics, is analyzed. We analyze two receiver structures. The first receiver (Chapter 4 or [16]) has a single antenna with the modified delayed signature two finger RAKE demodulator. The second (Chapter 5 or [17]) is a dual space diversity RAKE demodulator with two antennas, four fingers and a space-multipath diversity combiner is used at the receiver. We assume the baud interval is similar to the channel delays [18], [19] and the chip extends up to ± 7 chip intervals that results in four incoherent intersymbol interference terms.

We calculate the error rate for a given channel using the total probability theorem, standard Gaussian approximation and bounds [20], [21] in the presence of Gaussian noise and intersymbol interference. Upper bounds on error rate are derived using the Chernoff and Prabhu bounds while a lower bound is derived using Jensen's

inequality. The latter upper bound is expressed in terms of the error rate with two intersymbol interference terms and bounds on the marginal distribution of the smaller terms. In the case of bounds the true statistics of intersymbol interference is used instead of assuming it to be Gaussian. The unconditional error rate is obtained by Monte Carlo simulation over channel parameters and all methods are compared.

For the first receiver [16] or the non space diversity two finger RAKE, the Gaussian approximation error rate is pessimistic for a SNR $>$ 8 dB and 12 dB when compared to that obtained by the total probability theorem and Prabhu bound respectively. The upper bound on error rate obtained from the Prabhu bound is much tighter than that obtained by the Chernoff bound. High SNR conditions can exist when the mobile power cannot be reduced further by power control. It is understood that diversity reception with channel coding would improve this operating SNR. Upper and lower bounds show that the modified delayed signature RAKE effectively combats incoherent intersymbol interference.

In the second receiver or dual space diversity four finger RAKE, for per branch SNR $>$ 6 dB, the Prabhu upper bound on error rate is notably better than the Gaussian approximation. The dual space diversity RAKE combats intersymbol interference at low SNR's while the immunity it offers decreases considerably for SNR $>$ 10 dB. At 10^{-3} error rate a dual space diversity RAKE provides an 8 dB space diversity gain [17].

The main difference between this study and previous work is that we use the true statistics of intersymbol interference instead of assuming it is Gaussian. The Gaussian approximation may work for low data rate systems [7], [8], however, more accurate methods are required for high data rate links. We use analytical techniques while [9], [10] use simulation. We consider chips that extend up to ± 7 chip intervals and four intersymbol interference terms while [8] considers rectangular chips and

two intersymbol interference terms. In [9] intersymbol interference causes error rate degradation while we show minimum degradation.

In this dissertation we derive an accurate analytical expression for the spectral density of a DS-SS BPSK signal with Gold and PN sequences. We show that the signal can be expressed mathematically as a linear digital modulated waveform that enables [22] determination of its spectral density. In our case, one signature period with chips that have square-root raised-cosine characteristics results in a unique signaling pulse. The information sequence is assumed to be wide sense stationary as is conventionally done. We directly utilize the spectral density of [2], [11] by deriving the Fourier transform of this unique baud rate signaling pulse along with the ensemble autocorrelation sequence of the information. The spectral density is a function of the chip Fourier transform, the signature coefficients and autocorrelation sequence of the information. We compute the spectral density and fractional containment bandwidth for different sequences and filter rolloffs. Finally, for front end SNR, we derive the received signal power from the spectral density and average it over the channel.

Our spectral density derivation is different from previous work [14], [15] in several ways. We correctly use wide sense stationarity for the information sequence and do not randomize the delay of the information sequence. We treat the signature sequence as deterministic instead of a random signal. Our spectral density does not have spectral lines like the spectral density in Eq. 8 of [14]. Also the measured spectral density in Fig. 3.32 of [23] does not have spectral lines. Our spectral density is a function of the signature coefficients, while the spectral density in Eq. 21 of [15] is a function of the periodic auto-correlation function.

1.2 Packet Wait Times and Outage in Voice over IP Wireless Links

For packet wireless, evaluation of Erlang capacity at a given expected voice packet wait time and packet error rate is an important consideration. For medium quality voice [24], the packet wait times should be less than 300 ms between mobile devices. Packet wait times introduced by queuing at the base station must be a much smaller fraction of this limit. In addition the probability of outage or the probability that packet wait times exceeds a threshold, when quality of voice is unacceptable, is important for capacity determination.

In [25], a packetized voice process was fed to a T1 1.543 Mb / sec system to obtain expected packet wait times. A single user's packet stream consisted of talkspurts and a silence interval both having mean durations. The talkspurts packets was geometrically distributed, while the silence interval was exponentially distributed. The packet interarrival times was a renewal process with successive interarrival times being independent. For multiple independent voice users, the cumulative distribution function of the aggregate packet interarrival times, obtained by superposition, was very nearly exponential. The aggregate packet interarrival times, were obtained by monte carlo simulation of the superposition process of multiple users. The expected packet wait times, obtained by monte carlo simulation of the G/D/1 queue was compared to those obtained from the M/D/1 queue [26], [27]. For utilization factors greater than 0.8 (or users > 110), expected packet wait times were underestimated by the M/D/1 queue approximation due to correlation between packet interarrival times.

For spread spectrum wireless voice over IP forward links [28], the base stations have a single queue and schedule packet transmission over a single high bit rate radio channel with 1% packet error rate. The packet wait times due to traffic induced queueing and radio retransmission was lumped together and obtained by using a modified M/D/1 queue. On the reverse link [28] each voice over IP user was assigned

a high bit rate traffic channel for the duration of the call. Erlang capacity was determined by modifying the Erlang B formula [29], [30] for the M/M/m queue. Packet wait times was due to voice packet allignment with available frames and frame retransmissions. For the forward and reverse links the probability of outage was defined as 2% of packet wait times being greater than a delay bound [28] of 70 ms. In [31] the probability of packet loss is obtained for a high data rate channel with a low number of voice over IP users using the M/M/1 queue with independent arrivals. Recently in [32] the batch arrivals process was used to approximate bursty correlated arrivals for an On-Off-G/D/1 queue to determine expected packet wait times. Hence, there is no analytical expected packet wait times for correlated interarrival times at $G/D/S_T$ queues. Also, there is no analytical probability of outage for traffic induced packet wait times.

For packetized data traffic reverse links [33], each mobile user has its own queue with forward and reverse dedicated control channels used to schedule traffic over a high bit rate bursting data channel. The radio channel can support a finite number of simultaneous high bit rate bursts at acceptable packet error rate. For the reverse link multiple queues and multiple radio channels or servers complicates determination of expected packet wait times.

In chapter 7 we derive the modified Little's-multinomial approximation for traffic induced expected packet wait times in voice over IP wireless reverse links with the G/D/1 queue and scheduled transmission. We assume a voice coding scheme [34] with header compression, voice packet duration of 20 ms at 9.6 Kb / sec. We modify [35] the parameters of the single and multiple voice user packet interarrival time model [25]. We assume that the reverse radio channel can support a single high bit rate bursts at 174.2 Kb / sec [16] with duration of 1.5 ms at a low packet error rate. Each voice over IP mobile has its own queue with forward and reverse dedicated control

channels that are used to schedule traffic over a high bit rate bursting data channel. We assume a single virtual queue at the base station is equivalent to many physical mobile queues. This virtual queue has correlated interarrival times for the superposition of all links. If the radio channel supports one high bit rate burst (or server) at any time with acceptable packet error rate, then all mobiles share usage of this one burst that is coupled to a G/D/1 virtual queue at the base station. We apply Little's theorem [26], [36], [37], [38], [39] to a reference users talkspurt-silence duration or the busy period divided into three intervals. Statistically independent packet arrival times from individual users are used to determine conditional expected packet wait time and carry over delays, given overlapping talkspurts. The probability of overlapping talkspurts determined from the multinomial distribution is used to obtain expected packet wait times by applying total probability theorem. At high utilization factors (operating point of interest), the modified Little's-multinomial analytical approximation provides a better estimate than the M/D/1 queue approximation when compared to simulations of the superposition process for multiple users and G/D/1 queue.

In Chapter 8, for voice over IP wireless reverse links which supports two simultaneous radio burst (or two servers) at any time with acceptable packet error rate, traffic induced expected packet wait times are obtained using the modified Little's-multinomial analytical approximation. Two servers increase the number of packets present per interval and reduce the carryover delays from one interval to the next. We compare the expected packet wait times obtained by the dual server modified Little's-multinomial analytical approximation to the Kingman upper bound [40] approximation and simulation. For high utilization factors where correlation between packet interarrival times results in high wait times, the modified Little's-multinomial analytical approximation provides a better estimate of packet expected wait times. Using the modified Little's-multinomial analytical approximation for expected packet

wait times, the dual burst reverse link provides a capacity gain of 2.16 over a single burst reverse link.

In this dissertation, Steffensens inequality is used to derive an upper bound on the probability of outage. Although the bound is applicable for any wait time thresholds we use 30 ms to 60 ms for analysis. Statistically only an analytical approximation on the first moment of packet wait time is known. The Kingman [40] upper bound on the tails of the waiting time distribution cannot be applied since wait times and interarrival times are correlated. The Chernoff bound cannot be used since the moment generating function of the wait time is not known. The Chebyshev inequality cannot be used as the second moment of wait times is not known and the Markov inequality is a weak upper bound.

There are several difference between our work and previous studies. We derive the modified Little's-multinomial analytical approximation for expected packet wait time in voice over IP wireless reverse links with the G/D/1 queue, at high utilization factors, for the first time. In [25] expected packet wait times are obtained for a land line T1 system with packetized voice at high utilization by simulation and using the M/D/1 queue approximation. Similarly, [28] assumes a high data rate continuous channel for the voice over IP reverse link and uses the modified M/M/m queue and [31] assumes a high bit rate channel with the M/M/1 queue. Additionally our analysis treats traffic induced packet wait time separately, while [28] lumps traffic induced and retransmission wait times together. This enables assessment of radio layer introduced wait times due to retransmission separately. Finally, [32] uses the batch arrivals process to approximate bursty correlated arrivals while we use the single user voice over IP packet arrivals. Our Steffensens upper bound on probability of outage can be used for any wait time threshold while [28] is specific to a outage of 2%. Our Steffensens upper bound on probability of outage is for traffic induced packet wait

times while in [28] outage is for frame alignment and retransmission wait times. Our analytical methods can be used for system design, characterization of base station traffic induced wait times and Erlang capacity determination.

The modified Little's-multinomial approximation for expected traffic induced packet wait time's in voice over IP wireless reverse links which supports one or two simultaneous radio burst (or servers) at any time with acceptable packet error rate has been derived for the first time. This analytical techniques are applied to the advanced G/D/1 and G/D/2 queues. Furthermore an upper bound for the related probability of outage has been derived for the first time using the Steffensen's inequality. Our analytical methods can be used for wireless system design, characterization of base station traffic induced wait times and Erlang capacity determination. These analytical techniques can be extended to the G/D/K queue.

CHAPTER 2

PERFORMANCE / CAPACITY OF DS-SS WIRELESS SYSTEMS

In DS-SS wireless reverse links, the error rate performance enables determination of number of radio channels supported and hence Erlang capacity. Here we provide a summary of existing low bit rate RAKE receiver and circuit switched voice call models along with error rate and the $M/M/\infty$ queue capacity that is used for legacy DS-SS wireless reverse links.

Here these concepts are used to start developing some of the models for a high bit rate RAKE receiver and voice over IP that is used for state of the art DS-SS packetized wireless reverse links. Practical wireless system parameters are used in these academic mathematical models. These models are used in chapters 4, 5 and 6 to derive error rate of the high bit rate dual space diversity RAKE receiver. While in chapter 7 and 8 these models are used to derive packet wait times statistics in the advanced $G/D/S_T$ queue used for voice over IP wireless reverse links.

2.1 Introduction

In legacy and state of the art (Direct Sequence-Spread Spectrum) DS-SS or (Code Division Multiple Access) CDMA wireless systems, the main challenge has always been improving error rate performance and Erlang capacity while combating impairments introduced by the mobile radio channel. The error rate performance of the link enables determination of how many simultaneous radio channels can be supported which in turn allows us to obtain Erlang capacity.

In DS-SS, dynamic power control is used to combat long term fading as shown in chapters 3 to 6. The chips have raised cosine characteristics [41] and the frequency selective radio channel causes intersymbol interference. The RAKE receiver [1], [4], [5] is used for multipath diversity combining of strong multipath beams and is effective in mitigating intersymbol interference. This enables us to develop the high bit rate RAKE models used in Chapter 4, 5 and 6.

Legacy DS-SS systems carry circuit switched voice where a low bit rate radio channel is assigned for the duration of the call. Circuit switched voice call arrivals are Poisson and hold times (or service time) are negative exponential Markov processes. Pursley [6], derives derives the standard Gaussian approximation error rate of a DS-SS BPSK Multiple Access (MA) link.

State of the art wireless systems carry voice over IP, where a high bit rate bursting reverse data channel is assigned when there is voice packets to send. Here we develop the voice over IP model that is used in chapters 7 and 8. In voice over IP call sessions arrivals are Poisson and session hold times are negative exponential Markov processes. However, the underlying voice packet arrivals have a general distribution with correlated interarrivals and deterministic service times. If the radio channel supports S_T simultaneous high bit rate bursts (or servers) at acceptable packet error rate, then all mobiles share usage of these S_T bursts that are coupled to a $\mathrm{G/D/S_T}$ virtual queue at the base station. In recent error rate studies the standard gaussian assumption has been used for intersymbol interference. In chapters 4 and 5 error rates using standard Gaussian approximation for intersymbol interference is compared to more robust methods.

In CDMA with circuit voice, the reverse link Erlang capacity [29] is average carried load (traffic in Erlangs) for a Grade of Service (GOS). Viterbi's GOS for the $\mathrm{M/M/\infty}$ queue equals the probability of interference-to-noise density being greater

than 10 dB, given K active users, is less than 2%. To determine multiple access interference power and hence Erlang capacity; Viterbi assumes that each user's receiver requires an E_b/I_o (bit energy-to-interference density), that is a lognormal (with empirical moments), to achieve an $FER \approx 1\%$.

In voice over IP wireless, voice capacity is the number of simultaneous voice users for a given packet expected wait times and probability of wait time outage. The existing expected packet wait times for the M/D/1 and G/D/2 queues are provided here. In chapters 7 and 8 the expected packet wait times of these queues is compared to analytical expected wait times statitsics of the advanced G/D/1 and G/D/2 queues of voice over IP wireless reverse links.

2.2 Wireless Radio Channel

When a microwave signal is transmitted by a fixed base station and received at a moving mobile, the received signal shall exhibit amplitude and phase variations along with signal distortion. For analytical analysis, the mobile radio channel is modeled by a linear impulse response with statistical parameters [42], [43] and a reasonable assumption [44] is that the channel is time invariant over several symbols. The mobile radio channel introduces long term or lognormal fading, short term or Rayleigh fading, uniform phase, multipath propagation with delayed beams and time dispersion that causes signal distortion.

2.2.1 Narrow Band Channel

In a mobile radio system, when a continuous wave carrier is transmitted from a base station, the median path loss depends on the carrier frequency, the distance between the transmitter and mobile, the base station and mobile antenna heights and the environment (urban, suburban or rural). In a mobile radio environment, a

large number of different obstructions such as buildings, hills, trees etc. attenuate the signal. Hence, this radio wave attenuation, measured in dB's, can be assumed to be a Gaussian random variable that represents long term fading. The received signal is a sum of multipath signals that have been scattered by random obstructions which introduces a different attenuation and phase for each of these signals. This phenomenon, modeled by a Rayleigh random variable, is termed short term fading.

The n^{th} diversity channel impulse response for a mobile user k

$$H_k^{(n)}(t) = L_k h_k^{(n)}(t) \tag{2.1}$$

where $L_k = \sqrt{\left[\mathcal{K}/d_{k,km}^{\gamma}\right] 10^{\zeta_k/10}}$ results in the local mean signal strength, depends on environment and shall be the same [43] for all diversity paths. The constant $\mathcal{K}$ depends on the antenna height and frequency, while $d_{k,km}$ is mobile to base station distance in km, γ is path loss exponent, ζ_k is normal random variable with $m_\zeta = 0\,\text{dB}$ and $\sigma_\zeta = 6$ to $13\,\text{dB}$. In chapters 2, 3, and 4, L_k is compensated for by ideal power control. Using baseband to passband conversion [2], the passband multi-path fading impulse response for mobile k on the statistically independent n^{th} diversity channel

$$h_k^{(n)}(t) = 2Re\left[c_k^{(n)}(t)\exp\left(j2\pi f_c t\right)\right] \tag{2.2}$$

where the baseband response

$$c_k^{(n)}(t) = r_k^{(n)}\exp\left(-j\phi_k^{(n)}\right). \tag{2.3}$$

The Rayleigh fading, $r_k^{(n)}$, has a pdf (with $E\left[r^2\right] = 2\sigma_r^2$)

$$p(r) = \frac{r}{\sigma_r^2}e^{-r^2/2\sigma_r^2} \qquad r \geq 0 \tag{2.4}$$

and assume $2\sigma_r^2 = 1$ [45]. The uniform phase $\phi_k^{(n)} = 2\pi f_c \tau_k^{(n)}$, where $\tau_k^{(n)}$ are clustered around very small values [4] $\pm 1/f_c$ (or ± 1.1 ns for 900 MHz) with pdf

$$p(\phi) = \frac{1}{2\pi} \qquad 0 \leq \phi < 2\pi. \tag{2.5}$$

A minimum signal power for user k is required to sustain an adequate error rate performance [46] and Erlang capacity. Rayleigh fading and uniform phase increases the minimum required signal power and impacts Erlang capacity (see chapter 3).

2.2.2 Frequency Selective Multipath Fading

The predominant characteristic of urban and suburban mobile radio channels is multiple propagation paths with varying degrees of delay and amplitude [5], [18]. In this case, the channel introduces time dispersion that causes signal distortion. The Cox wideband channel power delay profile measurements [18] show delay spreads of 0.24 μs and 2.05 μs. In some measurements [18] strong multipath Rayleigh beams appear at 1.1 μs and 4.3 μs relative to the earliest main Rayleigh beam. Longer delay spreads are usually found in urban environments. At fixed delays signal level distributions are Rayleigh. The baseband channel impulse response, for mobile k,

$$c_k^{(n)}(t) = \sum_{g=1}^{2} \rho_{k,g}^{(n)} r_{k,g}^{(n)} \exp\left(-j\omega_c \tau_{k,g}^{(n)}\right) \delta\left(t - \tau_{k,g}^{(n)}\right) \tag{2.6}$$

has been used [47], [44] for analytical receiver performance analysis. The g^{th} Rayleigh fading beam; $r_{k,g}^{(n)} = \sqrt{\left\{\alpha_{k,g}^{(n)}\right\}^2 + \left\{\beta_{k,g}^{(n)}\right\}^2}$, where $\alpha_{k,g}^{(n)}$ and $\beta_{k,g}^{(n)}$ are zero mean Gaussian random variables. Each beam has a relative amplitude $\rho_{k,g}^{(n)}$ and a delay $\tau_{k,g}^{(n)} = \tan^{-1}\left[\alpha_{k,g}^{(n)}/\beta_{k,g}^{(n)}\right]$. In chapter's 4, 5 and 6 different delay characteristics are used for the secondary beam of the transmitted signal and asynchronous multiple access interference when determining error rate performance.

The coherence bandwidth [43] of the channel is the maximum frequency difference for which a signal envelope correlation is 0.5. The coherence bandwidth $BW_c = 1/(2\pi\sigma_D)$ where σ_D is the delay spread. A channel is considered frequency selective [2] or time dispersive if signal bandwidth $BW > BW_c$. A time dispersive channel severely distorts the transmitted signal.

2.3 AMPS/TDMA Wireless System

The Advanced Mobile Radio System (AMPS) system first introduced by Bell Labs in the late 1970's was a Frequency Division Multiple Access (FDMA) system. Each user's voice frequency modulated a carrier and the passband signal occupied a bandwidth of 30 kHz. In a cluster of seven cells, a unique set of carriers was allocated for each cell. In 1981 Time Division Multiple Access (TDMA) systems that used QPSK modulation and FDMA were deployed. In the 30 kHz bandwidth, three users used separate time slots which resulted in a three-fold increase in capacity. The capacity was limited by available carriers and carrier to co-channel interference or C/I thresholds that defined the distance between cells using the same carriers. Circuit switched voice call arrival and hold time processes are described in Sec. 2.4.1.

2.4 DS-SS Wireless Systems and Error Rate

A simple theoretical DS-SS or CDMA system (Fig. 2.1) comprises of a cluster of seven omni-directional hexagonal cell sites with central base stations (BTS's) towers connected to a Mobile Trunk Exchange/Base Station Controller (MTX/BSC) by a backhaul system. The MTX/BSC has the reverse link selection function which is required for reverse link soft handoff diversity reception. Each BTS uses one frequency on the forward link and another, with adequate separation, on the reverse link. At the transmitter user data is multiplied (or spread) by a unique code sequence and up-converted. At the receiver the incoming signal is down-converted and multiplied by the same unique code sequence that is used at the transmitter. If rectangular chips were used at the transmitter then the correlation signal demodulator (based on the integrate and dump principle) and threshold detector (based on output energy per bit) can be used at the receiver.

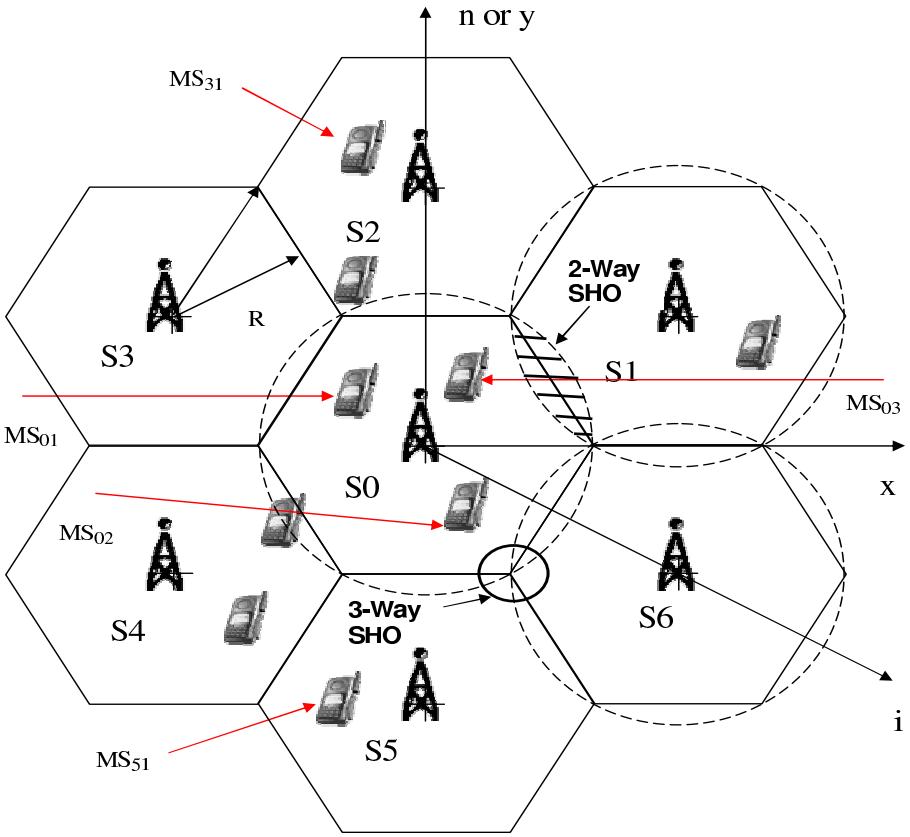

Figure 2.1. DS-SS system - cluster of seven cell sites.

If shaped chips are used at the transmitter then the matched filter signal demodulator with maximum likelihood detection can be used at the receiver. For real systems, square root raised-cosine filters at the transmitter and receiver shall enable spread spectrum communications with chips that satisfy the Nyquist criteria. In this case the practical receiver (see chapter 3, 4, 5 and 6) with matched filtering and RAKE processing followed by threshold detection (based on signal voltage) can be used. In a Multiple Access (MA) system the desired signal is corrupted by other user interference and Additive White Gaussian Noise (AWGN). Pseudonoise (PN) or Gold sequences are used to suppress interference due to their cross-correlation properties.

Dynamic power control and soft handoff (SHO), where mobiles communicate with multiple BTS's, help minimize interference.

2.4.1 Circuit Switched Voice Low Bit Rate Reverse Links

In one DS-SS system, all mobile stations (MS) transmit at the same frequency f_1 and have bandwidth $BW = 1.25$ MHz. A simple system with BPSK symbol modulation and 127 chip Gold sequence for spreading is used for our analytical analysis [1]. The unique sequence is also used for the user's address. A chip duration of $T_c = 0.82\,\mu$s, signal bandwidth $BW \approx 1/T_c = 1.2288$ MHz and symbol duration $T = 104.2\,\mu$s (or bit rate $R_b = 9.6$ kb / sec) similar to real CDMA systems is assumed.

In the sector multiple access interference is caused by other user transmissions. Each user's mobile signal has a call arrival time τ_a as shown in Fig. 2.2. The time between adjacent arrivals or the inter-arrival time have a negative exponential pdf;

$$p_a(t) = \lambda \exp\left[-\lambda t\right] \tag{2.7}$$

where the expected inter-arrival time, $E[t] = 1/\lambda$. The call arrivals are Poisson distributed with pdf

$$p_k = \frac{(\lambda t)^k}{k!} e^{-\lambda t}. \tag{2.8}$$

where λ is the expected call arrival rate. The service time or call hold time has a negative exponential pdf;

$$p_b(t) = \mu \exp\left[-\mu t\right] \tag{2.9}$$

where the expected call hold time, $E[t] = 1/\mu$.

Consider the reverse link signals received at the base station receiver for the central cell site $S0$ of the single cluster system shown in Fig. 2.1. As shown in Fig.

[1] In IS2000/IS856 [48] systems the mobile use a 42-Stage Long PN (different phase offset) and 15-Stage Short PN synchronized to the BTS phase with QPSK and QAM symbol modulation

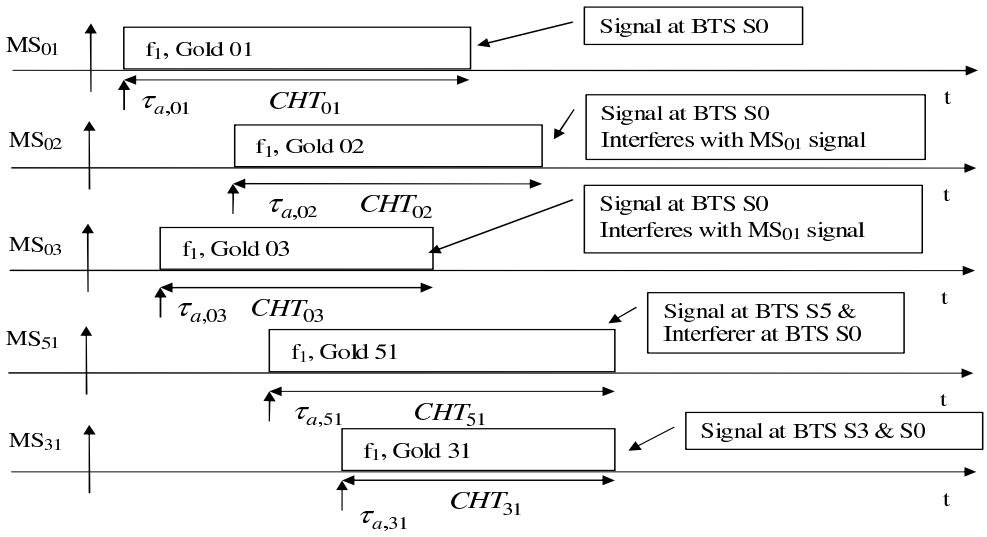

Figure 2.2. Reverse link multiple access interference at the central base station receiver.

2.2, the desired signal from mobile station MS_{01} at base station $S0$ uses a signature Gold sequence $Gold\ 01$, that has a time of arrival $\tau_{a,01}$ and a Call Hold Time CHT_{01}. The desired signal for MS_{01} is corrupted by same cell multiple access interference from mobiles MS_{02} and MS_{03}. The desired signal for MS_{01} is also corrupted by other cell multiple access interference from mobiles MS_{51} and MS_{31}.

2.4.2 RAKE Receiver

For a delay spread $\sigma_D = 2.05\mu$s, the signal bandwidth BW is much greater than the coherence bandwidth $BW_c = 77.6$ KHz. Delay spreads of $\sigma_D = 2.05\,\mu$s and strong multipath Rayleigh beams (at $1.1\,\mu$s and $4.3\,\mu$s relative to the main beam) have delays that are significantly larger than the chip duration $T_c = 0.82\mu$s. For low data rate links with symbol duration $T = 104.2\ \mu$s, strong multipath propagation with large delays introduces intersymbol interference due to multipath interference. However, due to the auto-correlation properties of the desired users signal these multiple beams can be resolved by the receiver and utilized for multipath diversity reception. Multipath

interference causes a reduction in Erlang capacity, hence, optimal transmission and reception is required to combat the mobile radio channel.

For a delay spread $\sigma_D = 0.24\mu sec$, the signal bandwidth BW is greater than the coherence bandwidth $BW_c = 663.0$ KHz. Hence, the channel distorts the transmitted chip due to time dispersion resulting in inter chip interference [4] which degrades error rate performance. If the multipath has delays $\leq T_c$, then these multipath echoes cannot be resolved. Such chip distortion is not considered here.

In PAM radio systems the signaling pulse [49], [50] and [20] has a raised-cosine frequency characteristic which satisfies the Nyquist criteria. Similarly in DS-SS links the chip has a raised-cosine frequency characteristic [41] that satisfies the Nyquist criterion. At the transmitter a square root raised-cosine filter is used for chip shaping prior to upconversion and transmission. At the receiver the signal demodulator comprises of a down converter, square root raised cosine filter and RAKE. The RAKE receiver, used for multipath maximal ratio combining of strong multipath beams with large delays, is effective in mitigating intersymbol interference. Multipath signals with large delays can be resolved at the receiver and constructively used by de-spreading the echoes with the unique code sequence that was used at the transmitter [1],[4].

In a sector, at the base station, two antennas are used for space diversity. Each diversity signal is expected to have more than one multipath Rayleigh fading beam (Eq. 2.6). The RAKE receiver structure has four fingers to track up to four multipath signals from the two antennas and it is a tapped delay line where each tap is synchronized to one of the fading echoes. The outputs from each tap are weighted in proportion to the received signal and phase corrected before being combined. Delays are reinserted into desired detected echoes so that the echoes fall in step and hence the RAKE receiver is effective in mitigating intersymbol interference. The diversity

RAKE receiver provides space and multipath diversity gains along with intersymbol interference mitigation as shown in chapters 4, 5 and 6.

The RAKE receiver is also used for soft handoff which provides diversity that reduces interference. Packet retransmission or time diversity combats short term fading. While dynamic power control combats long term fading and minimizes interference.

2.4.2.1 Price and Green RAKE Receiver

The original Price and Green [1] RAKE receiver (Fig. 2.3) was significantly different from that used for IS-2000 radios. The transmitted mark or space signal

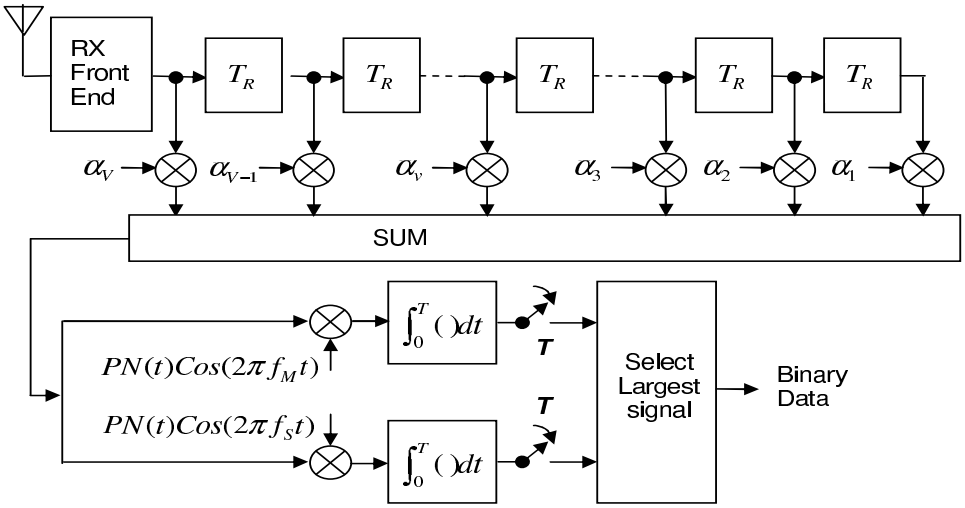

Figure 2.3. The Price and Green RAKE receiver.

in one baud interval T [4]

$$s_l(t) = PN(t)\cos(2\pi f_l t) \qquad l = M, S \tag{2.10}$$

where $PN(t)$ is the maximal length binary shift register sequence which has a bandwidth W. The frequencies f_M and f_S represent the mark and space symbols re-

spectively while $|f_M - f_S|$ is chosen so that the waveforms are uncorrelated. For a multipath fading channel the received signal,

$$r(t) = \sum_{g=0}^{G} \alpha_g s_l (t - \tau_g), \tag{2.11}$$

where g is the number of beams with complex amplitude α_g and delay τ_g. The RAKE receiver is comprised of three sections. The first section is the transversal filter, in which case signals from a periodically tapped delay line are weighted appropriately and summed up. The second section consists of space and mark correlators that have separate integrate and dump circuits. Finally, the outputs of the two correlator are processed at decision device where an estimate is made on whether a space or mark was transmitted. The impulse response of the transversal filter [5] $h_{RAKE}(t) = \sum_{v=0}^{V} \widehat{\alpha_v} \delta (t + vT_R)$ which has a total of V taps that extract the signal from a delay line at periodic delays T_R where $T_R = 1/W$. Each tap has complex weights $\widehat{\alpha_v}$. The output from the transversal filter $r_{TF}(t) = r(t) \otimes h_{RAKE}(t)$ or

$$r_{TF}(t) = \sum_{v=0}^{V} \sum_{g=0}^{G} \widehat{\alpha_v} \alpha_g PN [t - \tau_g + vT_R] \cos [2\pi f_l (t - \tau_g + vT_R)]. \tag{2.12}$$

The composite signal at the output of the transversal filter is then fed to separate correlators whose output $r_O(t) = \int_0^T r_{TF}(t) PN(t) \cos(2\pi f_l t)\, dt$. The ouput from the correlator, that is an estimate of the transmitted signal,

$$r_O(t) = \sum_{v=0}^{V} \sum_{m=0}^{M} \widehat{\alpha_v} \alpha_m R_{PN} [\tau_m - vT_R] \cos [2\pi f_l (\tau_m - vT_R)] \tag{2.13}$$

where $R_{PN} [\tau_m - vT_R]$ is the auto correlation function of the sequence $PN(t)$.

The signal correlator output, assuming $M = 1$, $V = 1$, $\tau_0 = 0$, and $\tau_1 = T_R$,

$$\begin{aligned} r_O(t) = {} & \widehat{\alpha_0} \alpha_0 R_{PN} [0] \cos [0] + \widehat{\alpha_1} \alpha_0 R_{PN} [-T_R] \cos [2\pi f_l T_R] \\ & + \widehat{\alpha_0} \alpha_1 R_{PN} [-T_R] \cos [2\pi f_l T_R] + \widehat{\alpha_1} \alpha_1 R_{PN} [0] \cos [0], \end{aligned} \tag{2.14}$$

where the first and fourth term represent two path maximal ratio combining. The second and third terms represent the intersymbol interference.

2.4.3 Error Rate - Low Bit Rate

In [6] Pursley determines the error rate of a DS-SS multiple access BPSK system with a uniform phase, delay radio channel and additive white gaussian noise by deriving the standard Gaussian approximation. Over the years the standard Gaussian approximation error rate [6] was extended [7], [8] by assuming that multipath interference is Gaussian. The approximation is good [7] for a single branch receiver with a 31 rectangular chip signature. In the low data rate RAKE system [8] with a 127 rectangular chip signature, two intersymbol interference terms were considered.

2.4.3.1 Standard Gaussian Approximation Error Rate

Pursley [6] determines the performance of a DS-SS multiple access BPSK system (Fig. 2.4)in which the transmitted signal for the k_{th} user's data symbols are spread by unique code sequences with rectangular chips. The transmitted signal for user k

$$s_k(t) = \sqrt{2P} \sum_{l=-\infty}^{\infty} b_{k,l} p_T(t - lT) \sum_{j=-\infty}^{\infty} a_{k,j} p_{T_c}(t - jT_c) \cos(\omega_c t + \theta_k) \qquad (2.15)$$

where $\sqrt{2P}$ is the amplitude, $b_{k,l} = \pm 1$ is the equal probability symbols for user

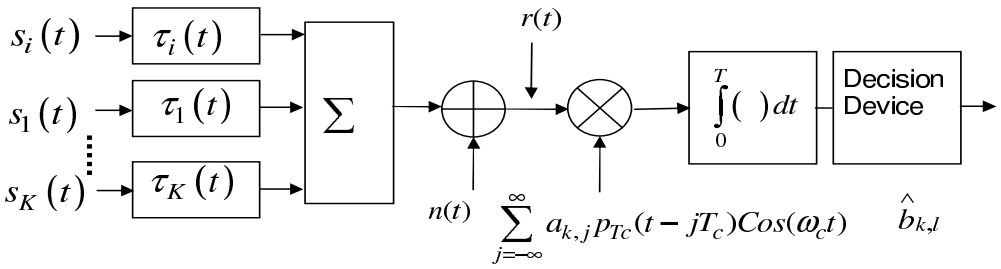

Figure 2.4. Pursley correlation receiver.

k, l is the baud, $p_T(t) = \Pi(t/T)$ is a rectangular function, T is the symbol duration, $a_{k,j} = \pm 1$ represents an element of the Gold code sequence, $p_{T_c}(t) = \Pi(t/T_c)$ is

the chip pulse with duration T_c. The period of the Gold sequence $N = T/T_c$. The pass-band desired and interfering signals are perturbed by the radio channel (uniform phase and delays) and AWGN. The overall received signal

$$r(t) = \sum_{k=1}^{K} \sqrt{2P} \sum_{l=-\infty}^{\infty} b_{k,l} p_T \left(t - lT - \tau_k\right) \times \sum_{j=\infty}^{\infty} a_{k,j} p_{T_C} \left(t - jT_c - \tau_k\right) \cos\left(\omega_c t + \phi_{k,1}\right) + n(t). \tag{2.16}$$

Here the delay $0 \leq \tau_k < T$ is uniformly distributed or $p(\tau_k) = 1/T$. The uniform phase $\phi_{k,1}^{(n)} = \theta_k - \omega_c \tau_{k,1}^{(n)}$ has pdf $p(\phi_k) = 1/2\pi$. The AWGN $n(t)$ has a two sided power spectral density of $N_o/2$ (W/Hz).

A correlation signal demodulator, based on integrate and dump principle, is used at the receiver. The incoming signal is down-converted, multiplied with the same unique code sequence used at the transmitter, integrated over the symbol interval and sampled at the symbol rate. The sampled signal at the correlator output,

$$r_O(t) = \sqrt{\frac{P}{2}} b_{i,0} T + \sum_{\substack{k=1 \\ k \neq i}}^{K} \sqrt{\frac{P}{2}} \cos\left(\phi_{k,1}\right) \left\{ b_{k,-1} R_{k,i}\left(\tau_k\right) + b_{k,0} \hat{R}_{k,i}\left(\tau_k\right) \right\} + \int_0^T n(t) \sum_{j=-\infty}^{\infty} a_{i,j} p_{T_C}\left(t - jT_c\right) \cos\left(\omega_c t\right), \tag{2.17}$$

is fed to a threshold detector which evaluates the energy per bit to decide which symbol was transmitted. Here the continuous time partial cross correlation functions

$$R_{k,i}\left(\tau_k\right) = \int_0^{\tau} \sum_{j=-\infty}^{\infty} a_{k,j} p_{T_C}\left(t - jT_c - \tau_k\right) \sum_{j=-\infty}^{\infty} a_{i,j} p_{T_C}\left(t - jT_c\right)$$

$$\hat{R}_{k,i}\left(\tau_k\right) = \int_{\tau}^{T} \sum_{j=-\infty}^{\infty} a_{k,j} p_{T_C}\left(t - jT_c - \tau_k\right) \sum_{j=-\infty}^{\infty} a_{i,j} p_{T_C}\left(t - jT_c\right). \tag{2.18}$$

As the multiple access interference is assumed to be Gaussian; so the error rate,

$$P_e = \frac{1}{2}\text{erfc}\left[\sqrt{\frac{A_s^2}{2\sigma_G^2}}\right], \tag{2.19}$$

where $A_s = \sqrt{P/2} \quad T$. The variance of the asynchronous multiple access interference plus noise,

$$\sigma_G^2 = \frac{P}{4}\sum_{\substack{k=1 \\ k\neq i}}^{K}\left\{E\left[R_{k,i}^2\left(\tau_{k,1}\right)\right] + E\left[\hat{R}_{k,i}^2\left(\tau_{k,1}\right)\right]\right\} + \frac{TN_0}{4}, \tag{2.20}$$

is determined by statistical averaging over mutually independent random variables $b_{k,0}$, $b_{k,-1}$, $\tau_{k,1}$ and $\phi_{k,1}$ and the filtered gaussian noise.

Aalo [51] studied error rate performance of a multi cell CDMA system with DS-SS BPSK reverse links that use rectangular chips at the transmitter, has imperfect power control while the channel introduces shadow fading, frequency selective Rayleigh fading and path delays. The demodulator comprises of a RAKE receiver with correlators. The error rate, averaged over Rayleigh fading, is determined in terms of receiver output signal-to-noise-plus-interference ratio that depends on the energy per bit, noise variance, multiple access and multipath induced interpath interference.

In [52] the error rate of a multi-carrier DS-SS MA system for a mutipath channel with flat Rayleigh fading beams and doppler spreads is determined by using the standard gaussian approximation for multiuser and intersymbol interference. In [53] upper and lower bounds on the error rate for DS-SS multiple access systems are derived for a correlation receiver with rectangular chips. Similarly, in [54], [55] the standard gaussian approximation error rate is used.

2.4.4 Voice over IP High Bit Rate Reverse Links

For a real DS-SS wireless Voice over IP (VoIP) system, on the forward links [28], the base stations have a single queue and schedule packet transmission over a single high bit rate radio channel with an acceptable packet error rate. On the reverse

link [28] each voice over IP user was assigned a high bit rate traffic channel for the duration of the call.

In DS-SS systems like CDMA2000 [56] and UMTS [33] the transmission bandwidth and the chip duration remain the same as the bit rate of the link increases. For this the number of chips per symbol decreases at the expense of a decrease in the processing gain. The models in chapter 4, 5 and 6 use a high bit rate of 174.2 kb/ sec, with $T_c = 0.82\,\mu$s and 7 bits per symbol.

In the reverse link [33] user data transmission is scheduled. The mobile transmits a dedicated reverse control channel, on a separate orthogonal spreading code than that used for the uplink traffic channel, which informs the base station that the mobile has data to transmit. A forward dedicated control channel for each user informs the mobile when to transmit data. The reverse traffic or data channel is transmitted only when the user has data to send and the base station authorizes transmission. In our model the control channels is equivalent to the reservation channel.

In real CDMA packet reverse links [56], the packet transmitted by the mobile consists of 4 sub packets that carries the same user data. In packet retransmission (transmit time diversity), if a sub packet is received the remaining packets are not transmitted. The duration of each sub packet is 1.25 ms. For a high bit rate $R_b =$ 174.2 kb / sec, each sub packet contains $N_b = 218$ bits. Similarly in UMTS [33] packet reverse links, the transmit time interval or packet duration for the data channel can be 10 ms or 2 ms. In chapter 7 and 8 it is assumed that a single sub packet is equal to one packet and the packet duration, $D = 1.5$ ms, carries 261 bits.

2.4.4.1 Statistical Model for Voice over IP on Wireless Reverse Links

Consider many voice over IP mobile users in a single sector where call session arrivals are Poisson with exponential call session hold times. Each call session hold

time is composed of talkspurts and silence intervals. During each talkspurts speech packets of duration T_{vp} ms arrive. The packetized voice model, presented here, uses the ITU G.729 voice coding standard to modify the Sriram/Whitt [25] model.

2.4.4.2 Modified Single Voice over IP Source Model

The pdf for the packet interarrival time used in chapters 7 and 8 is described here. The ITU G.729 coding scheme [57], [34] for speech which uses code excited linear prediction compression is assumed. Voice is coded into 8 kb / sec streams and a speech frame is produced every 10 ms. To reduce overhead bits, two speech frames are packed into a single voice packet of 20 ms. Thus the packet has 160 bits (20 bytes). Transmission of voice over IP shall require the addition of the IP (Internet Protocol) header of 20 bytes in size, the RTP (Real Time Protocol) header of 8 bytes and UDP (User Datagram Protocol) of 12 bytes. This amounts to a header for IP/RTP/UDP of 40 bytes (or 320 bits) being added to the voice packet. It is assumed that header compression reduces the IP/RTP/UDP header to 4 bytes before it is added to the voice packet. Hence, the voice over IP packet has 192 bits (24 bytes). The voice coder with headers produces voice packets 20 ms long at a rate of 9.6 kb / sec.

The single voice user packet interarrival time pdf of Sriram/Whitt [25] is modified based on the G.729 coding scheme. The voice packetization period $T_{vp} = 20$ ms instead of $T_{vp} = 16$ ms like the Sriram/Whitt model. The assumed mean talkspurt duration $\alpha^{-1} = 360$ ms instead of $\alpha^{-1} = 352$ ms like the Sriram/Whitt model. The mean number of packets per talkspurt $E[N_{vp}] = 18$ instead of $E[N_{vp}] = 22$ like the Sriram/Whitt model. Hence, for wireless reverse links, the pdf of interarrival times,

$$f_{IA}(t) = \begin{cases} 0 & t < T_{vp} \\ p\delta(t - T_{vp}) + (1-p)\beta e^{-\beta(t-T_{vp})} & t \geq T_{vp} \end{cases}, \qquad (2.21)$$

where $p = \frac{17}{18}$ instead of $p = \frac{21}{22}$ like the Sriram/Whitt model.

2.4.4.3 Common Virtual Queue Model

In this section multiple mobile voice over IP users with individual queues are modeled as a single virtual queue (see Fig. 2.5). The base station has a First-In-First-Out (FIFO) scheduler. The shared radio channel can support $S_T = 1, 2$ simultaneous high bit rate bursts that are coupled to a virtual G/D/S_T queue.

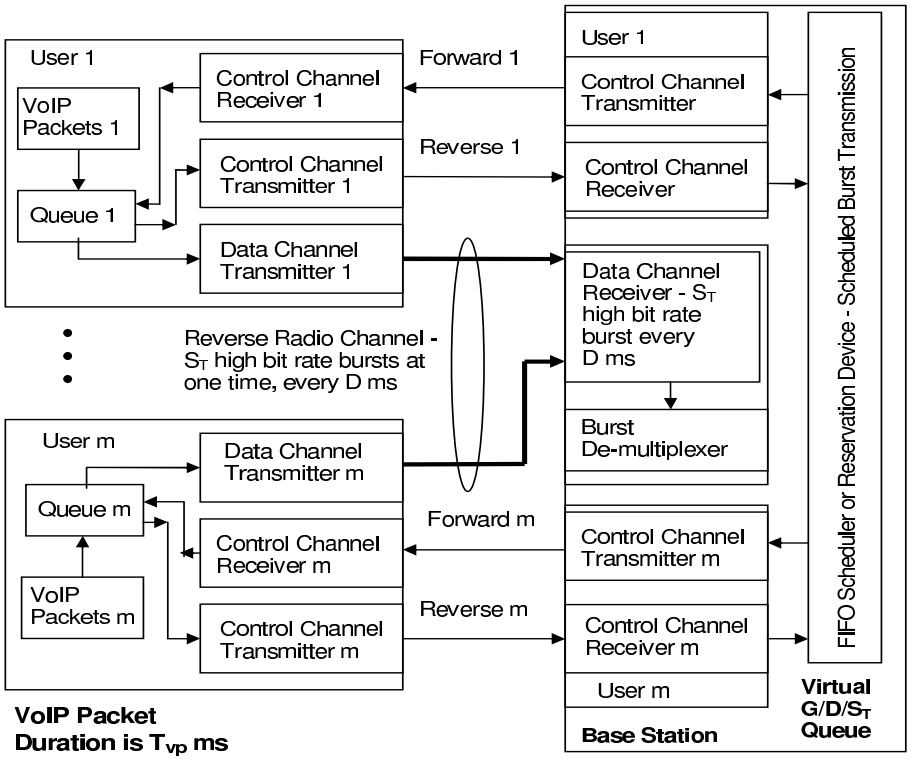

Figure 2.5. Multiple VoIP users terminal equipment and base station.

Consider speech packets (Fig. 2.6) that arrive at the respective queues of the terminal equipment for user 1 and 2. Two control channel communicate with a reservation device at the base station and the packets are transmitted over a single

burst shared radio channel or server. A reservation request is sent on the reverse control channel to the base station reservation device or scheduler which determines when the user can transmit the reverse data channel and sends a reservation granted message to user 1 using the forward control channel. User 1 terminal equipment transmits the burst of speech data on the reverse data channel. If the scheduler receives a reservation request from user 2, it shall wait until it completely receives user 1's burst before sending a reservation grant message to user 2. Hence user 2's burst waits in its queue.

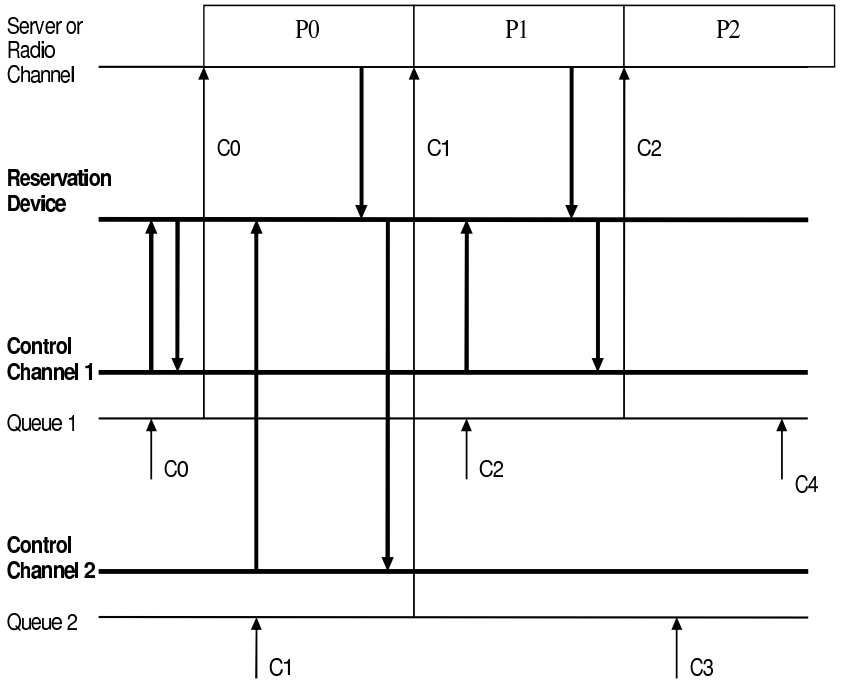

Figure 2.6. Transmission of two VoIP users packets by a single server.

The delays introduced by the control channel and reservation device are assumed to be negligible. The time required to transmit a reservation request, propagation time for the reservation request, processing time for the reservation request, the time required to transmit the reservation response and the propagation time for

the reservation response are all assumed to be negligible. As shown in Fig. 2.7, conceptually there is a single virtual queue at the base station even though there is one physical queue per mobile VoIP user. A similar concept was introduced for queues of multiple earth stations in satellite communications [58].

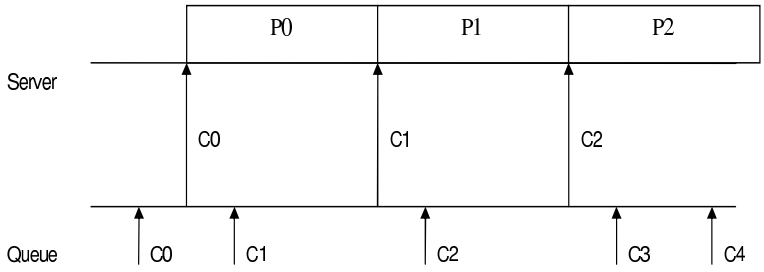

Figure 2.7. The common virtual queue.

2.4.4.4 Multiple Voice over IP User Model

It has been shown that the multiple VoIP users packet arrivals can be modeled as packets arriving at a single virtual queue at the base station. The model for multiple packetized voice users, provided by Sriram/Whitt, [25], with parameters adjusted to meet the ITU G.729 coding scheme can be used. In this model the interarrival times are correlated. In chapters 7 and 8 the packet interarrival time pdf's, described above, for a single and multiple VoIP users are utilized.

2.4.5 Error Rate - High Bit Rates

For a wideband frequency selective channel, with delay spreads of $\sigma_D = 2.05\,\mu$s; strong multipath Rayleigh beams (at 1.1 μs and 4.3 μs relative to the main beam) have delays that are significantly larger than the chip duration $T_c = 0.82\ \mu$s. For high bit rate links the symbol duration $T = 5.75\ \mu$s and hence strong multipath

propagation with large delays shall introduce much severe intersymbol interference, due to multipath interference, than that observed in low bit rate links. For high bit rates with up to 8 chip signatures, error rate was determined by simulation [9], [10].

In chapter 4 for a high bit rate DS-SS BPSK over wideband channels, the original delayed signature and modified [3] delayed signature RAKE demodulator structures error rate is determined. In chapters 5, the error rate of a dual space diversity RAKE demodulators is determined with intersymbol interference. In chapters 4 and 5 we evaluate the accuracy of the standard gaussian approximation error rate. Finally, in chapter 6, the packet error rate of a dual space diversity RAKE demodulators with intersymbol and same cell multiple access interference is determined. This enables determination of the number of simultaneous bursts that can be supported by the radio channel at an acceptable packet error rate.

2.5 Queuing Theory and Erlang Capacity of Wireless Links

The commodity that flows through a circuit switched voice and voice over IP wireless links is user calls and user data packets respectively. The queuing system [26], [36] is described by the pdfs of the interarrival times, the amount of demand or the service times and the number of servers used for transmission of the commodity.

A queuing system, as it applies to circuit switched voice wireless transmission, is a system in which user calls at the transmitter flows through one or more finite capacity channels and end up at the receiver. The call arrivals are Poisson and the service times are negative exponential random variables (Sec's. 2.3 and 2.4.1). The servers are dedicated low bit rate radio channels that are setup and maintained during the life of the call. The measure of performance is carried Erlangs and percentage of blocked users.

A queuing system, as it applies to voice over IP wireless transmission, is a system in which user data packets at the transmitter flows through one or more finite capacity channels and end up at the receiver. The voice packet arrivals have pdf's described in Sec. 2.4.4 and the packet service duration is deterministic or D ms. The queuing system includes storage or queue for waiting packets which is typically assumed to be infinite. This queue is a part of the scheduler and the queuing discipline is the first-come-fist-serve discipline. The server is high bit rate radio bursts, hence, if the radio channel can support a single burst at any time, it is said to have one server. If the radio channel can support two bursts at any time, it is said to have two servers and so on. The measure of performance is the number of simultaneous voice users being serviced by the queuing system for a given expected packet wait times and probability of packet wait time outage. In voice over IP wireless transmission Erlang capacity can be determined based on call session arrivals and hold times.

Central to queuing theory, is the Markov process in which the past history affects the future of the process by only the current value of the process, or

$$\begin{aligned}\Pr\left[X\left(t_{n+1}\right)=x_{n+1}\middle|\, X\left(t_n\right)=x_n, X\left(t_{n-1}\right)=x_{n-1}, ..., X\left(t_1\right)=x_1\right] \\ = \Pr\left[X\left(t_{n+1}\right)=x_{n+1}\middle|\, X\left(t_n\right)=x_n\right]. \end{aligned} \tag{2.22}$$

In continuous time Markov chains, state changes can occur at any time. The time spent in the current state should have a distribution that is memoryless as the past history has to be completely summarized by the current state. The negative exponential distribution is a continuous distribution that is memoryless. While the discrete geometric distribution has a probability mass function that is memoryless.

The Kendall shorthand notation [36] $a/b/c$ is widely used to describe the queuing model. Where a is the arrival time distribution, b is the service time distribution and c is the number of servers.

2.5.1 AMPS/TDMA - Erlang B M/M/K Queue

In this queuing system, for circuit switched voice transmission, the call inter-arrival times and hold times or service times are exponentials (Sec's. 2.3 and 2.4.1) that are memoryless and Markov processes. This system has K servers or dedicated channels. The state transitions or the birth-death process is the blocked calls cleared model where unserved users are lost and assumed to return after a random time.

The Erlang capacity is the average offered load per sector for a specified Grade of Service (GOS), with K servers or channels. Offered load [42], [43] or traffic (Erlangs), $A = \lambda/\mu$, where λ is the expected call arrival rate and $1/\mu$ is the expected call hold time. Offered load is also the amount of time that a number of users desire to use the channels. The GOS is the fraction of call attempts that encounter busy channels or the probability of blocking

$$P_b = Pr[Number\ of\ active\ users\ > K\ |K \text{ channels}]. \tag{2.23}$$

The offered Erlang capacity, A, is determined from Erlang B formula [26] for probability of blocking ;

$$P_b = \frac{A^K/K!}{\sum_{k=0}^{K}(A^k/k!)}. \tag{2.24}$$

In this case the carried traffic [59] $A_c = A\,[1 - P_b]$; which is required for capacity comparisons. For example, an AMPS sector with 19 channels has $A = 12.3$ Erlangs with $P_b = 2\%$ where $\lambda = 246$ Calls/Hour and $1/\mu = 180$ seconds.

2.5.2 Viterbi DS-SS - Erlang B M/M/∞ Queue

In this queuing system, for circuit switched voice transmission, the call inter-arrival times and hold times or service times are exponential (Sec. 2.4.1) that are memoryless and Markov processes. The system is assumed to have infinite servers or low bit rate dedicated channels. The state transitions or the birth-death process is

the blocked calls held model where unserved users make another attempt in one call hold time and remain in the system, while the GOS is a soft probability of blocking.

In CDMA circuit switched voice reverse links the Erlang capacity, is the average offered load per sector for a defined GOS. The Offered load [42], [43] or traffic (Erlangs), $A = \lambda/\mu$, where λ is the expected call arrival rate and $1/\mu$ is the expected call hold time. Viterbi's [29] CDMA reverse link sector Erlang capacity equals the probability of interference density to noise density being greater than 10 dB, given K active users, is less than 2% GOS or the probability of blocking;

$$P_b = Pr\left[Interference\,to\,Noise\,Density\ >\ 10dB\,|\,K\ \text{users}\right]. \tag{2.25}$$

This is expected to result in an acceptable average frame error rate, $FER \approx 1\%$, for all users. Using Molina's formula [42], with an infinite number of channels and Poisson distributed call arrivals the probablity of blocking;

$$P_b = \sum_{k=K}^{\infty} \left(A^k/k!\right) e^{-A}. \tag{2.26}$$

This is the sum of the Poisson pdf tails or the K^{th} user causes unacceptable interference. Where the number of active users have a Poisson probability mass function $p_k = \left(A^k/k!\right) e^{-A}$. Sector Erlang capacity is obtained by using Monte Carlo simulation to determine P_b. The simulation based P_b is compared to blocking probability obtained by a gaussian model. In the gaussian model

$$P_b = Pr\left[Z > \frac{BW_T}{R}\left(1 - \frac{N_o}{I_o}\right)\right] \tag{2.27}$$

where it is assumed that the random variable

$$Z = \sum_{k=1}^{K} \vartheta_k \frac{E_{b,k}}{I_o}, \tag{2.28}$$

is a gaussian function based on the central limit theorem. Here the ratio of the total spread spectrum available bandwidth to data rate $BW_T/R = 1280$; assuming 10 channels, $BW_T = 10 \times 1.2288 \times 10^6$ Hz where the signal bandwidth $BW = 1.2288$ MHz

and $R = 9.6$ kb / sec. The voice activity factor $\vartheta_k = \pm 1$ has a pdf of $Pr[\vartheta_k = 1] = \rho_\vartheta$ where a good assumption is that $\rho_\vartheta = 0.4$. Furthermore, Viterbi defines the threshold noise density to interference density ratio $N_o/I_o = 0.1$ which results in acceptable $FER \approx 1\%$. The required energy per bit to interference density $E_{b,k}/I_o$, for each user k, is lognormal based on CDMA IS-95 field data [29] and analytical analysis [3], [60] that shows the corresponding gaussian has moments, $G(m \approx 7.5 \text{ dB}, \sigma \approx 2.5 \text{ dB})$. Here the interference density I_o is the interference power normalized by BW. The gaussian model, with other cell interference represented by a factor, is used for cluster Erlang capacity. The probability of blocking [29]

$$P_b \approx Q\left[\frac{B - A\rho_\vartheta(1+f)\exp\left[\{\beta\sigma\}^2/2\right]}{A\rho_\vartheta(1+f)\exp\left[2\{\beta\sigma\}^2\right]}\right] \tag{2.29}$$

where A is offered Erlang capacity and $B = \frac{BW_T}{R}\left(1 - \frac{N_o}{I_o}\right)/\exp[\beta m]$ with $\beta = (\ln 10)/10$. Here $Q(k) = 1/\sqrt{2\pi}\int_k^\infty e^{-\lambda^2/2}d\lambda$. For a single sector $f = 0$ and with a $P_b = 1\%$ the offered Erlang capacity $A = 395$ using the gaussian model. This compares closely with the Erlang capacity of $A \approx 400$ that is obtained from Monte Carlo simulations and hence validates the gaussian model. Similar results were obtained with our C programs, for Monte Carlo simulations. Similarly for a cluster $f = 0.55$ and for $P_b = 2\%$; the offered Erlang capacity $A = 258$.

The gaussian pdf for the required $E_{b,k}/I_o$, used for Erlang capacity determination, is also obtained by simulation and analytical analysis for an IS-95 reverse link [3] and [60] operating at an $FER \approx 1\%$ with non-optimum power control. The link has a transmitter with a 64-ary modulator, a wideband channel and a correlation receiver with a modified delayed signature RAKE demodulator.

Kim/Prabhu [61] compare the capacity of forward link CDMA systems with a frequency reuse factor of unity to the capacity of two new systems with a frequency reuse factor of three and with cell splitting. Capacity is defined as the maximum

number of simultaneous users that can be supported for a required probability of outage, $P_{out} = P_r\left[E_b/I_o < E_b/I_o|_{req}\right]$, crieteria. Here E_b/I_o is the bit energy to interference density at the mobile and $E_b/I_o|_{req} = 7$ dB. The error rate performance is not evaluated and the Poisson call arrival rate is not used.

2.5.3 Voice over IP - G/D/S_T Queue

In these queuing systems, for voice over IP transmission, the packets interarrival times have a general pdf (Sec's. 2.4.4.1 through 2.4.4.4) and successive interarrival times are correlated. The packet service duration is deterministic or D ms. If the radio channel supports S_T simultaneous high bit rate bursts (or servers) at acceptable packet error rate, then all mobiles share usage of these S_T bursts that are coupled to a G/D/S_T virtual queue at the base station. In voice over IP wireless, voice capacity is the number of simultaneous voice users for a given packet expected wait times and probability of wait time outage. Here we provide analytical wait times for two queue models that are used for comparison purposes in chapters 7 and 8.

2.5.3.1 Expected Packet Wait Times - M/D/1 Queues

In this queuing system the packet interarrival times are exponential which is memoryless or a Markov processes. The packet expected interarrival times is $E[t]$ and for a one server or channel, the expected packet wait time at the queue

$$E[w] = \frac{\rho_1 D}{2(1-\rho_1)} \tag{2.30}$$

where the utilization factor $\rho_1 = D/E[t]$.

2.5.3.2 Expected Packet Wait Times - G/D/2 Queues

In this queuing system the packet interarrival times have a general pdf. For two servers or channels, with statistically independent interarrivals, the Kingman upper bound on the expected packet wait times at the queue

$$E[w] \leq \frac{Var[t] + (D^2/4)}{2E[t](1-\rho_2)} \tag{2.31}$$

where the expected packet interarrival times $E[t]$, the utilization factor $\rho_2 = D/2E[t]$ and the variance of packet interarrival times $Var[t]$.

2.5.3.3 DS-SS Wireless Link Voice over IP Capacity

For spread spectrum wireless voice over IP forward links [28], the base stations have a single queue and schedule packet transmission over a single high bit rate radio channel with an acceptable packet error rate. The expected packet wait times due to traffic induced queuing and radio retransmission was lumped together and obtained by using a modified M/D/1 queue. On the reverse link [28] each voice over IP user was assigned a high bit rate traffic channel for the duration of the call. The Erlang capacity was determined by modifying the Erlang B formula [29], [30] for the M/M/m queue. For the forward and reverse links the probability of outage was defined as 2% of the packet wait time being greater than a delay bound [28] of 70 ms. In chapters 7 and 8, the packet wait times first moment and probability of outage are derived for the G/D/S_T queue.

CHAPTER 3

MODIFIED ERLANG CAPACITY OF DS-SS REVERSE LINKS IMPAIRED BY RAYLEIGH FADING

Performance of direct sequence spread spectrum (DS-SS) BPSK systems that transmit rectangular chips and use correlation demodulators have been analyzed with error rate as a function of receiver output signal-to-noise-plus-interference ratio and in terms of energy per bit. We have presented a DS-SS BPSK demodulator with three branch maximal ratio combining that uses identical conventional theoretical transmit and receive filters. This receiver combats a non frequency selective mobile radio channel (with Rayleigh fading and uniform phase) asynchronous multiple access interference and additive white Gaussian noise. The unconditional error rate derived here is expressed in terms of per branch front end average signal-to-noise power ratio averaged over the Rayleigh fading, cross correlation functions and spreading factor. Using the direct analytical method for Erlang capacity of reverse links, presented here, the three branch receiver provides a 4 Erlangs increase in capacity or 5 dB diversity gain over the two branch receiver. Our grade of service (GOS) equals the probability of average frame error rate (FER) for all users being greater than a threshold, given a number of active users, is less than a blocking probability. This GOS is different from the existing GOS based on threshold interference-to-noise density ratio.

3.1 Introduction

DS-SS cellular systems for circuit voice and packet data services (e.g. email, www, etc.) have been deployed while Voice over IP and video telephony for enhanced

user experience are under development. As spectrum is expensive, radio transmission capacity improvements are desired for higher data rates, reduced latency and maximum number of users per carrier. The design of complicated receiver structures to combat frequency selective radio channel is one challenge.

Pursley [6] determines the error rate performance of a multiple access DS-SS BPSK system by assuming asynchronous multiple access interference is Gaussian. The transmitted signal for each user, which is data symbols spread by unique codes using rectangular chips, is perturbed by a radio channel with uniform delays and additive white Gaussian noise. The demodulator uses a correlator that integrates the product of the received signal and replica of the transmitted symbol waveform over one symbol interval. The error rate depends on the receiver output signal-to-noise-plus-interference ratio that is determined from the energy per bit, interference variance (obtained from the received signal power and continuous time partial cross correlation functions) and noise variance.

More recently Aalo [51] studied error rate performance of a multi cell CDMA system with DS-SS BPSK reverse links that use rectangular chips at the transmitter, has imperfect power control while the channel introduces shadow fading, frequency selective Rayleigh fading and path delays. The demodulator comprises of a RAKE receiver with correlators. The error rate, averaged over Rayleigh fading, is determined in terms of receiver output signal-to-noise-plus-interference ratio that depends on the energy per bit, multiple access with multipath induced interpath interference and noise variance.

In this chapter, the unconditional error rate for a three branch maximal ratio combining [42], [2] DS-SS BPSK receiver with conventional filtering is derived and expressed in terms of the per branch front end average signal-to-noise ratio. A single cell, non frequency selective channel [42], [43] (with Rayleigh fading and uniform

phase), accurate dynamic power control, coherent detection with no pilot and asynchronous multiple access interference is assumed. Three antennas are coupled to three receiver chains of the demodulator with weighted coherent downconverters and receive filters identical to the transmit filter. Optimal weights are derived (using Schwartz inequality [62]), to minimize error rate, in terms of the Rayleigh amplitudes, front end interference power, noise density and discrete partial cross correlation functions. Theoretical filters result in rectangular chip waveforms at the receive filter output, while the diversity signal waveforms are sampled, processed, combined at chip rates and finally an accumulator sends the baud rate discrete signal to a threshold detector. In practice [20], [43], a threshold detector can estimate the transmitted symbol from the received signal voltage corrupted by interference and Gaussian noise voltages. The conditional error rate is averaged over the Rayleigh vector representing branch amplitudes and unconditional error rate is expressed in terms of front end signal and interference power, that is derived from the received passband waveforms. Our intent is evaluation of the demodulator and it is understood that encoding and decoding would improve performance.

In CDMA IS-95, Viterbi's reverse link Erlang capacity [29] is average carried load (traffic in Erlangs) for a GOS. Viterbi's GOS equals the probability of interference to noise density being greater than 10 dB, given K active users, is less than 2%. To determine multiple access interference density, Viterbi assumes that each user's maximum likelihood detection rake receiver with matched filters requires an E_b/I_o (bit energy-to-interference density), that is a lognormal (with empirical moments), to achieve a FER $\approx 1\%$. In this chapter a direct method for reverse link carried Erlang capacity, that uses a GOS based on robust analytical techniques, is presented. This GOS equals the probability of average FER for all users being greater than 1%, given

K active users, is less than 2%. New calls are blocked when average FER is greater than 1% (or any other threshold).

For a non frequency selective channel the carried Erlang capacity for DS-SS BPSK reverse links with three and two branch maximal ratio combining receivers is 5.2 and 1.0 Erlangs respectively, at an FER = 1%. Increasing the number of users requires a higher average signal-to-noise power ratio (for all users) to maintain FER = 1%. However, as users increase and front end multiple access interference-to-noise power ratio exceeds a limit, increasing the desired signal's average power does not reduce the FER to 1%. This trend follows Viterbi's GOS for Erlang capacity of a IS-95 reverse link that uses 64-ary orthogonal modulation. Real CDMA systems use bandwidth limited chips [4] [52], that satisfy the Nyquist criteria and can use conventional transmit and recieve filters. The mobile radio channel is frequency selective and introduces signal distortion [19] which degrades capacity. Furthermore, receivers use various processing techniques to improve performance. Analytical techniques presented here have the potential of extension to systems using chips with raised cosine fourier functions, or to different DS-SS modulation schemes and evaluation of complicated receiver structures with many degradations.

3.2 Single Sector DS-SS Cellular System

Consider a single sector (or cell) with multiple users. A reverse link with mobile transmitter, radio channel and base station receiver is shown in Figures 3.1 and 3.2. At the transmitter, the symbol waveforms representing user data are spread with a

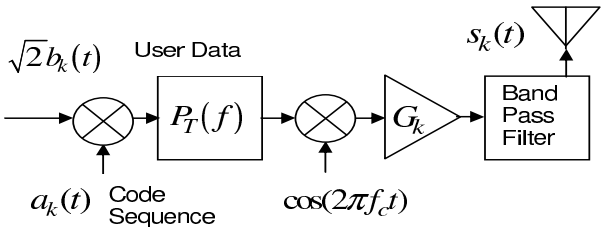

Figure 3.1. Mobile transmitter for user k.

unique periodic Gold sequence and a transmit filter is used for chip shaping prior to up-conversion. The overall transmitted waveform for user k is given by

$$s_k(t) = \sqrt{2} \sum_{l=-\infty}^{\infty} B_{k,l} b_{k,l} p_b(t - lT) \times \sum_{j=0}^{N-1} a_{k,j} p_T(t - jT_c - lT) \cos(2\pi f_o t + \theta_k) \tag{3.1}$$

where $B_{k,l}$ is a scalar multiplier, symbol $b_{k,l} = \pm 1$ represent the k^{th} user's equal probability digitized voice information (or binary digits) for baud index l with $p_b(t) = \Pi(t/T)$ as the symbol waveform and T is the symbol duration. The Gold code sequence has elements $a_{k,j} = \pm 1$, $p_T(t)$ is the transmit chip waveform with duration T_c, the sequence period $N = T/T_c$ is the spreading factor and θ_k is the carrier phase.

The n^{th} diversity mobile radio channel passband impulse response $h_k^{(n)}(t)$ for user k is is assumed to be non frequency selective or narrow band. For the k^{th} user, the n^{th} diversity channels baseband impulse response [42], [2], [43]

$$c_k^{(n)}(t) = L_k r_k^{(n)} \exp\left(-j\Theta_k^{(n)}\right) \delta\left(t - \tau_k^{(n)}\right), \tag{3.2}$$

where $L_k = \sqrt{\left[\mathcal{K}/d_{k,km}^{\gamma}\right] 10^{\zeta_k/10}}$ results in the local mean signal strength, depends on environment and shall be the same [43] for all diversity paths. The constant $\mathcal{K}$ depends on the antenna height and frequency, while $d_{k,km}$ is mobile to base station distance in km, γ is path loss exponent, ζ_k is normal random variable with $m_\zeta = 0\,\text{dB}$ and $\sigma_\zeta = 6$ to $13\,\text{dB}$. The Rayleigh amplitude $r_k^{(n)}$ has a probability density function

(pdf) $f(r) = (r/\sigma_r^2)\, e^{-r^2/2\sigma_r^2}, \quad r \geq 0$ that is normalized so that $2\sigma_r^2 = 1$. The random phase $\Theta_k^{(n)}$ is discussed later. While the delay $0 \leq \tau_k^{(n)} < T$ is assumed to be uniform or $f(\tau) = 1/T$. Although the local mean signal strength, Rayleigh amplitude, uniform delay and random phase are time varying, it is assumed that the channel is time invariant for a few baud intervals. For this analysis it is assumed that the amplitude $r_k^{(n)}$, phase $\Theta_k^{(n)}$ and delay $\tau_k^{(n)}$ for user k at the antenna are statistically independent [19]. It is also assumed that the amplitudes (and phases) at each diversity antenna are statistically independent for the same or any user. The equivalent baseband received signal $r_{BB,k}^{(n)}(t) = s_{BB,k}^{(n)}(t) \otimes c_k^{(n)}(t)$ where $s_{BB,k}^{(n)}(t)$ is the basedband transmitted signal, is used to derive the passband received signal [2].

We shall further assume local mean signal strength is maintained at a desired value by means of the dynamic power control gain $B_{k,l}^2 = \lambda_{k,l}^2 E_{k,l}^2 / L_k^2$ at the transmitter. Here $E_{k,l}^2 = 10^{\epsilon/10}$ [51], where ϵ is the power control error in decibels with $m_\epsilon = 0$ dB and $\sigma_\epsilon = 2.5$ *to* 3.0 dB. For ideal power control $E_{k,l}^2 = 1$ and the resulting gain or attenuation of the link for user k is $\lambda_{k,l}^2 = B_{k,l}^2 L_k^2$.

3.3 Receiver Structure and Error Rate

The two branch maximal ratio combining receiver (Figure 3.2) has two diversity antennas (or $n = 2$), with adequate spatial separation, coupled to two receiver chains. The demodulator receive filters are identical to the transmit filter and the chip waveform at receive filter output is rectangular.

3.3.1 Demodulator with Conventional Filters

The k^{th} users, n^{th} diversity received passband signal and additive white Gaussian noise

$$r_{R,k}^{(n)}(t) = \sqrt{2}\, r_k^{(n)} \sum_{l=-\infty}^{\infty} \lambda_{k,l} b_{k,l} p_b \left(t - lT - \tau_k^{(n)}\right)$$
$$\times \sum_{j=0}^{N-1} a_{k,j} p_T \left(t - jT_c - lT - \tau_k^{(n)}\right) \cos\left(2\pi f_o t + \phi_k^{(n)}\right)$$
$$+ n^{(n)}(t); \qquad n = 1, 2. \tag{3.3}$$

Here the uniform phase $\phi_k^{(n)} = \theta_k - \Theta_k^{(n)}$, where $0 < \phi_k^{(n)} \leq 2\pi$ has pdf $f(\phi_k) = 1/2\pi$. The zero mean additive white Gaussian noise $n^{(n)}(t) = n_c^{(n)}(t)\cos(2\pi f_o t) + n_s^{(n)}(t)\sin(2\pi f_o t)$ has two-sided power spectral density $N_0/2$ (W/Hz). The overall n^{th} diversity received signal

$$r_R^{(n)}(t) = \sum_{k=1}^{K} \sqrt{2}\, r_k^{(n)} \sum_{l=-\infty}^{\infty} \lambda_{k,l} b_{k,l} p_b \left(t - lT - \tau_k^{(n)}\right)$$
$$\times \sum_{j=0}^{N-1} a_{k,j} p_T \left(t - jT_c - lT - \tau_k^{(n)}\right) \cos\left(2\pi f_o t + \phi_k^{(n)}\right)$$
$$+ n^{(n)}(t); \qquad n = 1, 2. \tag{3.4}$$

At each receiver chain, the desired signal for user i is coherently down-converted with adequate weights $A_i^{(n)}$ and baud index $l = 0$ is used to derive error rate performance. In real CDMA systems the mobile also transmits a pilot, that is used by the receiver to estimate the phase and amplitude of the recieved signal. As the relative phase shifts are modulo 2π and relative time delays are modulo T, at the receiver chain $\phi_i^{(n)} = 0$ and $\tau_i^{(n)} = 0$. The n^{th} receiver chain's filtered signal for user i , $r_F^{(n)}(t) = \left[r_R^{(n)}(t) \times A_i^{(n)} \cos(2\pi f_o t)\right] \otimes p_R(t)$ with $K - 1$ interferers is

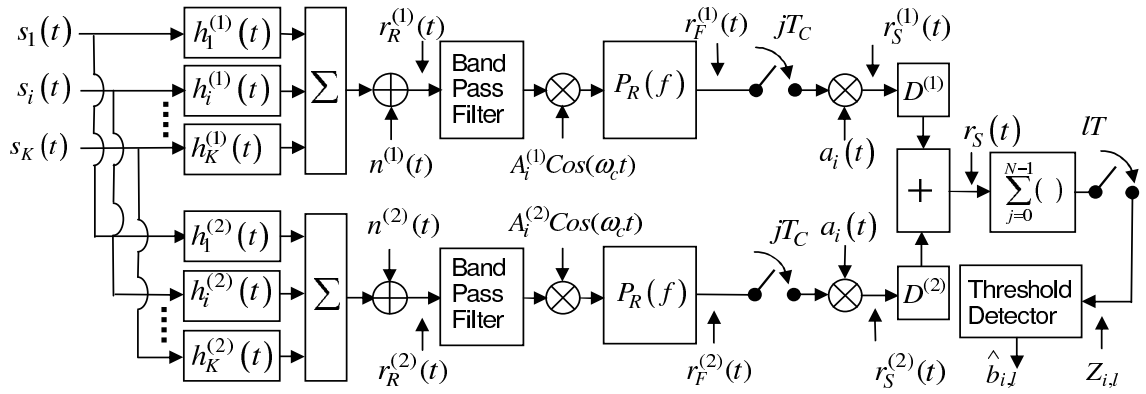

Figure 3.2. Maximal ratio combining receiver with conventional filters..

$$
\begin{aligned}
r_F^{(n)}(t) &= \sqrt{\frac{1}{2}}\, r_i^{(n)} A_i^{(n)} \lambda_{i,l} b_{i,0} p_b(t) \sum_{j=0}^{N-1} a_{i,j} p(t - jT_c) \\
&+ \left[\sum_{\substack{k=1 \\ k \neq i}}^{K} \sqrt{\frac{1}{2}}\, r_k^{(n)} A_i^{(n)} \cos\left(\phi_k^{(n)}\right) \lambda_{k,l} \times \right. \\
&\left\{ b_{k,-1} p_b\left(t + T - \tau_k^{(n)}\right) \sum_{j=0}^{N-1} a_{k,j} p(t - jT_c + T - \tau_k^{(n)}) \right. \\
&\left. \left. + b_{k,0} p_b\left(t - \tau_k^{(n)}\right) \sum_{j=0}^{N-1} a_{k,j} p(t - jT_c - \tau_k^{(n)}) \right\} \right] \\
&+ g_F^{(n)}(t); \qquad\qquad n = 1, 2
\end{aligned}
\tag{3.5}
$$

where filtered noise $g_F^{(n)}(t) = (A_i^{(n)}/2) n_c^{(n)}(t) \otimes p_R(t)$ is Gaussian. The chip $p(t) = \Pi\left[\frac{t - T_c/2}{T_c}\right]$ with characteristic $P(f) = T_c \mathrm{sinc}(fT_c) e^{-j2\pi f T_c/2}$, where $P_T(f) = P_R(f) = |P(f)|^{1/2} \exp\left[ArgP(f)/2\right]$ are theoretical filters. In this chapter theoretical filters are assumed in order to simplify correlation functions. The filter output is sampled at the chip rate, multiplied by the i^{th} users discrete Gold code $a_i(t) = \sum_{l=-\infty}^{\infty} \sum_{j=0}^{N-1} a_{i,j} \delta(t - jT_c - lT)$ where $\delta(t)$ is the unit impulse and this results in the discrete signal $r_S^{(n)}(t) = r_F^{(n)}(t) \times a_i(t)$. For synchronous combining, the diversity signal's $r_S^{(n)}(t)$ are time aligned by ideal delay's $D^{(n)}$. The ideal combiner's signal, $r_S(t) = \sum_{n=1}^{2} r_S^{(n)}(t)$, is fed

to a chip summer, whose output signal $Z_{i,l} = SUM\left[r_S(t)\right]_{\text{Over Period N}}$. The $SUM[.]$ function accepts chip rate samples and adds $N-1$ samples for a specific baud. Every T sec, the discrete voltage $Z_{i,l}$ is sent to the threshold detector and the chip summer is reset. The discrete decision variable for baud index $l = 0$,

$$\begin{aligned} Z_{i,0} &= \sum_{n=1}^{2} \sqrt{\frac{1}{2}}\, r_i^{(n)} A_i^{(n)} \lambda_i b_{i,0} N \\ &+ \sum_{\substack{k=1 \\ k\neq i}}^{K} \sum_{n=1}^{2} \sqrt{\frac{1}{2}}\, r_k^{(n)} A_i^{(n)} \cos\left(\phi_k^{(n)}\right) \lambda_k \left\{ b_{k,-1} R_{k,i}\left(\tau_k^{(n)}\right) \right. \\ &\qquad \left. + b_{k,0} \hat{R}_{k,i}\left(\tau_k^{(n)}\right) \right\} + \sum_{n=1}^{2} \sum_{j=0}^{N-1} g_F^{(n)}(jT_c). \end{aligned} \tag{3.6}$$

The voltage $Z_{i,0} = A_S b_{i,0} + A_I + g_T$, where $A_S b_{i,0}$ is the desired signal, A_I is multiple access interference due to $K-1$ users and g_T is total Gaussian noise. As the channel is invariant over several baud intervals $\lambda_{k,l} = \lambda_k$. The autocorrelation function

$$R_{i,i}(0) \;= \sum_{j=0}^{N-1} a_{i,j} a_{i,j} p(0T_c) = N \tag{3.7}$$

where $p(0T_c) = 1$.

Pursley [6] defines continuous time partial cross correlation functions while the discrete partial cross correlation functions for our receiver are

$$R_{k,i}\left(\tau_k^{(n)}\right) = \begin{cases} 0 & \tau_k^{(n)} = 0 \\ \sum\limits_{j=0}^{U-1} a_{k,j-U} a_{i,j} p\left(\Delta T_c\right) & 0 < \tau_k^{(n)} \leq T \end{cases}$$

$$\hat{R}_{k,i}\left(\tau_k^{(n)}\right) = \begin{cases} \sum\limits_{j=0}^{N-1} a_{k,j} a_{i,j} p(0) & \tau_k^{(n)} = 0 \\ \sum\limits_{j=U}^{N-1} a_{k,j-U} a_{i,j} p\left(\Delta T_c\right) & 0 < \tau_k^{(n)} \leq T. \end{cases} \tag{3.8}$$

These functions depends on chip number $U = 1, 2, \cdots, N$, such that $(U-1)T_c < \tau_{k,1}^{(n)} \leq UT_c$. Within the chip interval $\tau_k^{(n)} = (U-\Delta)T_c, \quad 0 \leq \Delta < 1$ and we use $B_{-l} = B_{N-l}$.

3.3.2 Optimum Weights for Error Rate Minimization

At the receiver a threshold detector is used and if $b_{i,0} = -1$ was transmitted then an error is made if $Z_{i,0} > 0$. As the symbols $b_{i,0} = \pm 1$ have equal apriori probabilities, the conditional error rate [6], [43]

$$\begin{aligned} P_e[\,|\,\mathbf{r_i^{(n)}}] &= 1/2\,\Pr[Z_{i,0} > 0\,|\,b_{i,0} = -1] \\ &\quad +1/2\,\Pr[Z_{i,0} < 0\,|\,b_{i,0} = +1] \\ &= \frac{1}{2}\mathrm{erfc}\left(\sqrt{\frac{A_S^2}{2\sigma_G^2}}\right) \end{aligned} \tag{3.9}$$

where it is assumed that $G = A_I + g_T$ is Gaussian random variable $G(m_G, \sigma_G)$. Here $\mathbf{r_i^{(n)}}$ is the vector of diversity Rayleigh fading random variables. It can be proved that

$$\frac{A_S^2}{2\sigma_G^2} = \frac{\lambda^2 N^2}{4}\left[\sum_{n=1}^{2} r_i^{(n)} A_i^{(n)}\right]^2 \Big/ \left[\sum_{n=1}^{2}\left\{A_i^{(n)}\right\}^2 I\right]. \tag{3.10}$$

Using statistical techniques it can be shown that $m_G = 0$ and $\sigma_G^2 = \sum_{n=1}^{2}\left\{A_i^{(n)}\right\}^2 I$ where

$$I = \frac{2\sigma_r^2\lambda^2}{4}\sum_{\substack{k=1\\k\neq i}}^{K}\left\{E\left[R_{k,i}^2(\tau_k)\right] + E\left[\hat{R}_{k,i}^2(\tau_k)\right]\right\} + \frac{NN_0}{4} \tag{3.11}$$

as $\phi_k^{(1)}$, $\phi_k^{(2)}$ and $\phi_p^{(1)}$ (where $k \neq p$) etc. are statistically independent, the symbols $b_{k,l}$ for different baud indices are statistically independent while at both receiver chains the expectation of square of partial cross correlation functions is the same for an interferer. It is assumed that λ^2 is fixed for a given number of users and shall be the same for all users. The noise variance $E\left[\left\{g_F^{(n)}(t)\right\}^2\right] = \left\{A_i^{(n)}\right\}^2 N_0/4$ where the power spectral density of $n_c(t)$ is N_0(W). At the diversity antennas the Rayleigh fading and phase are statistically independent which makes the Gaussian multiple access interference at each receiver chain uncorrelated. Hence the interference variance at the demodulator output is the sum of the interference variance for each receiver chain.

To minimize error rate, maximal ratio combining [62] maximizes the signal voltage and minimizes the standard deviation of noise plus multiple access interference. Hence to maximize $A_S^2/2\sigma_G^2$, the optimum down-converter weights

$$A_i^{(n)} = \frac{r_i^{(n)}}{I}, \tag{3.12}$$

where I, defined in Eq. 3.11, can be related to the per branch average received signal power, averaged over the Rayleigh fading $\mathcal{P}_k$ (Eq. 3.23) or

$$I = \frac{\mathcal{P}_k T_c}{4} \sum_{\substack{k=1 \\ k \neq i}}^{K} \left\{ E\left[R_{k,i}^2(\tau_k)\right] + E\left[\hat{R}_{k,i}^2(\tau_k)\right] \right\} + \frac{NN_0}{4} \tag{3.13}$$

and hence the conditional error rate

$$P_e\left[\left|\mathbf{r_i^{(n)}}\right.\right] = \frac{1}{2}\text{erfc}\left[\sqrt{\frac{\lambda^2 N^2}{4} \sum_{n=1}^{2} \frac{\left\{r_i^{(n)}\right\}^2}{I}}\right]. \tag{3.14}$$

By statistical averaging [63] [64], the unconditional error rate for a two branch maximal ratio combining receiver

$$P_e = \frac{1}{2} - \frac{1}{4} \frac{\sqrt{\eta}\,[3 + 2\eta]}{[1+\eta]^{3/2}} \tag{3.15}$$

where $\eta = 2\sigma_r^2 \lambda^2 N^2 / 4I$ is in terms of the demodulator output signal square and total interference plus noise variance. In terms of per branch average received signal power, averaged over the Rayleigh fading $\mathcal{P}_k$ (Eq. 3.23), it can be shown that

$$\eta = \frac{\mathcal{P}_k N^2}{\mathcal{P}_k \sum_{\substack{k=1 \\ k \neq i}}^{K} \left\{ E\left[R_{k,i}^2(\tau_k)\right] + E\left[\hat{R}_{k,i}^2(\tau_k)\right] \right\} + NN_0 \frac{1}{T_c}}. \tag{3.16}$$

Similarly for three branch receiver the unconditional error rate

$$P_e = \frac{1}{2} - \frac{1}{16} \frac{\sqrt{\eta}\,[15 + 20\eta + 8\eta^2]}{[1+\eta]^{5/2}}. \tag{3.17}$$

3.4 Signal to Noice Power Ratio

For receiver design and comparison purposes the threshold average signal-to-noise ratio, before the receive passband filter, that results in a threshold error rate performance $P_{e,th}$ for a given number of users is required. At the threshold detector's input the desired i^{th} user's signal voltage and interferer's voltage are directly proportional to $\lambda_{i,l}$ and $\lambda_{k,l}$ respectively as the chip waveform at the sampling instant is normalized to unity. This local mean signal strength $\lambda_{k,l}$ is related to the average received power. With ideal power control, the required average received power for all user's would be equal. Assuming chips limited to T_c, for user i the average received signal power [43] (for a 1-ohm impedence), averaged over the Rayleigh fading,

$$\mathcal{P}_i = E\left[\lim_{\Omega\to\infty}\frac{1}{2\Omega T_c}\int_{-\Omega T_c}^{\Omega T_c}\left\{r_{R,i}^{(n)}(t)\right\}^2 dt\right]_{r_i^{(n)},b_{i,l}} \tag{3.18}$$

is before the receive passband filter. The integer $\Omega >> N$, hence we truncate the received signal for mathematical convenience. Here the user i's received signal,

$$\begin{aligned} r_{R,i}^{(n)}(t) = \sqrt{2}\, r_i^{(n)} &\sum_{l=-\Omega/N}^{\Omega/N}\lambda_{i,l}b_{i,l}p_b\left(t-lT\right) \\ &\times\sum_{j=0}^{N-1}a_{i,j}p_T\left(t-jT_c-lT\right)\cos\left(2\pi f_o t\right). \end{aligned} \tag{3.19}$$

As statistical averaging and integration are linear and interchangeable

$$\mathcal{P}_i = \lim_{\Omega\to\infty}\frac{1}{2\Omega T_c}\int_{-\Omega T_c}^{\Omega T_c}E\left[\left\{r_{R,i}^{(n)}(t)\right\}^2\right]_{r_i^{(n)},b_{i,l}} dt \tag{3.20}$$

As the chips do not overlap in time,

$$\begin{aligned} E\left[\left\{r_{R,i}^{(n)}(t)\right\}^2\right]_{r_i^{(n)},b_{i,l}} &= 2E\left[\left\{r_i^{(n)}\right\}^2\right]\lambda_i^2 \\ \times\sum_{l=-\Omega/N}^{\Omega/N}E\left[b_{i,l}^2\right]&\sum_{j=0}^{N-1}p_T^2\left(t-jT_c-lT\right)\cos^2\left(2\pi f_o t\right). \end{aligned} \tag{3.21}$$

In this case for a fixed number of users, $\lambda_{i,l} = \lambda_i$. As summation and integration are interchangeable linear operations,

$$\mathcal{P}_i = \lim_{\Omega\to\infty} \frac{2\sigma_r^2\lambda_i^2}{\Omega T_c} \times \sum_{l=-\Omega/N}^{\Omega/N} \sum_{j=0}^{N-1} \int_{-\Omega T_c}^{\Omega T_c} p_T^2(t)\cos^2(2\pi f_o t)\, dt. \tag{3.22}$$

Using mathematical limits and Rayleigh's energy theorem,

$$\mathcal{P}_i = 2\sigma_r^2 \frac{\lambda^2}{T_c} \int_{-\infty}^{\infty} |P_T(f)|^2\, df = 2\sigma_r^2 \mathcal{P}_{R,i} \tag{3.23}$$

where $\mathcal{P}_{R,i} = \lambda^2/T_c$ is average power. For ideal power control, considered here, $\mathcal{P}_{R,i}$ shall not fluctuate for a fixed number of users and shall be the same for all users. As calls are initiated (within Erlang capacity limits) in the sector the required $\mathcal{P}_{R,i}$, for all users, increases to attain the desired $P_{e,th}$. The per branch front end average signal-to-noise power ratio, averaged over the Rayleigh fading, before the receiver's band pass filter

$$\rho = \frac{\mathcal{P}_i}{No/T_c} = \frac{2\sigma_r^2\mathcal{P}_{R,i}}{No/T_c}, \tag{3.24}$$

where No/T_c is the front end thermal noise power in the Nyquist band. Similarly, for a threshold error rate performance the front end average interference-to-noise power ratio, averaged over Rayleigh fading, is $(K-1)\,\mathcal{P}_i/\left[No/T_c\right]$.

3.5 Single Sector Erlang Capacity

To obtain Erlang capacity of multiple access DS-SS reverse links, the GOS presented and used here is blocking probability

$$P_b = \Pr\ [\text{Average FER over all users } > 1\%|K \text{ users}] \tag{3.25}$$

where FER $= 1 - \left[\{1 - P_e\}^{N_S}\right]$ and N_S is number of symbols / frame. This definition of GOS depends directly on a threshold FER or error rate while Viterbi's GOS or the blocking probability,

$$P_b = \Pr\ [\text{Interference to Noise Density} > 10\,\text{dB}|K\ \text{users}]\,. \tag{3.26}$$

Assuming the blocked calls held model [42], [29], $P_b = \sum_{k=K}^{\infty} \left(A^k/k!\right) e^{-A}$. which is the sum of a Poisson distribution tails, when the K^{th} user causes unacceptable FER. Offered load A is mean number of call arrivals per call hold time. The probability of k active users $p_k = \left(A^k/k!\right) e^{-A}$ is Poisson. The carried traffic $A_c = A\,[1 - P_b]$.

3.6 Numerical Results

For the two receiver structures carried Erlang capacity is determined (Table 3.1). Two primitive polynomials of degree $m = 7$ with octal representations 211E and 217E are used for preferred maximum-length sequences that generate [2] Gold codes with period $N = 2^m - 1 = 127$. The two maximum-length sequences are generated by simple shift register generators (SSRG) with feedback connections specified by the polynomials. Although $129\,(2^m + 1)$ unique Gold codes can be generated by the modulo-2 sum of SSRG outputs, only 2 Gold codes are used as equal multiple access interference for all users is assumed. The cross correlation and off-peak autocorrelation functions are three valued $\{-1, -17, 15\}$. The bit rate $R_b = 9.6$ kb / sec, $T_c = 8.2 \times 10^{-07}$ sec, $N_S = 192$, front end noise figure $F = 5$ dB and $No = 4 \times 10^{-21}$ W/Hz.

The statistical average of the squared partial cross correlation functions (Eq. 3.8), obtained by simulation, are used to calculate interference variance. All other numerical results (Table 3.1) and the signal-to-noise ratio ρ verses error rate P_e curves (Figure 3.3) are obtained directly from the analytical functions.

Table 3.1. Carried Erlang capacity of 2 and 3 branch receiver

Parameter	*2 branch*	*2 branch*	*3 branch*	*3 branch*
Number of Users K	3	4	10	11
RF Power (dBm) $\mathcal{P}_{R,i}$	-103	-100	-107.7	-100.5
Signal to Noise Ratio (dB) ρ	10.1	12.7	5.4	12.7
Signal Power / (Noise + Interference power) (dB)	-3.2	-4.8	-9.7	-10.0
Interference Power / Noise Power (dB)	13.1	17.4	14.9	22.7
Interference Variance / Noise Variance (dB)	7.9	12.2	9.7	17.4
Error Rate P_e	5×10^{-5}	1×10^{-4}	5×10^{-5}	5.6×10^{-5}
FER (%)	1.0	1.9	1.0	1.1
Carried Erlangs A_c	1.0	1.5	5.2	5.9

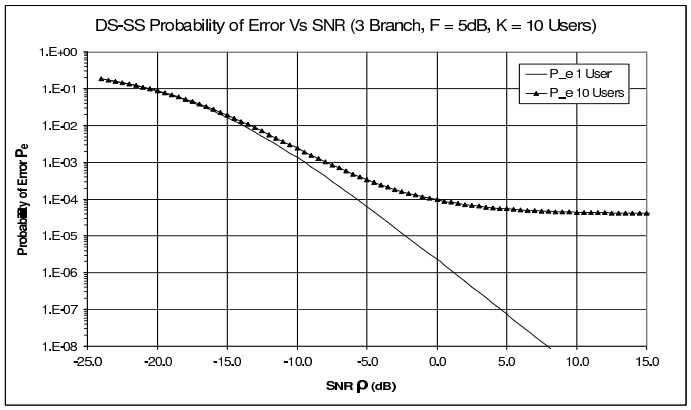

Figure 3.3. Signal-to-noise power ratio verses error rate for 1 and 10 Users.

3.7 Conclusions

For rectangular chips Pursley [6] and Aalo [51] have analyzed DS-BPSK receivers with correlator demodulators and obtain error rate as a function of receiver output signal-to-noise-plus-interference ratio and in terms of the energy per bit. We have presented and analyzed a DS-SS BPSK demodulator with three branch maximal ratio combining that uses conventional theoretical receive filters which are identical to the transmit filter and preserve temporal structure of the rectangular chip waveform

at its output. This receiver combats a non frequency selective mobile radio channel (with Rayleigh fading and uniform phase) asynchronous multiple access interference and additive white Gaussian noise. Output diversity waveforms are sampled at chip rates, multiplied by the user code, diversity combined and after the discrete samples are despread the baud rate desired signal voltage corrupted by noise plus interference voltages is sent to a threshold detector. Discrete autocorrelation of the user's signature code and the discrete partial cross correlation of the user and interferer's signature codes are derived from the chip waveform. Demodulator branch weights, derived to minimize error rate, are a function of the desired signal's per branch Rayleigh fading amplitude, front end average interference power, cross correlation functions and spreading factor. The unconditional error rate (Eq.'s 3.15 and 3.17) of a two and three branch maximal ratio combining receiver, is expressed in terms of per branch front end average signal-to-noise power ratio, cross correlation function and spreading factor. For average signal-to-noise ratio (Eq. 3.24) at the bandpass filter input, the per branch average received power averaged over the Rayleigh fading is derived (Eq. 3.20). The direct analytical method (Eq. 3.25) for Erlang capacity of DS-SS reverse links, presented here is used to compare the receiver structures. Here the GOS equals the probability of average FER for all users being greater than 1%, given K active users, is less than 2%. New calls are blocked when average FER for all users is greater than 1% (or any other threshold) instead of using the a threshold interference-to-noise density as used by Viterbi [29].

The carried Erlang capacity (at $P_b = 2\%$) of three and two branch maximal ratio combining receiver's are 5.2 and 1.0 Erlangs respectively. The three branch receiver provides a 5 dB diversity gain over the two branch receiver that results in a 4 Erlang increase in capacity. As new calls are setup a higher average signal-to-noise power ratio (for all users) to maintain FER = 1% is required. As new calls are setup

and the front end per branch multiple access interference-to-noise power ratio exceeds 14.7 dB (or 13.1 dB), for the three (or two) branch receiver, increasing the desired signal's average power does not reduce the FER to 1%. This trend follows Viterbi's GOS recommedation, where interference-to-noise density greater than 10 dB results in blocking. Our analysis shows that higher interference-to-noise power ratios can be tolerated by the reciever to acheive an FER = 1%. Some of the difference between ours and Viterbi's results is because Viterbi analyzes a different modulation, detector and includes power control errors, other cell interference and voice activity factors. Furthermore, this analysis proves that FER = 1% when the front end interference-to-noise power ratio is 14.9 dB (or 13.1 dB). In Viterbi's [29] analysis it is assumed that an interference-to-noise density equal to 10 dB results in FER $\approx$ 1%. The error rate performance of our one branch receiver with conventional filters and the correlation receiver [6] is similar, for the same channel, received power and number of users. Negligible difference is due to discrete de-spreading function. Error rate performance differences between our three branch receiver and Aolo's [51] three branch RAKE receiver with correlators is because we do not consider power control errors, multipath induced interpath interference and other cell interference. Analytical techniques introduced here are being extended to determine Erlang capacity of more complicated receiver's for systems with chips that have raised cosine characteristics.

CHAPTER 4

SOME CONSIDERATIONS OF DS-SS BPSK SPECTRAL DENSITY AND ERROR RATE OF A HIGH BIT RATE RAKE

As cellular technologies evolve, evaluation of modulation schemes with frequency selective fading is an important consideration. We present methods to evaluate a high data rate DS-SS BPSK reverse link, over a wideband channel, with filters and a modified delayed signature dual finger RAKE. For several years the standard Gaussian approximation has been used to estimate error rate of DS-SS BPSK. We derive simple upper and lower bounds on the conditional error rates. The upper bound is in terms of the error rate obtained with two intersymbol interference terms and bounds on the marginal distribution of the smaller terms. The Gaussian approximation error rate is pessimistic for SNR's greater than 8dB and 12dB when compared to that obtained by the total probability theorem and upper bound respectively. Intersymbol interference is not Gaussian and at high front end signal-to-noise ratio's (SNR's) our error rate bound is a better estimate. We have also derived the bandwidth occupancy in a rigorous way for the first time by developing a method to compute the spectral density. The fractional containment bandwidth with two Gold codes is smaller than that with a PN sequence. The spectral density has no discrete lines while it is a function of the signature coefficients and chip Fourier transform. Within the bandwidth the spectral density of a set of frequencies is 15dB greater than at other frequencies and this set varies from signature to signature. Finally, we show that a modified delayed signature RAKE combats multipath interference. These methods can be used and to select signatures that minimize adjacent and co-channel interference.

In Chapter 5 we evaluate a dual space diversity four finger RAKE by using these methods. We show that this receiver provides an 8 dB diversity gain in Chapter 5.

4.1 Introduction

DS-SS cellular systems for packet data, Voice over IP and video services with higher data rates and reduced latency are evolving. Evaluation of spectral efficiency and capacity of transmission schemes that combat frequency selectivity are main challenges. This requires determination of error rate, operating SNR and bandwidth where the last two are obtained from the spectral density. Spectral density is also used to assess adjacent and co-channel interference impacts.

For DS-SS BPSK over wideband channels, the delayed signal [1]-[2], original delayed signature and modified [3] delayed signature RAKE demodulator structures can be used. The first RAKE mitigates intersymbol interference and the second retains coherent intersymbol interference in DS-SS FSK [1]. For one user, the desired symbol at the RAKE output is corrupted by correlated Gaussian noise and multipath [5] interference. Over the years the standard Gaussian approximation error rate [6] was extended [7], [8] by assuming that multipath interference is Gaussian. The approximation is good [7] for a single branch receiver with a 31 rectangular chip signature. In the low data rate RAKE system [8] with a 127 rectangular chip signature, two intersymbol interference terms were considered. For high bit rates with up to 8 chip signatures, error rate was determined by simulation [9], [10]. For a single branch receiver at 10^{-3} error rate, intersymbol interference degrades [9] the required SNR by 4dB.

It is established [2], [11] that the spectral density of a linear digital modulated signal is obtained by the Fourier transform of its autocorrelation function. First the ensemble autocorrelation function is obtained assuming that the information sequence

is wide sense stationary. Next the time variable of the periodic autocorrelation function, is eliminated by averaging over time. The spectral density is the product of the pulse Fourier transform magnitude square and the Fourier transform of the information autocorrelation sequence. Various methods have been developed for the spectral density of GMSK [12] and DS-SS signals [13], [14], [15]. The spectral density [13], of a periodic PN sequence with shaped chips was determined from the discrete Fourier transform of the signatures temporal autocorrelation sequence. In [14] the spectral density for a DS-SS BPSK signal, with discrete lines, was obtained by expressing it as a linear digital modulated signal and direct use of its density [2]. It was assumed [14] that the product of information and signature sequences results in a wide sense stationary chip rate sequence. For DS-SS BPSK with Gold or PN sequences this assumption [14] of wide sense stationarity is not theoretically feasible. The spectral density of DS-SS BPSK signal with rectangular chips was determined [15] by assuming the information sequence has a random delay uniformly distributed over the baud. The PN sequence ensemble autocorrelation sequence is used by assuming [15] the signature has statistical properties like the information sequence and random pulse train. In CDMA [4] mobiles are synchronized to base stations that are synchronized to GPS and the mobile signal has small delay shifts. A PN sequence is not truly random unless it has infinite length. The models used in references [14] and [15] are not consistent with real applications. Hence, there is no accurate analytical expression for spectral density of DS-SS BPSK with deterministic signatures and small spreading factors.

In this chapter [16] a high data rate DS-SS BPSK reverse link, with a 7 chip signature and chips with raised-cosine characteristics, is analyzed. The receiver has an original or modified delayed signature two finger RAKE demodulator. We assume

the baud interval is similar to the channel delays [18], [19] and the chip extends up to ± 7 chip intervals that results in four incoherent intersymbol interference terms.

We calculate the error rate for a given channel using the total probability theorem, standard Gaussian approximation and bounds [20], [21] in the presence of Gaussian noise and intersymbol interference. Upper bounds on error rate are derived using the Chernoff and Prabhu bounds while a lower bound is derived using Jensen's inequality. The latter upper bound is expressed in terms of the error rate with two intersymbol interference terms and bounds on the marginal distribution of the smaller terms. In the case of bounds the true statistics of intersymbol interference is used instead of assuming it to be Gaussian. The unconditional error rate is obtained by Monte Carlo simulation over channel parameters and all methods are compared. The Gaussian approximation error rate is pessimistic for SNR's $>$ 8dB and 12dB when compared to that obtained by the total probability theorem and Prabhu bound respectively. The upper bound on error rate obtained from the Prabhu bound is much tighter than that obtained by the Chernoff bound. High SNR conditions can exist when the mobile power cannot be reduced further by power control. It is understood that diversity reception with channel coding would improve this operating SNR. Upper and lower bounds show that the modified delayed signature RAKE effectively combats incoherent intersymbol interference. While the original structure has severe error rate degradation due to coherent intersymbol interference. This analysis can be extended to consider design of a dual space diversity four finger RAKE, the impact of changing filter rolloff factors and signatures.

The main difference between this study and previous work is that we use the true statistics of intersymbol interference instead of assuming it is Gaussian. The Gaussian approximation may work for low data rate systems [7], [8], however, more accurate methods are required for high data rate links. We use analytical techniques

while [9], [10] use simulation. We consider chips that extend up to ± 7 chip intervals and four intersymbol interference terms while [8] considers rectangular chips and two intersymbol interference terms. In [9] intersymbol interference causes error rate degradation while we show minimum degradation.

In this chapter we derive an accurate analytical expression for the spectral density of a DS-SS BPSK signal with Gold and PN sequences. We show that the signal can be expressed mathematically as a linear digital modulated waveform that enables [22] determination of its spectral density. In our case, one signature period with chips that have square-root raised-cosine characteristics results in a unique signaling pulse. The information sequence is assumed to be wide sense stationary as is conventionally done. We directly utilize the spectral density of [2], [11] by deriving the Fourier transform of this unique baud rate signaling pulse along with the ensemble autocorrelation sequence of the information. The spectral density is a function of the chip Fourier transform, the signature coefficients and autocorrelation sequence of the information. We compute the spectral density and fractional containment bandwidth for different sequences and filter rolloffs. Finally, for front end SNR, we derive the received signal power from the spectral density and average it over the channel.

Our spectral density derivation is different from previous work [14], [15] in several ways. We correctly use wide sense stationarity for the information sequence and do not randomize the delay of the information sequence. We treat the signature sequence as deterministic instead of a random signal. Our spectral density does not have spectral lines like the spectral density in Eq. 8 of [14]. Also the measured spectral density in Fig. 3.32 of [23] does not have spectral lines. Our spectral density is a function of the signature coefficients, while the spectral density in Eq. 21 of [15] is a function of the periodic auto-correlation function.

4.2 System Description

Consider the single sector reverse link in Fig. 4.1 with a transmitter, channel and dual finger RAKE receiver.

4.2.1 DS-SS BPSK Transmitter

The transmit signal

$$s(t) = \sqrt{2} \sum_{l=-\infty}^{\infty} B_l b_l \sum_{u=0}^{N-1} a_u p_T(t - uT_c - lT) \cos(2\pi f_o t + \theta) \tag{4.1}$$

where ideal power control gain $B_l^2 = \lambda^2/L^2$, information symbols $b_l = \pm 1$ for baud index l are equi-probable with duration T. The Gold sequence with period $N = T/T_c$ has elements $a_u = \pm 1$ and chip $p_T(t)$ with square-root raised-cosine characteristic, is transmitted every T_c sec with carrier phase θ. In CDMA systems, $T_c = 0.82\,\mu$sec and bandwidth ≈ 1.536 MHz is greater than coherence bandwidth [4], [43]. For high bit rates, with $T_c = 0.82\,\mu$sec, we assume $R_b = 174.2$ and 39.4 kb/ sec for $N = 7$ and 31 respectively.

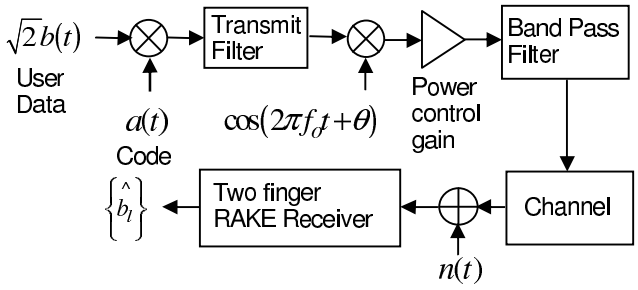

Figure 4.1. The reverse link with wideband channel and zero mean additive white Gaussian noise $n(t)$ which has two-sided spectral density $N_o'/2$ where $N_o' = 4 \times 10^{-21}$ W/Hz. .

4.2.2 Wideband Channel

The baseband channel impulse response [2], [19], [18],

$$c(t) = L \sum_{g=1}^{2} r_g \exp\left(-j\Theta_g\right) \delta\left(t - \tau_g\right) \tag{4.2}$$

is invariant over a few bauds, where L represents propagation path loss and shadowing. We assume Rayleigh amplitude r_g, phase Θ_g and delay τ_g are statistically independent [19]. The probability density function (pdf) of r_g is normalized with $2\sigma_r^2 = 1$. We assume that $\tau_1 = 0$ and τ_2 is uniformly distributed between $2T_c$ and $6T_c$.

4.2.3 Modified Delayed Signature Dual Finger RAKE

The demodulator in Fig. 4.2 has optimal adaptive finger weights and oscillator phase. For this structure delay 1 and 2 are equal to τ_2 and 0 respectively. At the receive filter output chip, $p(t)$ has raised-cosine characteristic with $p(0) = 1$. The discrete voltage for $l = 0$,

$$Z_0 = A_S b_0 + \gamma_0 b_0 + \sum_{l=-2}^{2}{}' \varsigma_l b_l + n_T, \tag{4.3}$$

where $\sum_{l}{}'$ excludes $l = 0$. The desired signals amplitude

$$A_S = \frac{\lambda}{\sqrt{2}} \sum_{g=1}^{2} r_g^2 \sum_{u=0}^{N-1} a_u^2. \tag{4.4}$$

The amplitude of interpath interference

$$\gamma_0 = \frac{\lambda Y}{\sqrt{2}} \left[R_0\left(\tau_2\right) + R_0\left(-\tau_2\right)\right], \tag{4.5}$$

and the pre and post-cursor symbol interference amplitude

$$\varsigma_l = \frac{\lambda Y}{\sqrt{2}} \left[R_l\left(\tau_2\right) + R_l\left(-\tau_2\right)\right]. \tag{4.6}$$

Here Laplacian $Y = r_1 r_2 \cos(\phi_2 - \phi_1)$ and uniform phase $\phi_g = \theta - \Theta_g$, $[0, 2\pi]$. Although tails of the chip $p(t)$ extend up to infinity, they decay as $1/t^3$. Intersymbol interference is caused by bauds $l = \pm 1, \pm 2$ as $p(t)$ has significant amplitude up to $t = \pm 7T_c$. The auto correlation function

$$R_l(\tau_2) = \sum_{\mu=0}^{N-1} \sum_{u=0}^{N-1} a_u p[(\mu - u - lN) T_c - \tau_2] a_\mu, \tag{4.7}$$

which is discrete can be expressed in matrix form

$$R_l(\tau_2) = \mathbf{a}\mathbf{p}_l\mathbf{a}^T. \tag{4.8}$$

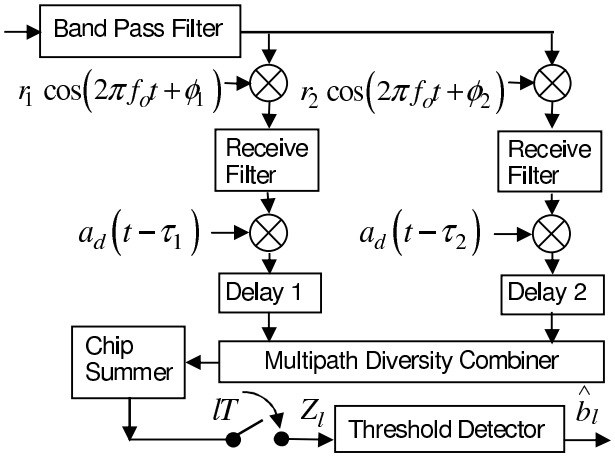

Figure 4.2. Two finger modified delayed signature RAKE demodulator. The receive filter is square-root raised-cosine (rolloff = 0.25) and discrete code $a_d(t) = \sum_l \sum_{\mu=0}^{N-1} a_\mu \delta(t - \mu T_c - lT)$. Delay 1 $= \tau_2$ and Delay 2 $= 0$. Chip summer or $\sum_{\mu_s=\mu_d}^{N-1+\mu_d}(.)$ is reset every T sec. Noise figure is 5 dB. Note: For original delayed signature RAKE Delay 1 and 2 = 0..

Here the $1 \times (N-1)$ matrix is the users Gold sequence

$$\mathbf{a} = \begin{bmatrix} a_0 & a_1 & \dots & a_{N-1} \end{bmatrix}. \tag{4.9}$$

The $(N-1)\times(N-1)$ matrix

$$\mathbf{p}_l = \begin{bmatrix} p_{0,0} & \cdots & p_{0,\mu} & \cdots & p_{0,N-1} \\ \vdots & & \vdots & & \vdots \\ p_{u,0} & \cdots & p_{u,\mu} & \cdots & p_{u,N-1} \\ \vdots & & \vdots & & \vdots \\ p_{N-1,0} & \cdots & p_{N-1,\mu} & \cdots & p_{N-1,N-1} \end{bmatrix} \tag{4.10}$$

depends on the baud of interest and is obtained from the sampled chip $p_{\mu,u} = p\left[(\mu - u - lN)\,T_c - \tau_2\right]$. At the receiver output total noise n_T is a sum of narrow-band correlated Gaussian noise samples. For given RAKE state vectors $\mathbf{r_g}, \phi_\mathbf{g}, \tau_2$ and receive filter, the noise variance,

$$\begin{aligned} \sigma_n^2 &= \frac{N_o N}{4} \sum_{g=1}^{2} r_g^2 \\ &+ \frac{N_o Y}{2} \sum_{u=0}^{N-1} \sum_{v=0}^{N-1} a_v p\left[(u-v)\,T_c - \tau_2\right] a_u. \end{aligned} \tag{4.11}$$

4.3 Error Rate

For a given channel and intersymbol interference, the conditional error rate

$$\begin{aligned} P_2[\,|\,\mathbf{r_g}, \phi_\mathbf{g}, \tau_2, b_l] &= \frac{1}{2}\Pr\left[n_T + \sum_{l=-2}^{2}{}' \varsigma_l b_l > A_S + \gamma_0\right] \\ &+ \frac{1}{2}\Pr\left[n_T + \sum_{l=-2}^{2}{}' \varsigma_l b_l < -\left\{A_S + \gamma_0\right\}\right]. \end{aligned} \tag{4.12}$$

For a given channel, the conditional error rate $P_2 = P_2[\,|\,\mathbf{r_g}, \phi_\mathbf{g}, \tau_2] = \left\langle P_2[\,|\,\mathbf{r_g}, \phi_\mathbf{g}, \tau_2, b_l]\right\rangle$ can be evaluated by analytical methods that are presented here. The unconditional error rate $P_e^M = \left\langle P_2^M \right\rangle$, where $\langle . \rangle$ is statistical averaging over the channel vectors $\mathbf{r_g}, \phi_\mathbf{g}, \tau_2$ and method $M = T, G, C, U, L$.

4.3.1 Error Rate using Total Probability Theorem

Using total probability theorem for pre and post-cursor interfering symbols, the error rate

$$P_2 = P_2^T = \frac{1}{32} \sum_{\substack{i_l=0 \\ l\in\Omega}}^{1} \text{erfc} \left[\frac{A_S + \gamma_0 + \sum_{l=-2}^{2}{}' (2i_l - 1)\, \varsigma_l}{\sqrt{2}\ \ \sigma_n} \right], \tag{4.13}$$

where the set Ω consists of elements $\{-2, -1, 1, 2\}$.

4.3.2 Error Rate using Standard Gaussian Approximation

If intersymbol interference is assumed Gaussian, the standard Gaussian approximation error rate

$$P_2 \approx P_2^G = \frac{1}{2} \text{erfc} \left[\frac{A_S + \gamma_0}{\sqrt{2\left(\sigma_n^2 + \sigma_{ISI}^2\right)}} \right]. \tag{4.14}$$

Here $\sigma_{ISI}^2 = \sum_{l\in\Omega}{}' \varsigma_l^2$ is the conditional variance of intersymbol interference. For high data rate DS-SS BPSK, with spreading factor $N = 7$, amplitude ς_l shall not be Gaussian.

4.3.3 Upper Bound on Error Rate using Chernoff Bound

Using the Chernoff bound [2], the error rate

$$P_2 \leq P_2^C = \exp\left[-\upsilon_o \left(A_S + \gamma_0\right) + \frac{\upsilon_o^2 \sigma_n^2}{2} \right] \prod_{l=-2}^{2}{}' \cosh\left[\upsilon_o \varsigma_l\right]. \tag{4.15}$$

The Chernoff constant, $\upsilon_o > 0$, is expressed as

$$\upsilon_o = \frac{A_S + \gamma_0 - \sum_{l\epsilon\Lambda} |\varsigma_l|}{\sigma_n^2 + \sum_{l\epsilon\Lambda^c} \varsigma_l^2} \tag{4.16}$$

where the set Λ and Λ^c consists of elements $\{-2, -1, 1, 2\}$.

4.3.4 Upper Bound on Error Rate using Prabhu Bound

The cumulative distribution function of the sum of two random variables has a simple upper bound [21],

$$\Pr[z_N + z_R < A] \leq \Pr[z_N \leq A + \Delta] + \Pr[z_R \leq -\Delta] \tag{4.17}$$

in terms of their marginal distributions. The bound shall be tight if the spread of z_R is smaller than that of z_N. As intersymbol interference is symmetric, using this bound

$$\begin{aligned} P_2 \leq P_2^U = \Pr\left[n_T + \sum_{l\epsilon\Lambda}{}' \varsigma_l b_l < -\left(A_S + \gamma_0\right) + \Delta\right] \\ + \Pr\left[\sum_{l\epsilon\Lambda^c}{}' \varsigma_l b_l < -\Delta\right]. \end{aligned} \tag{4.18}$$

Applying total probability theorem and Chernoff bound to the first and second terms respectively, the error rate

$$\begin{aligned} P_2 \leq P_2^U = \frac{1}{8}\sum_{\substack{i_l=0 \\ l\in\Lambda}}^{1} \operatorname{erfc}\left[\frac{A_S + \gamma_0 + \sum_{l\epsilon\Lambda}{}' \left(2i_l - 1\right)\varsigma_l - \Delta}{\sqrt{2}\ \ \sigma_n}\right] \\ + \exp\left[-\upsilon_o \Delta\right] \prod_{l\in\Lambda^c}{}' \cosh\left[\upsilon_o \varsigma_l\right]. \end{aligned} \tag{4.19}$$

where Λ has two elements and constant, $\Delta > 0$, is determined numerically. The Chernoff constant, for $\mathcal{A}, \mathcal{B} \in \Lambda^c$,

$$\upsilon_o = \frac{\Delta - |\varsigma_{\mathcal{A}}|}{\varsigma_{\mathcal{B}}^2}. \tag{4.20}$$

4.3.5 Lower Bound on Error Rate using Jensen's Inequality

Using Jensens inequality [21], the error rate

$$P_2 \geq P_2^L = \frac{1}{2}\operatorname{erfc}\left[\frac{A_S + \gamma_0}{\sqrt{2}\sigma_n}\right]. \tag{4.21}$$

4.4 Power Spectral Density and SNR

With ideal power control the link operates at a threshold error rate $P_{e,th}$. As $p(0) = 1$, the signal voltage at the detector input is proportional to the local mean signal strength λ that is related to the received power. For the chip waveform used here, average received signal power and hence front end SNR can be obtained numerically. Alternatively, we derive the received signal power from the spectral density and average it over the wideband channel. From Eq. 5.1 the baseband transmit signal, prior to the dynamic gain,

$$s_{BB}(t) = \sqrt{2} \sum_{l=-\infty}^{\infty} b_l \sum_{u=0}^{N-1} a_u \delta\left(t - uT_c - lT\right) \otimes p_T(t), \tag{4.22}$$

where we have assumed that $\theta = 0$. The transmitter section and an example baseband waveform of Eq. 4.22 is illustrated in Fig. 4.3. This baseband waveform of Eq. 4.22 can also be expressed as a linear digital modulated waveform

$$s_{BB}(t) = \sqrt{2} \sum_{l=-\infty}^{\infty} b_l q(t - lT). \tag{4.23}$$

Here $q(t) = \sum_{u=0}^{N-1} a_u \delta\left(t - uT_c\right) \otimes p_T(t)$ is a unique signaling pulse that is expressed mathematically. This pulse depends upon the deterministic signature which is fixed for the duration of the call. An alternate representation for the transmitter section shown in Fig. 4.3a is illustrated in Fig. 4.4a. In Fig. 4.4a the filter with characteristic $Q(f)$ has a unique impulse response $q(t)$ that is shown Fig. 4.4c.

The transmitter of Fig. 4.4a is mathematically equivalent to the transmitter of Fig. 4.3a as the example baseband waveforms $s_{BB}(t)$ are the same in both Fig. 4.4d and 4.3d. Or Eq. 4.22 and Eq. 4.23 are different mathematical representations of the same baseband signal $s_{BB}(t)$.

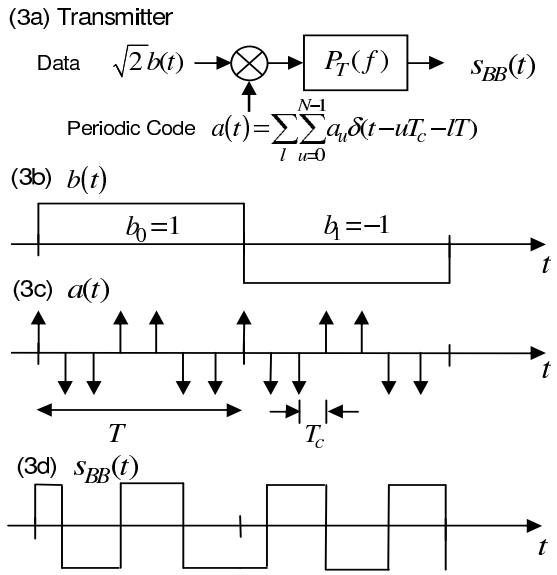

Figure 4.3. Transmitter section prior to dynamic power control gain and DS-SS BPSK baseband waveform with rectangular chips..

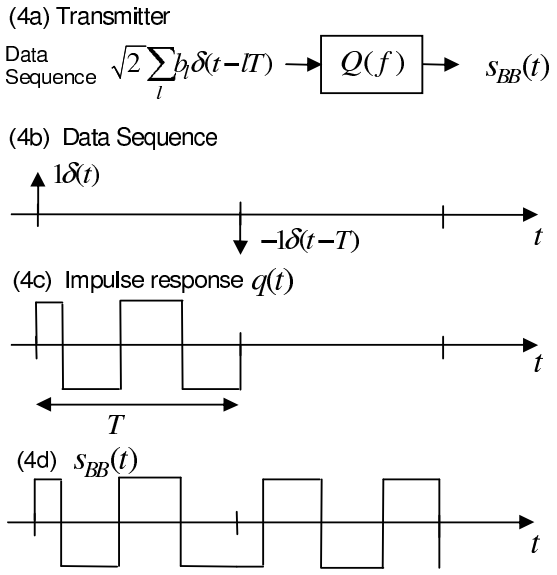

Figure 4.4. Equivalent transmitter model for that shown in Fig. 4.3a and baseband DS-SS BPSK waveform with rectangular chips..

The information symbols b_l are statistically independent and stationary. Hence, the spectral density of $s_{BB}(t)$ in Eq. 4.23 is obtained by direct use of the spectral density that is provided in [2], [11] for linear digital modulated signals.

Hence, the baseband spectral density,

$$P_{BB}(f) = \frac{2}{T} |Q(f)|^2 \sum_{m=-\infty}^{\infty} \Phi(m) e^{-j2\pi f m T} \tag{4.24}$$

Here $Q(f)$ is the Fourier transform of $q(t)$ and

$$\Phi(m) = E\left[b_{l+m} b_l\right] = \begin{cases} 1 & m = 0 \\ 0 & m \neq 0 \end{cases} \tag{4.25}$$

is the autocorrelation function of the information symbols.

The Fourier transform of the unique baud rate pulse $q(t)$,

$$Q(f) = P_T(f) \sum_{u=0}^{N-1} a_u e^{-j2\pi f u T_c}, \tag{4.26}$$

is used to obtain the spectral density

$$P_{BB}(f) = \frac{2}{T} |P_T(f)|^2 \left[\sum_{u=0}^{N-1} a_u^2 + 2 \sum_{v=1}^{N-1} \sum_{u=0}^{N-1-v} a_u a_{u+v} \cos(2\pi f v T_c) \right] \tag{4.27}$$

for the DS-SS BPSK baseband signal $s_{BB}(t)$. This spectral density is positive and real for all frequencies and has no discrete spectral lines. The same $P_{BB}(f)$ in Eq. 4.27 was derived by using the matrix method [22]. It was shown [22] that the passband transmit power spectral density $\mathcal{P}(f) = \frac{1}{4} P_{BB}(f - f_o) + \frac{1}{4} P_{BB}(-f - f_o)$. Hence, the average received signal power

$$\mathcal{P}_r = E\left[1/2 \int_{-\infty}^{\infty} P_{r,BB}\left(f, \mathbf{r_m}, \phi_{\mathbf{m}}, \tau_{\mathbf{m}}\right) df \right] \tag{4.28}$$

is obtained by ensemble averaging over the channel. Here the received baseband spectral density $P_{r,BB}(f) = P_{BB}(f) B_l^2 |C(f)|^2$ where $C(f)$ is the Fourier transform of the channel impulse response $c(t)$ given in Eq. 5.2. Finally

$$\mathcal{P}_r = \frac{\left[2\sigma_r^2 + 2\sigma_r^2\right] \lambda^2}{T_c} \tag{4.29}$$

relates the signal voltage, at the threshold detector input to front end average received signal power. The front end signal-to-noise power ratio averaged over the channel

$$\rho = \mathcal{P}_r / \left[No/T_c \right]. \tag{4.30}$$

Here No/T_c is noise power in the equivalent Nyquist band.

4.5 Numerical Results

In this study, the Gold code for $N = 7$ (or 31) uses primitive polynomials in octal units 13 and 15 (or 45 and 67). Here we use our mathematical methods for evaluation of high data rate DS-SS BPSK reverse links. First we compare the accuracy of different error rate methods by considering a single user link with a Gold sequence. Next we discuss the transmit power spectral density and bandwidths for the link with different signatures and potential adjacent channel interference impacts.

4.5.1 Error Rate Considerations

In Fig. 4.5 and 4.6 unconditional error rate, is obtained by Monte Carlo simulation of the channel vector and use of conditional error rates in Eq.'s 5.11, 5.12, 5.13, 5.17 and 5.19 at different SNR's as defined in Eq. 4.30.

As shown in Fig. 4.5, at high data rates of 174.2 kb/ sec or $N = 7$, for $\rho =$ 14dB, error rate by total probability theorem $P_e^T = 4.8 \times 10^{-4}$ and by the Gaussian approximation $P_e^G = 1.2 \times 10^{-3}$. It is clear from the graph that P_e^G is pessimistic for $\rho >$ 8dB. Similarly for $\rho >$ 12dB and $\rho >$ 16dB, P_e^G is pessimistic when compared to upper bounds on error rate P_e^U and P_e^C respectively. For moderate values of SNR, P_e^G and P_e^T gives the same result. From the curves for P_e^U, P_e^T and P_e^L it is apparent that incoherent intersymbol interference marginally degrades performance. The lower

bound on error rate P_e^L is equivalent to the error rate where intersymbol interference is ignored.

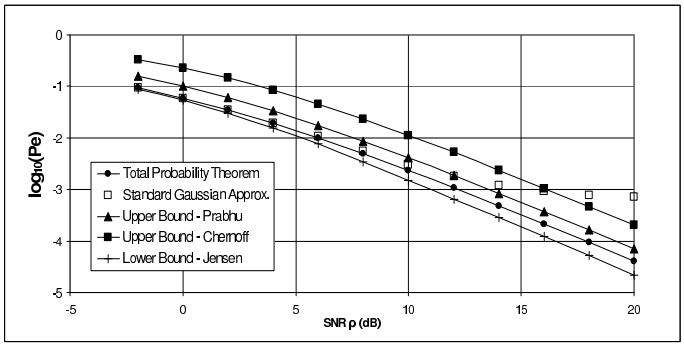

Figure 4.5. Error rate for the modified delayed signature RAKE demodulator at 174.2 kb/ sec or $N = 7$. Error rate by total probability theorem is P_e^T. Gaussian approximation error rate is P_e^G. Upper bound on error rate by Chernoff bound is P_e^C. Upper bound on error rate by Prabhu bound is P_e^U. Lower bound on error rate by Jensen inequality is P_e^L..

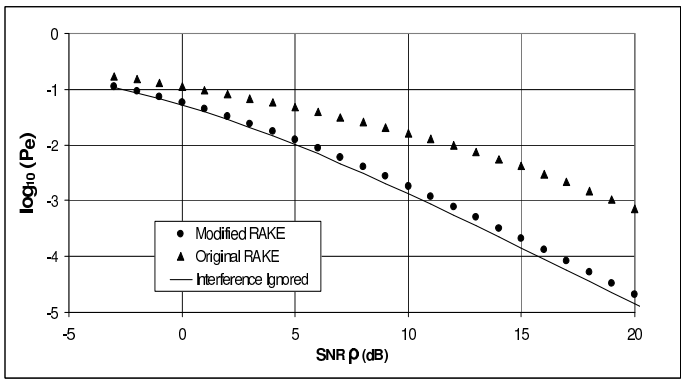

Figure 4.6. Error rate P_e^T for the original and modified delayed signature RAKE's at 174.2 kb/ sec or $N = 7$ for $\tau_2 = 3T_c$..

We also studied the error rate at a low data rate of 39.4 kb/ sec or $N = 31$. It was observed that P_e^T, P_e^G and P_e^L are the same, for $-5\text{dB} \leq \rho \leq 25\text{dB}$. For a high spreading factor of $N = 31$, noise is dominant relative to multipath interference. For a

single branch 174.2 kb/ sec receiver, P_e^T and P_e^G was the same which is consistent with [7] as conditional pdf of intersymbol interference is approximately Gaussian. While for the high data rate RAKE with $N = 7$ intersymbol interference is not Gaussian.

As shown in Fig. 4.6, for 174.2 kb/ sec with $\tau_2 = 3T_c$, the original and modified delayed signature RAKE's require ρ = 19dB and 11dB respectively at $P_e^T = 10^{-3}$. The former structure retains coherent intersymbol interference as shown in the Appendix (A.1 and A.2) while the latter combats intersymbol interference.

4.5.2 Power Spectral Density and Bandwidth Considerations

For high data rates, the spectral densities obtained from Eq. 4.27, for two Gold and one PN sequences and the same filter rolloff $\alpha = 1/4$, are compared in Fig. 4.7. The spectral density varies significantly for different Gold codes and PN signatures. For a given signature within the bandwidth, the spectral density at a set of frequencies is 15dB higher than at other frequencies. The set of frequencies with higher spectral density varies from signature to signature. As shown the PN sequence can potentially result in higher adjacent channel interference.

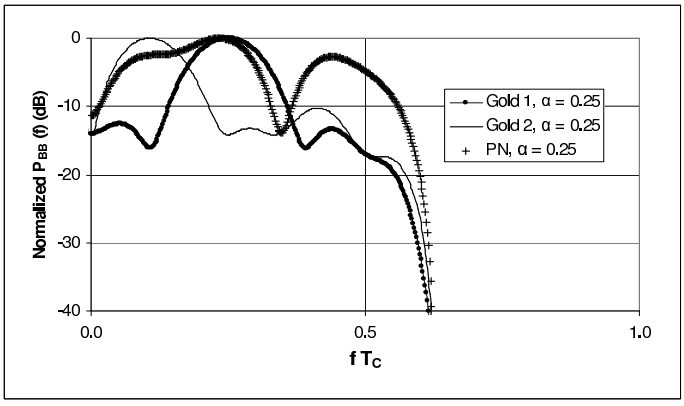

Figure 4.7. Spectral density for high data rate DS-SS BPSK, or $N = 7$, with two Gold sequences, one PN sequence and for filter rolloff $\alpha = 1/4$..

In Fig. 4.8 a filter rolloff of $\alpha = 1/2$ results in a side lobe of significant magnitude compared to the case where $\alpha = 1/4$ which depicts the impact of different filter characteristics.

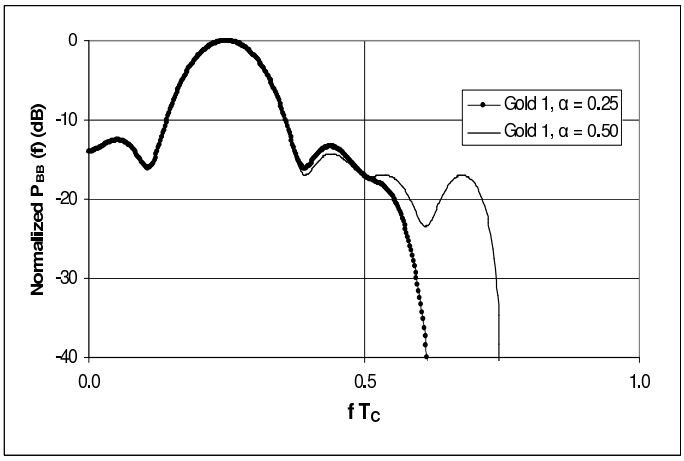

Figure 4.8. Spectral density for $N = 7$ or high data rate DS-SS BPSK using the same Gold sequence with filter rolloffs $\alpha = 1/4$ and $1/2$..

As shown in Table 4.1, the bandwidth (BW) that contains 99% of the signal power for Gold code 1 is $0.96/T_c$. For the same α, the two Gold codes have smaller fractional power containment bandwidth than the PN sequence.

Table 4.1. 1% Fractional Power Containment Bandwidth

Sequence	α	$BW\,T_c$
Gold 1	1/4	0.96
Gold 2	1/4	1.00
PN	1/4	1.10
Gold 1	1/2	1.26

Finally, the power spectral density of a low data rate transmitter with $N = 127$ and a Gold signature is shown in Fig. 4.9. The density varies uniformly between 0dB

and −15dB relative to the maximum for majority of the frequencies. However, a few distinct frequencies within the bandwidth of the signal are 30dB and 40dB down.

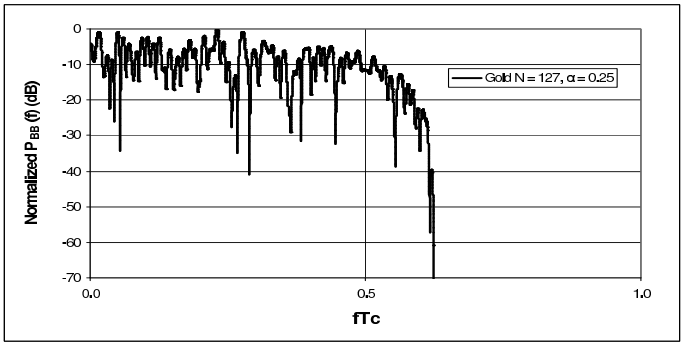

Figure 4.9. Spectral density for low data rate DS-SS BPSK with a Gold sequence..

4.6 Conclusions

We have evaluated the error rate at different operating SNRs, spectral density and bandwidth of a high data rate DS-SS BPSK reverse link. The signal with a 7 chip signature is transmitted over a frequency selective channel and the receiver has a dual finger RAKE demodulator. The chips have raised-cosine frequency characteristics that results in four non-coherent intersymbol interference terms.

We compare the standard Gaussian approximation error rate for this link to error rate obtained using the total probability theorem and bounds. Upper bounds on the error rate are derived using the Chernoff and Prabhu bounds while a lower bound on error rate is derived using Jensen's inequality. The latter upper bound is in terms of the error rate obtained with two intersymbol interference terms and bounds on the marginal distribution of the smaller terms. In the case of bounds the true statistics of intersymbol interference is used instead of a Gaussian assumption. The Gaussian approximation error rate is pessimistic for SNR's $>$ 8dB and 12dB when

compared to that obtained by the total probability theorem and the Prabhu bound respectively. For high data rates, intersymbol interference is not Gaussian and at high SNR's our error rate bound is a better estimate. Evaluation of a dual space diversity four finger RAKE demodulator will be evident to the reader.

We show that the modified delayed signature RAKE combats incoherent intersymbol interference, while the original structure has severe performance degradation due to coherent intersymbol interference.

We derive an accurate analytical expression for the transmit spectral density of this link by expressing the signal as a linear digital modulated waveform. The spectral density is a function of the chip Fourier transform, the signature coefficients and the autocorrelation sequence of the information. We determine the operating SNR by deriving the received signal power from the spectral density and average it over the wideband fading channel. Finally, the fractional containment bandwidth obtained from the spectral density for transmission with two Gold sequences is less than that with a PN sequence.

CHAPTER 5

ERROR RATE CONSIDERATIONS FOR A HIGH BIT RATE DS-SS BPSK DUAL SPACE DIVERSITY RAKE

In high bit rate DS-SS BPSK mobile radio reverse links with RAKE demodulators the frequency selective channel causes intersymbol interference. For many years the standard Gaussian approximation error rate has been used and for high bit rates its accuracy is not known. We compare the Gaussian approximation to error rate derived using total probability theorem, Chernoff and Prabhu bounds with true statistics of intersymbol interference. For signal-to-noise ratio's (SNR's) greater than 6dB (cases of interest), we show that the Gaussian approximation is a much looser upper bound than our bounds. The Prabhu bound which can be tailored to different intersymbol interference conditions is the tightest bound. We show that the RAKE combats incoherent intersymbol interference while the immunity it offers decreases for SNR's greater than 10dB. Finally, a dual space diversity RAKE provides an 8dB space diversity gain.

5.1 Introduction

DS-SS cellular systems for packet data services, Voice over IP and video telephony with higher bit rates and reduced latency are evolving. One main challenge is evaluation of capacity and performance with different transmission schemes that combat frequency selective fading. This requires determination of error rate for a given SNR. For DS-SS BPSK a modified delayed signature RAKE demodulator [2], [3] with two horizontally separated antennas [4] can be used. The dual space diversity

RAKE receiver combines the desired signal extracted from multiple delayed paths of each diversity channel. For one user, the desired symbol at the RAKE output is corrupted by correlated Gaussian noise and intersymbol interference.

Over the years the standard Gaussian approximation error rate [6] was extended [7], [8] by assuming intersymbol interference is Gaussian. The approximation is good [7] for a single branch receiver with a 31 rectangular chip signature. In the low bit rate single antenna RAKE [8] with a 127 rectangular chip signature, two intersymbol interference terms were considered. For high bit rates (8 chip signatures), error rate was determined by simulation [9], [10]. For a single branch receiver at 10^{-3} error rate, coherent intersymbol interference degrades [9] required SNR by 4dB. In a non space diversity two finger RAKE [16], the Gaussian approximation is pessimistic when compared to an upper bound on error rate, at SNR's $>$ 12dB.

In this chapter [17] a high bit rate DS-SS BPSK reverse link with a 7 chip signature and chips with raised-cosine characteristics is analyzed. A dual space diversity RAKE demodulator with two antennas, four fingers and a space-multipath diversity combiner is used at the receiver. We assume the baud interval is similar to the channel delay [18], [19] and the chip extends up to ± 7 chip intervals that results in four incoherent intersymbol interference terms.

We calculate the error rate for a given channel using the total probability theorem, standard Gaussian approximation and bounds [16], [21] in the presence of Gaussian noise and intersymbol interference. The upper bounds on error rate derived using the Chernoff and Prabhu bounds while the lower bound derived using Jensen's inequality all use the true statistics of intersymbol interference. The latter upper bound is expressed in terms of the error rate with two intersymbol interference terms and bounds on the marginal distribution of the smaller terms. The unconditional error rate is obtained by Monte Carlo simulation over the channel parameters. For

per branch SNR's > 6dB, the Prabhu upper bound on error rate is notably better than the Gaussian approximation. The dual space diversity RAKE combats intersymbol interference at low SNR's while the immunity it offers decreases considerably for SNR's > 10dB. At 10^{-3} error rate a dual space diversity RAKE provides an 8dB space diversity gain.

In contrast to previous work, this study uses the true statistics of intersymbol interference instead of a Gaussian assumption. The Gaussian approximation may work for low bit rates [7], [8], however, more accurate methods are required at high bit rates. We analytically treat four intersymbol interference terms while [8] considers two terms and [9], [10] use simulation. Unlike [9] we show minimal performance degradation due to intersymbol interference. We extend [16] to evaluate a dual space diversity RAKE.

5.2 System Description

Consider a single sector reverse link shown in Fig. 5.1.

5.2.1 DS-SS BPSK Transmitter

The transmit signal

$$s(t) = \sqrt{2} \sum_{l=-\infty}^{\infty} B_l b_l \sum_{u=0}^{N-1} a_u p_T(t - uT_c - lT) \cos(\omega_o t + \theta) \tag{5.1}$$

where ideal power control gain $B_l^2 = \lambda^2/L^2$, information symbols $b_l \in \{\pm 1\}$ for baud index l are equi-probable with duration T. The Gold sequence with period $N = T/T_c$ has elements $a_u \in \{\pm 1\}$ and chip $p_T(t)$ with square-root raised-cosine characteristic, is transmitted every T_c sec. In CDMA systems, $T_c = 0.82\ \mu$sec and bandwidth ≈ 1.536 MHz is greater than coherence bandwidth [4], [43]. We assume a high bit rate $R_b = 174.2$ kb/ sec with $N = 7$.

5.2.2 Wideband Channel Model

The ηth diversity baseband channel impulse response

$$c^{(\eta)}(t) = L \sum_{g=1}^{2} r_g^{(\eta)} \exp\left(-j\Theta_g^{(\eta)}\right) \delta\left(t - \tau_g\right) \quad \eta = 1, 2, \tag{5.2}$$

is assumed to be invariant over a few bauds. For typical antenna separations, the two paths are not independent [43] with respect to obstructions, so we assume propagation path loss and shadowing L is identical on both paths. For both diversity channels, as the signals are received from the same constellation of scatterers, we assume [44] delay τ_g to be identical. We assume Rayleigh amplitude $r_g^{(\eta)}$, phase $\Theta_g^{(\eta)}$ and τ_g are statistically independent [19]. We assume short term fading and phase on the diversity channels are statistically independent. The probability density function of $r_g^{(\eta)}$ is normalized with $2\sigma_r^2 = 1$. We assume $\tau_1 = 0$ and τ_2 is uniformly distributed between $2T_c$ and $6T_c$.

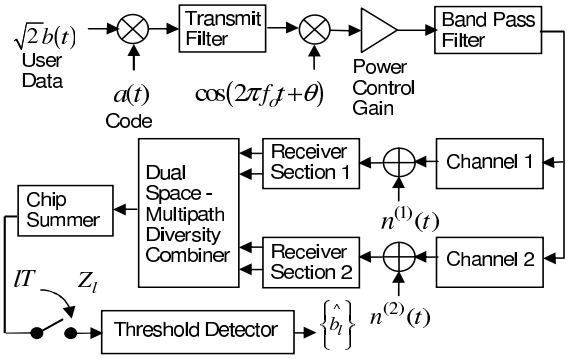

Figure 5.1. Reverse link with a dual space diversity RAKE receiver. Zero mean additive white Gaussian noise $n^{(\eta)}(t)$, $\eta = 1, 2$, has two-sided spectral density $N_o/2$ ($N_o = 4 \times 10^{-21}$ W/Hz). .

5.2.3 Dual Space Diversity RAKE Demodulator

At the receiver (Fig. 5.1) each section processes the space diversity signals independently. After the two multipath components are despread independently at each section (Fig. 5.2), the four multipath diversity signals are combined. At the receive filter output, chip $p(t)$ has raised-cosine characteristic with $p(0) = 1$. The discrete voltage for $l = 0$,

$$Z_0 = A_S b_0 + \gamma_0 b_0 + \sum_{l=-2}^{2}{}' \varsigma_l b_l + n_T, \tag{5.3}$$

where $\sum_{l}{}'$ excludes the term $l = 0$. The amplitude of the desired signal

$$A_S = \frac{\lambda}{\sqrt{2}} \sum_{\eta=1}^{2} \sum_{g=1}^{2} \left\{ r_g^{(\eta)} \right\}^2 \sum_{u=0}^{N-1} a_u^2. \tag{5.4}$$

The interpath interference amplitude

$$\gamma_0 = \frac{\lambda}{\sqrt{2}} \sum_{\eta=1}^{2} Y^{(\eta)} \left[R_0 \left(\tau_2 \right) + R_0 \left(-\tau_2 \right) \right], \tag{5.5}$$

and post and pre-cursor symbol interference amplitude

$$\varsigma_l = \frac{\lambda}{\sqrt{2}} \sum_{\eta=1}^{2} Y^{(\eta)} \left[R_l \left(\tau_2 \right) + R_l \left(-\tau_2 \right) \right]. \tag{5.6}$$

Here Laplacian $Y^{(\eta)} = r_1^{(\eta)} r_2^{(\eta)} \cos\left(\phi_2^{(\eta)} - \phi_1^{(\eta)} \right)$ and uniform phase $\phi_g^{(\eta)} = \theta - \Theta_g^{(\eta)}$, $[0, 2\pi]$. Although the tails of the chip $p\left(t\right)$ extend up to infinity, they decay as $1/t^3$. Bauds $l \in \{\pm 1, \pm 2\}$ cause intersymbol interference as the chip has significant amplitude up to $t = \pm 7 T_c$. The discrete [16] auto correlation function in matrix form

$$R_l \left(\tau_2 \right) = \mathbf{a} \mathbf{p}_l \mathbf{a}^T, \tag{5.7}$$

where the $1 \times N$ matrix $\mathbf{a} = \begin{bmatrix} a_0 & a_1 & \dots & a_{N-1} \end{bmatrix}$ is the users Gold sequence and,

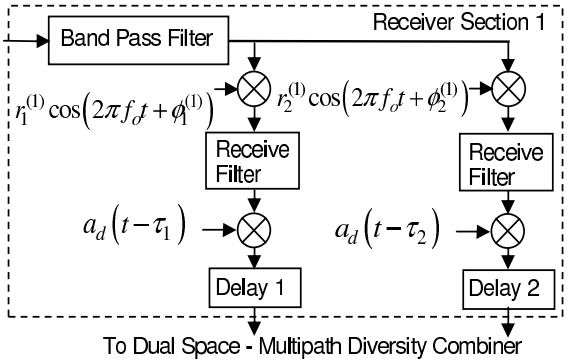

Figure 5.2. Receiver section 1 with square-root raised-cosine (rolloff = 0.25) filters. Noise figure is 5 dB, discrete code $a_d(t) = \sum_l \sum_{\mu=0}^{N-1} a_\mu \delta(t - \mu T_c - lT)$, Delay 1 $=\tau_2$ and Delay 2 =0..

$$\mathbf{p}_l = \begin{bmatrix} p_{0,0} & \cdots & p_{0,\mu} & \cdots & p_{0,N-1} \\ \vdots & & \vdots & & \vdots \\ p_{u,0} & \cdots & p_{u,\mu} & \cdots & p_{u,N-1} \\ \vdots & & \vdots & & \vdots \\ p_{N-1,0} & \cdots & p_{N-1,\mu} & \cdots & p_{N-1,N-1} \end{bmatrix}. \tag{5.8}$$

is an $N \times N$ matrix. Here sampled chip $p_{u,\mu} = p[(\mu - u - lN)T_c - \tau_2]$ depends on the baud of interest. At the receiver output total noise n_T is a sum of narrowband correlated Gaussian noise samples. For given RAKE state vectors $\mathbf{r}_\mathbf{g}^{(\eta)}, \phi_\mathbf{g}^{(\eta)}, \tau_2$ and receive filter the noise variance,

$$\sigma_n^2 = \frac{N_o' N}{4} \sum_{\eta=1}^{2} \sum_{g=1}^{2} \left\{ r_g^{(\eta)} \right\}^2 + \frac{N_o'}{2} \sum_{\eta=1}^{2} Y^{(\eta)} \mathbf{a} \mathbf{p}_0 \mathbf{a}^T. \tag{5.9}$$

5.3 Error Rate

For a given channel and intersymbol interference, the conditional error rate

$$P_2[\,|\,\mathbf{r}_\mathbf{g}^{(\eta)}, \phi_\mathbf{g}^{(\eta)}, \tau_2, b_l] = \frac{1}{2} \Pr\left[n_T + \sum_{l=-2}^{2\ \prime} \varsigma_l b_l > A_S + \gamma_0 \right]$$

$$+\frac{1}{2}\Pr\left[n_T+\sum_{l=-2}^{2}{}'\varsigma_l b_l<-\{A_S+\gamma_0\}\right]. \tag{5.10}$$

The conditional error rate $P_2 = P_2[|\,\mathbf{r}_{\mathbf{g}}^{(\eta)}, \phi_{\mathbf{g}}^{(\eta)}, \tau_2] = \left\langle P_2[|\,\mathbf{r}_{\mathbf{g}}^{(\eta)}, \phi_{\mathbf{g}}^{(\eta)}, \tau_2, b_l]\right\rangle$ can be evaluated by analytical methods presented here. The unconditional error rate $P_e^M = \left\langle P_2^M\right\rangle$, where $\langle . \rangle$ is statistical averaging over the channel vector $\mathbf{r}_{\mathbf{g}}^{(\eta)}, \phi_{\mathbf{g}}^{(\eta)}, \tau_2$ while method $M = T, G, C, U, L$ are described here.

5.3.1 Error Rate using Total Probability Theorem

Using total probability theorem for pre and post-cursor interfering symbols, the error rate

$$P_2 = P_2^T = \frac{1}{32}\sum_{\substack{i_l=0\\ l\in\Omega}}^{1}\operatorname{erfc}\left[\frac{A_S+\gamma_0+\sum_{l=-2}^{2}{}'(2i_l-1)\,\varsigma_l}{\sqrt{2}\;\;\sigma_n}\right], \tag{5.11}$$

where the set Ω consists of elements $\{-2,-1,1,2\}$.

5.3.2 Error Rate using Standard Gaussian Approximation

If intersymbol interference is assumed Gaussian, the standard Gaussian approximation error rate

$$P_2 \approx P_2^G = \frac{1}{2}\operatorname{erfc}\left[\frac{A_S+\gamma_0}{\sqrt{2\left(\sigma_n^2+\sigma_{ISI}^2\right)}}\right]. \tag{5.12}$$

Here $\sigma_{ISI}^2 = \sum_{l\in\Omega}{}'\varsigma_l^2$ is the conditional variance of intersymbol interference. For high bit rate DS-SS BPSK, with $N = 7$, the amplitude ς_l shall not be Gaussian.

5.3.3 Upper Bound on Error Rate using Chernoff Bound

Using the Chernoff bound [2], the error rate

$$P_2 \leq P_2^C = \exp\left[-\upsilon_o\left(A_S+\gamma_0\right)+\frac{\upsilon_o^2\sigma_n^2}{2}\right] \times \prod_{l=-2}^{2}{}' \cosh\left[\upsilon_o \varsigma_l\right]. \tag{5.13}$$

The Chernoff constant, $\upsilon_o > 0$, is expressed as

$$\upsilon_o = \frac{A_S+\gamma_0-\sum\limits_{l\epsilon\Lambda}|\varsigma_l|}{\sigma_n^2+\sum\limits_{l\epsilon\Lambda^c}\varsigma_l^2} \tag{5.14}$$

where Λ is a subset of $\{\pm 2, \pm 1\}$ and Λ^c is its compliment.

5.3.4 Upper Bound on Error Rate using Prabhu Bound

The cumulative distribution function of the sum of two random variables has a simple upper bound [21],

$$\Pr[z_N + z_R < A] \leq \Pr[z_N \leq A+\Delta] + \Pr[z_R \leq -\Delta] \tag{5.15}$$

in terms of marginal distributions and constant $\Delta > 0$. The bound shall be tight if spread of z_R is less than that of z_N. As intersymbol interference is symmetric, using Eq. 5.15,

$$P_2 \leq P_2^U = \Pr\left[n_T + \sum_{l\epsilon\Lambda}{}' \varsigma_l b_l < -\left(A_S+\gamma_0\right)+\Delta\right] + \Pr\left[\sum_{l\epsilon\Lambda^c}{}' \varsigma_l b_l < -\Delta\right]. \tag{5.16}$$

Applying total probability theorem and Chernoff bound to the first and second terms respectively, the error rate

$$P_2 \leq P_2^U = \frac{1}{8}\sum_{\substack{i_l=0 \\ l\in\Lambda}}^{1} \operatorname{erfc}\left[\frac{A_S+\gamma_0+\sum\limits_{l\epsilon\Lambda}{}'\left(2i_l-1\right)\varsigma_l-\Delta}{\sqrt{2}\ \ \sigma_n}\right]$$

$$+\exp\left[-\upsilon_o\Delta\right]\prod_{l\in\Lambda^c}{}'\cosh\left[\upsilon_o\varsigma_l\right]. \tag{5.17}$$

where Λ consists of two elements from $\{\pm 2, \pm 1\}$, Δ is determined numerically and Chernoff constant,

$$\upsilon_o = \frac{\Delta - |\varsigma_{\mathcal{A}}|}{\varsigma_{\mathcal{B}}^2}, \qquad \mathcal{A}, \mathcal{B} \in \Lambda^c. \tag{5.18}$$

C. Lower Bound on Error Rate using Jensen's Inequality

Using Jensens inequality [21], the error rate

$$P_e[\,|\,\mathbf{r}_{\mathbf{g}}^{(\eta)}, \phi_{\mathbf{g}}^{(\eta)}, \tau_2] \geq P_2^L = \frac{1}{2}\text{erfc}\left[\frac{A_S + \gamma_0}{\sqrt{2}\sigma_n}\right]. \tag{5.19}$$

5.4 SNR and Space Diversity Gain

With ideal power control the link operates at a threshold error rate $P_{e,th}$. As $p(0) = 1$, the signal voltage at the detector input is proportional to the local mean signal strength λ. The front end average received power [16]

$$\mathcal{P}_r = \frac{[2\sigma_r^2 + 2\sigma_r^2]\,\lambda^2}{T_c}, \tag{5.20}$$

at each branch. The front end per branch SNR $\rho = \mathcal{P}_r/\left[No/T_c\right]$ where No/T_c is the noise power in the equivalent Nyquist bandwidth. The performance gain of a dual space diversity RAKE demodulator in decibels

$$G_{Div} = \rho_{Div}\,|_{P_{e,th}} - \rho\,|_{P_{e,th}}. \tag{5.21}$$

Here $\rho_{Div}\,|_{P_{e,th}}$ and $\rho\,|_{P_{e,th}}$ is the SNR in dB with and without space diversity respectively at a given $P_{e,th}$.

5.5 Numerical Results

Here we compare the accuracy of different error rate methods by considering a single user high bit rate reverse link with a dual space diversity RAKE and known Gold sequence. The Gold code uses primitive polynomials in octal units 13 and 15. In Fig. 5.3 the unconditional error rate P_e^M (for all methods), obtained by Monte Carlo simulation of the channel parameters, is plotted. For 6dB $\leq \rho \leq$ 20dB the Prabhu upper bound on error rate P_e^U is the most accurate estimate when compared to the error rate P_e^T obtained by total probability theorem. Over the range of SNR's plotted P_e^U is within $<$ 1dB of P_e^T and it is a moderately tight upper bound. For $\rho >$ 6dB, the standard Gaussian approximation error rate P_e^G is pessimistic when compared to P_e^U. The inaccuracy of the Gaussian approximation is observed at $\rho =$ 10dB where $P_e^U = 5.6 \times 10^{-5}$ and $P_e^G = 2.8 \times 10^{-4}$. Furthermore, P_e^U is 2dB tighter than the Chernoff upper bound on error rate P_e^C.

From curves for P_e^U, P_e^T and P_e^L it is observed that incoherent intersymbol interference marginally degrades performance at low SNR's. While at high SNR's there is a decrease in immunity offered by the dual space diversity RAKE. For $\rho \leq$ 6dB, when $P_{e,th} \geq 10^{-3}$ intersymbol interference marginally degrades performance by $<$ 1dB. For 6dB $< \rho \leq$ 10dB, when $P_{e,th} < 10^{-3}$ intersymbol interference degrades performance by $\sim$ 1.5dB. These SNR conditions can exist in multiple access systems or when the mobile power cannot be reduced further by power control. At high SNR's intersymbol interference starts contributing more to the bit errors.

In Fig. 5 of [16] similar error rate curves for a non space diversity RAKE were obtained and for $\rho >$ 12dB, P_e^G is pessimistic compared to P_e^U. In the non space diversity RAKE incoherent intersymbol interference marginally degrades performance. At $P_{e,th} = 10^{-3}$ the non space diversity RAKE [16] required $\rho =$ 14dB.

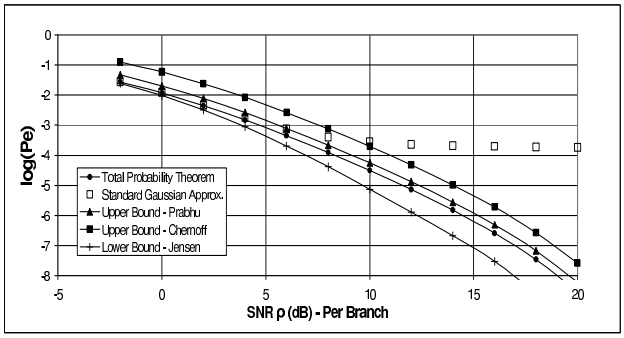

Figure 5.3. Dual space diversity RAKE error rate for $N = 7$..

Hence, at $P_{e,th} = 10^{-3}$ the dual space diversity RAKE provides a space diversity gain $G_{Div} = 8$dB.

5.6 Conclusion

We have evaluated the performance of a high bit rate DS-SS BPSK mobile radio reverse link with a dual space diversity RAKE. We calculate error rate for a given frequency selective channel using the total probability theorem, standard Gaussian approximation and bounds in the presence of Gaussian noise and intersymbol interference. The upper bounds on error rate derived using the Chernoff and Prabhu bounds while the lower bound derived using Jensen's inequality all use the true statistics of intersymbol interference. For per branch SNR's $>$ 6dB, the Prabhu upper bound on error rate is notably better than the Gaussian approximation. The dual space diversity RAKE combats intersymbol interference at low SNR's while the immunity it offers decreases considerably for SNR's $>$ 10dB. At 10^{-3} error rate a dual space diversity RAKE provides an 8dB space diversity gain.

CHAPTER 6

PACKET ERROR RATE FOR DS-SS BPSK REVERSE LINKS WITH DUAL HIGH BIT RATE BURSTS

A high bit rate DS-SS BPSK reverse link with a frequency selective channel and dual space diversity RAKE can support two simultaneous bursts at a reasonably acceptable packet error rate. Error rate of the link, with one continuous interferer, is determined by using the total probability theorem for intersymbol interference, by proving that the interference is conditionally Gaussian and Monte Carlo simulation of channel parameters. For per branch SNR's of 20 dB the packet error rate is 2.6%. Real systems have channel coding and decoding with packet retransmission while at any time 0, 1 or 2 users shall be bursting which shall reduce the packet error rate.

6.1 Introduction

DS-SS cellular systems for packet data voice, video and data services with higher bit rates and reduced latency are evolving. Evaluation of capacity requires determination of how many simultaneous high bit rate bursts can be supported at a given packet error rate and hence bit error rate. For the case of 2 users [54] with DS-SS QPSK and spreading factor of 32, error rate was evaluated. In his case 6 users [65] and spreading factors of 16 an approximate packet error rate was evaluated.

In this chapter it is determined that a high bit rate DS-SS BPSK reverse link can support two simultaneous bursts at a reasonably acceptable packet error rate. The desired user and interferer have Gold signatures of 7 chips with high bit rates of $R_b = 174.2$ kb / sec. We evaluate the error rate and packet error rate of the link with a

frequency selective channel, dual space diversity RAKE and one continuous interferer by using the total probability theorem for intersymbol interference and by proving that the multiple access interference is conditionally Gaussian. Unconditional error rate is obtained by Monte Carlo simulation of the channel parameters. Packet error rates of upto 2.6 % can be acheived at an SNR of 20 dB. Real systems have channel coding and decoding with packet retransmission which reduces the packet error rate. In packetized voice (chapters 7 and 8), depending upon the utilization factor, at any one instance there could be 0, 1 or 2 users transmitting high bit rate bursts. Hence, the packet error rate would be less than that determined in this chapter.

6.2 Multiple Access Dual Burst Packetized System Description

Consider a single sector reverse link with multiple users where only two users can transmit user data at the same time. As described in Sec. 2.4.4, in the reverse link user data transmission is scheduled with a packet of duration $D = 1.5$ ms. In packetized voice (chapters 7 and 8), depending upon the utilization factor, at any one instance there could be 0, 1 or 2 users transmitting high bit rate bursts. To determine the packet error rate with multiple users, error rate would need to be determined by considering user data packet arrivals for multiple users and scheduled transmission. A detailed link description for the single user and error rate was provided in chapters 4 and 5. The simplified analysis here, assumes two users are continuously transmitting high data rate bursts. Here we provide details for the second user or interferer.

6.2.1 Interferer's DS-SS BPSK Transmitter

The transmit signal for second user

$$s_1(t) = \sqrt{2} \sum_{l=-\infty}^{\infty} B_{1,l} b_{1,l} \sum_{u=0}^{N-1} a_{1,u} p_T(t - uT_c - lT) \cos(2\pi f_o t + \theta_1) \qquad (6.1)$$

where $B_{1,l}^2 = \lambda^2/L_1^2$ is the ideal power control gain and $b_{1,l} \in \{\pm 1\}$ are the information symbols for baud index l, are equi-probable with duration T. The Gold sequence for the second user with period $N = T/T_c$ has elements $a_{1,u} \in \{\pm 1\}$ where T_c is the chip duration. We assume a high bit rate $R_b = 174.2$ kb / sec with $N = 7$. Here the transmitter oscillator phase θ_1 is a uniform random variable $[0, 2\pi]$.

6.2.2 Interferer's Wideband Channel Model

The ηth diversity baseband channel impulse response for the second user,

$$c_1^{(\eta)}(t) = L_1 \sum_{g=1}^{2} r_{1,g}^{(\eta)} \exp\left(-j\Theta_{1,g}^{(\eta)}\right) \delta\left(t - \tau_{1,g}\right) \quad \eta = 1, 2, \tag{6.2}$$

where we assume $\tau_{1,1}$ is uniformly distributed between $2T_c$ and $6T_c$. The delayed path $\tau_{1,2}$ is uniformly distributed and satisfies the condition $\tau_{1,1} + 2T_c \leq \tau_{1,2} \leq \tau_{1,1} + 6T_c$. For a cell radius of 2 km and using the speed of light, the propagation delay incurred by the signal from cell edge is $\approx 8T_c$. It is assumed that the desired user is close to the antenna, while the interfering user moves anywhere in the cell. Although $\tau_{1,1}$ is not uniformly distributed, we make this simplifying assumption.

6.2.3 Dual Space Diversity RAKE with Interference

For the case of two users, the desired symbol at the RAKE output is corrupted by correlated Gaussian noise, intersymbol interference and multiple access interference. The discrete voltage for $l = 0$,

$$Z_0 = A_S b_0 + \gamma_0 b_0 + \sum_{l=-2}^{2\ \prime} \varsigma_l b_l + I_1 + n_T, \tag{6.3}$$

where $I_1 = \sum_{\eta=1}^{2} I_1^{(\eta)}$. The amplitude of the interferer at the ηth diversity branch

$$I_1^{(\eta)} = \frac{\lambda}{\sqrt{2}} r_1^{(\eta)} \sum_{g=1}^{2} r_{1,g}^{(\eta)} \cos\left(\phi_{1,g}^{(\eta)} - \phi_1^{(\eta)}\right) \times \sum_{l=-3}^{3} b_{1,l} R_{1,l}\left(\tau_{1,g}\right)$$
$$+ \frac{\lambda}{\sqrt{2}} r_2^{(\eta)} \sum_{g=1}^{2} r_{1,g}^{(\eta)} \cos\left(\phi_{1,g}^{(\eta)} - \phi_2^{(\eta)}\right) \times \sum_{l=-3}^{3} b_{1,l} R_{1,l}\left(\tau_{1,g} - \tau_2\right) \tag{6.4}$$

The discrete cross correlation function,

$$R_{1,l}(\tau) = \sum_{\mu=0}^{N-1} \sum_{u=0}^{N-1} a_{1,u} p\left[(\mu - u - lN) T_c - \tau\right] a_\mu, \tag{6.5}$$

and the phased $\phi_{1,g}^{(\eta)} = \theta_1 - \Theta_{1,g}^{(\eta)}$. In this case both θ_1 and $\Theta_{1,g}^{(\eta)}$ are statistically independent having uniform distributions between $[0, 2\pi]$. Details of noise variance and the intersymbol interference terms are provided in the chapter 5.

6.3 Statistical Characteristics of Multiple Access Interference

Here we show that the conditional probability denisty function of the interferer is Gaussian. The interferer amplitude,

$$I_1 = \frac{\lambda}{\sqrt{2}} \sum_{l=-3}^{3} I_{1,l} = \frac{\lambda}{\sqrt{2}} \sum_{l=-3}^{3} X_{1,l} b_{1,l} \tag{6.6}$$

where $X_{1,l} = \sum_{\eta=1}^{2} X_{1,l}^{(\eta)}$ and $X_{1,l}^{(\eta)} = \sum_{g=1}^{2} K_{c,1,g,l}^{(\eta)} X_{c,1,g}^{(\eta)} + \sum_{g=1}^{2} K_{s,1,g,l}^{(\eta)} X_{s,1,g}^{(\eta)}$. The dual space diversity RAKE demodulator structure state vectors $\mathbf{r}_{\mathbf{g}}^{(\eta)}$, $\phi_{\mathbf{g}}^{(\eta)}$, τ_2 are fixed for the desired users given channel condition. In order to obtain the conditional probability density function of I_1 we shall assume that the interferers transmitter oscillator phase θ_1 and channel introduced delays $\tau_{1,g}$ are fixed. Hence, for these given desired user channel parameters and interferer transmitter oscillator phase and channel delays, we define the following conditional constant,

$$K_{c,1,g,l}^{(\eta)} = r_1^{(\eta)} \cos\left(\theta_1 - \phi_1^{(\eta)}\right) R_{1,l}\left(\tau_{1,g}\right) + r_2^{(\eta)} \cos\left(\theta_1 - \phi_2^{(\eta)}\right) R_{1,l}\left(\tau_{1,g} - \tau_2\right) \tag{6.7}$$

and

$$K_{c,1,g,l}^{(\eta)} = r_1^{(\eta)} \sin\left(\theta_1 - \phi_1^{(\eta)}\right) R_{1,l}\left(\tau_{1,g}\right) + r_2^{(\eta)} \sin\left(\theta_1 - \phi_2^{(\eta)}\right) R_{1,l}\left(\tau_{1,g} - \tau_2\right) \quad (6.8)$$

for $\eta = 1, 2$ and $g = 1, 2$. The interferer terms,

$$X_{c,1,g}^{(\eta)} = r_{1,g}^{(\eta)} \cos\left(\Theta_{1,g}^{(\eta)}\right) \quad (6.9)$$

$$X_{s,1,g}^{(\eta)} = r_{1,g}^{(\eta)} \sin\left(\Theta_{1,g}^{(\eta)}\right) \quad (6.10)$$

are statistically independent Gaussian random variables. Hence, it can be shown that $E\left[X_{c,1,g}^{(\eta)}\right] = 0$, $E\left[X_{s,1,g}^{(\eta)}\right] = 0$, $E\left[\left\{X_{c,1,g}^{(\eta)}\right\}^2\right] = 1/2$ and $E\left[\left\{X_{s,1,g}^{(\eta)}\right\}^2\right] = 1/2$. Similarly it can be shown that $E\left[X_{c,1,g}^{(\eta)} X_{c,1,\acute{g}}^{(\acute{\eta})}\right] = 0$, $E\left[X_{c,1,g}^{(\eta)} X_{s,1,\acute{g}}^{(\acute{\eta})}\right] = 0$ and $E\left[X_{s,1,g}^{(\eta)} X_{s,1,\acute{g}}^{(\acute{\eta})}\right] = 0$ for $\acute{g} \neq g$ and $\acute{\eta} \neq \eta$.

As $K_{c,1,g,l}^{(\eta)}$ and $K_{c,1,g,l}^{(\eta)}$ are conditional constants, $X_{1,l}^{(\eta)}$ is comprised of a linear sum of statistically independent Gaussian random variables. Hence $X_{1,l}^{(\eta)}$ is a Gaussian random variable. The value of the cross correlation functions $R_{1,l}\left(\tau_{1,g}\right)$ and $R_{1,l}\left(\tau_{1,g} - \tau_2\right)$ depend upon the interfering signal baud l. Hence, for different interfering signal bauds l, $X_{1,l}^{(\eta)}$ are correlated Gaussian random variables.

The product term $I_{1,l}^{(\eta)} = X_{1,l}^{(\eta)} b_{1,l}$ is a Gaussian random variable. The characteristic function of this product term

$$E\left[\exp\left\{j\omega I_{1,l}^{(\eta)} b_{1,l}\right\}\right] = \frac{1}{2} E\left[\exp\left\{j\omega X_{1,l}^{(\eta)}\right\}\right] + \frac{1}{2} E\left[\exp\left\{-j\omega X_{1,l}^{(\eta)}\right\}\right] \quad (6.11)$$

where we have first taken the expectation with respect to $b_{1,l}$. We know that for a zero mean Gaussian random variable X, $E\left[\exp\left\{\pm j\omega X\right\}\right] = \exp\left\{-\omega^2 \sigma_X^2\right\}$. Hence

$$E\left[\exp\left\{j\omega X_{1,l}^{(\eta)} b_{1,l}\right\}\right] = \exp\left\{-\omega^2 \sigma^2\right\} \quad (6.12)$$

where $\sigma^2 = E\left[\left\{X_{1,l}^{(\eta)}\right\}^2\right]$.

The interference term $I_1^{(\eta)}$ is a sum of statistically independent Gaussian random variables. As $E\left[X_{1,l}b_{1,l}X_{1,\acute{l}}b_{1,\acute{l}}\right] = 0$ for $\acute{l} \neq l$, the covariance $\mathbf{COV}\left[X_{1,l}b_{1,l}, X_{1,\acute{l}}b_{1,\acute{l}}\right] = 0$. If two normal random variables are uncorrelated than they are independent. Since I_1 is a linear sum of statistically independent Gaussian randome variables, I_1 is Gaussian. We have assumed that the RAKE state vectors $\mathbf{r}_{\mathbf{g}}^{(\eta)}, \phi_{\mathbf{g}}^{(\eta)}, \tau_2$ and interferer transmitter oscillator phase and channel delays are fixed. Hence $I_1^{(\eta)}$ is conditionally a Gaussian random variable. Since the fading and uniform phase of the diversity paths are statistically independent, it can be shown that $I_1 = \frac{\lambda}{\sqrt{2}} \sum_{l=-3}^{3} X_{1,l}b_{1,l}$ is a Gaussian random variable, with conditional mean

$$E\left[I_1 \,|\, \mathcal{C}\right] = 0, \tag{6.13}$$

where space $\mathcal{C}$ represents a given set $\mathbf{r}_{\mathbf{g}}^{(\eta)}, \phi_{\mathbf{g}}^{(\eta)}, \tau_{\mathbf{2}}, \theta_1, \tau_{\mathbf{1,g}}$ and the conditional variance

$$\sigma^2_{I_1|\mathcal{C}} = \frac{\lambda^2}{2}\left[\frac{1}{2}\sum_{\eta=1}^{2}\left\{r_1^{(\eta)}\right\}^2 \sum_{l=-3}^{3}\sum_{g=1}^{2} R^2_{1,l}\left(\tau_{1,g}\right) + \frac{1}{2}\sum_{\eta=1}^{2}\left\{r_2^{(\eta)}\right\}^2 \sum_{l=-3}^{3}\sum_{g=1}^{2} R^2_{1,l}\left(\tau_{1,g}-\tau_2\right)\right.$$
$$\left. + \sum_{\eta=1}^{2} r_1^{(\eta)} r_2^{(\eta)} \cos\left(\phi_2^{(\eta)} - \phi_1^{(\eta)}\right) \sum_{l=-3}^{3}\sum_{g=1}^{2} R_{1,l}\left(\tau_{1,g}\right) R_{1,l}\left(\tau_{1,g}-\tau_2\right)\right], \tag{6.14}$$

does not depend on the transmitter oscillator phase θ_1.

6.4 Packet Error Rate with Multiple Access Interference

For a given channel and intersymbol interference, the conditional error rate

$$P_2[\,|\,\mathbf{r}_{\mathbf{g}}^{(\eta)}, \phi_{\mathbf{g}}^{(\eta)}, \tau_2, b_l, \tau_{\mathbf{1,g}}, \theta_1] = \frac{1}{2}\Pr\left[n_T + I_1 + \sum_{l=-2}^{2}{}' \varsigma_l b_l > A_S + \gamma_0\right]$$

$$+\frac{1}{2}\Pr\left[n_T + I_1 + \sum_{l=-2}^{2}{}' \varsigma_l b_l < -\left\{A_S + \gamma_0\right\}\right]. \tag{6.15}$$

The conditional error rate $P_2 = P_2[\,|\,\mathbf{r}_{\mathbf{g}}^{(\eta)}, \phi_{\mathbf{g}}^{(\eta)}, \tau_2, \tau_{\mathbf{1,g}}] = \left\langle P_2[\,|\,\mathbf{r}_{\mathbf{g}}^{(\eta)}, \phi_{\mathbf{g}}^{(\eta)}, \tau_2, b_l, \tau_{\mathbf{1,g}}]\right\rangle$ can be evaluated by the total probability theorem for the intersymbol interference

terms. The unconditional error rate $P_e = \langle P_2 \rangle$, where $\langle . \rangle$ is statistical averaging over the channel vector $\mathbf{r}_{\mathbf{g}}^{(\eta)}, \phi_{\mathbf{g}}^{(\eta)}, \tau_2$ and the interferers delay vector $\tau_{\mathbf{1},\mathbf{g}}$.

Using total probability theorem for pre and post-cursor interfering symbols, the error rate

$$P_2 = P_2^T = \frac{1}{32} \sum_{\substack{i_l=0 \\ l \in \Omega}}^{1} \operatorname{erfc} \left[\frac{A_S + \gamma_0 + \sum_{l=-2}^{2}{}' (2i_l - 1) \varsigma_l}{\sqrt{2 \quad \left(\sigma_n^2 + \sigma_{I_1}^2 \right)}} \right], \tag{6.16}$$

where the set Ω consists of elements $\{-2, -1, 1, 2\}$. In this case we have used the fact that the RAKE state vectors $\mathbf{r}_{\mathbf{g}}^{(\eta)}, \phi_{\mathbf{g}}^{(\eta)}, \tau_2$ and interferer transmitter oscillator phase and channel delays are fixed and hence I_1 is conditionally a Gaussian random variable. Thus the sum of the noise and interference terms are conditionally Gaussian.

If a packet has a size of N_b bits, then the probability of m bits in error [42],

$$P_m \left(N_b, m \right) = \frac{N_b!}{(N_b - m)! m} \left(1 - P_e \right)^{(N_b - m)} P_e^m. \tag{6.17}$$

One definition of packet error rate is the probability that all N_b bits are in error. Hence, the packet error rate

$$\begin{aligned} P_p &= 1 - P_m \left(N_b, 0 \right) \\ &= 1 - \left(1 - P_e \right)^{N_b}. \end{aligned} \tag{6.18}$$

6.5 Numerical Results

The conditional error rate is obtained from Eq. 6.16, while the unconditional error rate P_e obtained by Monte Carlo simulation of channel parameters and plotted in Fig. 6.1 is used to obtain packet error rate P_p (Eq. 6.18). For per branch SNR's $\rho = 14$ dB and 20 dB, P_p is 4% and 2.6% respectively.

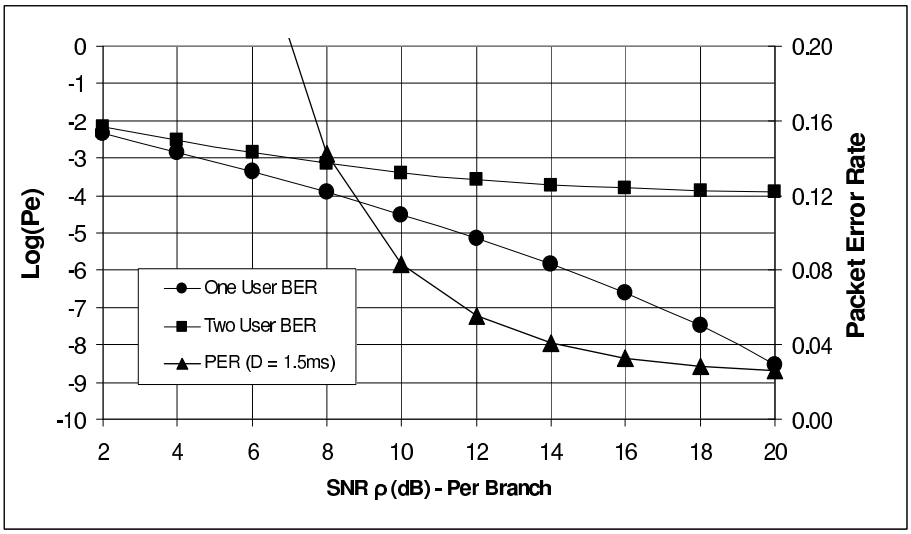

Figure 6.1. Packet Error Rate for a dual space diversity RAKE with 2 simultaneous bursts.

6.6 Conclusions

We determine that a high bit rate DS-SS BPSK reverse link can support two simultaneous bursts at a reasonably acceptable packet error rate. The error rate of the link with a frequency selective channel, dual space diversity RAKE and one continuous interferer is evaluated by using the total probability theorem for inter-symbol interference and by proving that the interference is conditionally Gaussian. Unconditional error rate is obtained by Monte Carlo simulation of the channel parameters. For per branch SNR's $\rho = 14$ dB and 20 dB the packet error rate is 4% and 2.6% respectively. Real systems shall have channel coding and decoding with packet retransmission which shall reduce the packet error rate. In packetized voice links (chapters 7 and 8), depending on the utilization factor, at any one instance there could be 0, 1 or 2 users transmitting high bit rate bursts. Hence, in packetized voice links the packet error rate would be lesser than that determined in this study.

CHAPTER 7

PACKET WAIT TIMES AND OUTAGE IN VOICE OVER IP SINGLE BURST WIRELESS REVERSE LINKS

For voice over IP wireless reverse links with a G/D/1 queue, where the radio channel supports only one radio burst (or one server) at any time with acceptable packet error rate, traffic induced expected packet wait times are obtained by deriving the modified Little's-multinomial analytical approximation for the first time. At high utilization factors where correlation between interarrival times results in high wait times, this method provides a better estimate of expected packet times than the M/D/1 queue approximation. An upper bound on the probability of outage, derived for the first time using Steffensen's inequality, is tighter than the Markov upper bound. These methods can be used to characterize base station traffic induced wait times for end-to-end delay budgets and Erlang capacity determination. At a 2% probability of outage and 60 ms wait time threshold, the voice over IP users supported by the G/D/1 queue is 26.

7.1 Introduction

Packetized wireless cellular systems with concurrent voice over IP [28], [33] and packet data services are evolving. Evaluation of Erlang capacity at a given expected voice packet wait time and packet error rate is an important consideration for spectral efficiency. For medium quality voice [24], the packet wait times should be less than 300 ms between mobile devices. Packet wait times introduced by queuing at the

base station must be a much smaller fraction of this limit. In addition obtaining probability of wait time outage, when quality of voice is unacceptable, is important.

In [25], a packetized voice process was fed to a T1 1.543 Mb / sec system to obtain expected packet wait times. A single user's packet stream consisted of talkspurts and a silence interval both having mean durations. The talkspurts packets was geometrically distributed, while the silence interval was exponentially distributed. The packet interarrival times was a renewal process with successive interarrival times being independent. For multiple independent voice users, the cumulative distribution function of the aggregate packet interarrival times, obtained by superposition, was very nearly exponential. The aggregate packet interarrival times, were obtained by monte carlo simulation of the superposition process of multiple users. The expected packet wait times, obtained by monte carlo simulation of the G/D/1 queue was compared to those obtained from the M/D/1 queue [26], [27]. For utilization factors greater than 0.8 (or users > 110), expected packet wait times were underestimated by the M/D/1 queue approximation due to correlated packet interarrival times.

For spread spectrum wireless voice over IP forward links [28], the base stations have a single queue and schedule packet transmission over a single high bit rate radio channel with 1% packet error rate. The packet wait times due to traffic induced queuing and radio retransmission was lumped together and obtained by using a modified M/D/1 queue. On the reverse link [28] each voice over IP user was assigned a high bit rate traffic channel for the duration of the call. Erlang capacity was determined by modifying the Erlang B formula [29], [30] for the M/M/m queue. Packet wait times was due to voice packet allignment with available frames and frame retransmissions. For the forward and reverse links the probability of outage was defined as 2% of packet wait times being greater than a delay bound [28] of 70 ms. In [31] probability of packet loss is obtained for a high data rate channel with low number

of voice over IP users using the M/M/1 queue with independent arrivals. Recently in [32] the batch arrivals process was used to approximate bursty correlated arrivals at an On-Off-G/D/1 queue to determine expected packet wait times. Hence, there is no analytical expected packet wait times for correlated interarrival times at G/D/1 queues. Also, there is no analytical probability of outage for traffic induced packet wait times.

For packetized data traffic reverse links [33], each mobile user has its own queue with forward and reverse dedicated control channels used to schedule traffic over a high bit rate bursting data channel. The radio channel can support a finite number of simultaneous high bit rate bursts at acceptable packet error rate. For the reverse link multiple queues and multiple radio channels or servers complicates determination of expected packet wait times.

In this chapter we derive the modified Little's-multinomial approximation for traffic induced expected packet wait times in voice over IP wireless reverse links with the G/D/1 queue and scheduled transmission. We assume a voice coding scheme [34] with header compression, voice packet duration of 20 ms at 9.6 kb / sec. We modify [35] the parameters of the single and multiple voice user packet interarrival time model [25]. We assume that the reverse radio channel can support a single high bit rate bursts at 174.2 kb / sec. [16] with duration of 1.5 ms at a low packet error rate. Each voice over IP mobile has its own queue with forward and reverse dedicated control channels that are used to schedule traffic over a high bit rate bursting data channel. We assume a single virtual queue at the base station is equivalent to many physical mobile queues. This virtual queue has correlated interarrival times for the superposition of all links. If the radio channel supports one high bit rate burst (or server) at any time with acceptable packet error rate, then all mobiles share usage of this one burst that is coupled to a G/D/1 virtual queue at the base station. We

apply Little's theorem [26], [36], [37], [38], [39] to a reference users talkspurt-silence duration or the busy period divided into three intervals. Statistically independent packet arrival times from individual users are used to determine conditional expected packet wait time and carry over delays, given overlapping talkspurts. The probability of overlapping talkspurts determined from the multinomial distribution is used to obtain expected packet wait times by applying total probability theorem. At high utilization factors (operating point of interest), the modified Little's-multinomial analytical approximation provides a better estimate than the M/D/1 queue approximation when compared to simulations of the superposition process for multiple users and G/D/1 queue.

In this chapter, Steffensens inequality is used to derive an upper bound on the probability of outage that is applicable at any wait time thresholds. Statistically only an analytical approximation on the first moment of packet wait time and the probability of wait time being zero is known. The Kingman [40] upper bound on the tails of the waiting time distribution cannot be applied as wait times and interarrival times are correlated. The Chernoff bound and Chebyshev inequality cannot be used as the moment generating function and second moment of the wait time is not known while the Markov inequality is a weak upper bound. Using our bound at a 2% probability of outage and 60 ms wait time threshold, the voice over IP users supported by the G/D/1 queue is 26, which is 4.8% less than that compared to simulation results.

There are several differences between our work and previous studies. We derive the modified Little's-multinomial analytical approximation for expected packet wait time in voice over IP wireless reverse links with the G/D/1 queue, at high utilization factors, for the first time. In [25] expected packet wait times are obtained for a land line T1 system with packetized voice at high utilization by simulation and using the M/D/1 queue approximation. Similarly, [28] assumes a high data rate continuous

channel for the voice over IP reverse link and uses the modified M/M/m queue. While [31] assumes a high bit rate channel with the M/M/1 queue. Additionally our analysis treats traffic induced packet wait time separately, while [28] lumps traffic induced and retransmission wait times together. This enables assessment of radio layer introduced wait times due to retransmission separately. Finally, [32] uses the batch arrivals process to approximate bursty correlated arrivals while we use the single user voice over IP packet arrivals. Our Steffensens upper bound on probability of outage is for traffic induced packet wait times while in [28] outage is for frame alignment and retransmission wait times. In addition our Steffensens upper bound on probability of outage can be used for any wait time threshold while [28] is specific to a outage of 2%. Our analytical methods can be used for system design, characterization of base station traffic induced wait times and Erlang capacity determination. Finally, our methods are applied in the next chapter to reverse links which can support two simultaneous bursts coupled to a G/D/2 queue.

7.2 Voice over IP Wireless Reverse Links

We consider many voice over IP mobile users in a single sector where call session arrivals are Poisson with exponential call session hold times while speech packets have a duration of T_{vp} ms. As shown in Fig. 7.1 each voice over IP mobile has its own queue with forward and reverse dedicated control channels that are used to schedule traffic over a high bit rate bursting data channel. Speech packets are transmitted, by a bursting high bit rate data channel at 174.2 kb / sec [16] with a frame duration of $D = 1.5$ ms whose transmission is scheduled by the base station. The base station has a scheduler that uses the First-In-First-Out (FIFO) queuing discipline. We assume a single virtual queue at the base station is equivalent to many physical mobile queues. This virtual queue has correlated interarrival times for the superposition of all links.

If the radio channel supports S_T simultaneous high bit rate bursts (or servers) at acceptable[1] packet error rate, then all mobiles share usage of these S_T bursts that are coupled to a G/D/S$_T$ virtual queue at the base station. In this chapter $S_T = 1$ and in chapter 8 $S_T = 1$.

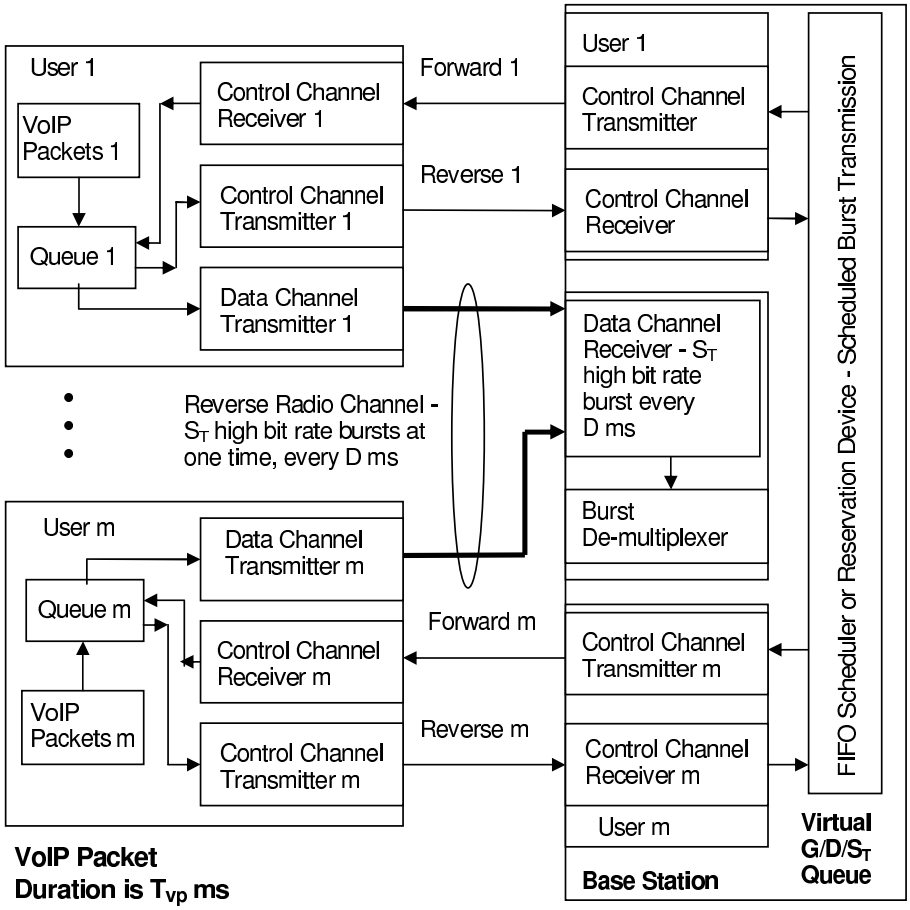

Figure 7.1. Multiple voice over IP users reverse links, radio channel or server that supports S_T simultaneous bursts every D ms and virtual G/D/S_T queue model at the base station.

[1]In Chapter 6 the radio channel supports at maximum two simultaneous high bit rate bursts at reasonably acceptable packet error rates $\approx 2.6\%$ with no coding or retransmission.

7.2.1 Single Voice over IP User Interarrival Times

We use the ITU G.729 coding scheme [34] for speech where two speech frames are packed into a single voice packet. The voice coder with a compressed header of 4 bytes generates voice packets 20 ms long at a rate of 9.6 kb / sec. We modify the packet interarrival time probability density function of [25] for a single packetized voice source using above specification for voice packets. The voice packetization period $T_{vp} = 20$ ms, number of packets N_{vp} in the talkspurt is geometrically distributed, mean talkspurt duration $\alpha^{-1} = 360$ ms and mean number of packets per talkspurt $E[N_{vp}] = 18$. While silence periods are exponentially distributed with mean silence duration $\beta^{-1} = 650$ ms. For a single voice over IP user the probability density function of the packet interarrival times

$$f_{IA}(t) = \begin{cases} 0 & t < T_{vp} \\ p\delta(t - T_{vp}) & t = T_{vp} \\ (1-p)\beta e^{-\beta(t-T_{vp})} & t > T_{vp} \end{cases}, \tag{7.1}$$

where $p = 17/18$. The expected packet interarrival time for a single user

$$\frac{1}{\lambda_{vp}} = \frac{\beta T_{vp} + 1 - p}{\beta}. \tag{7.2}$$

7.2.2 Multiple Voice over IP User Interarrival Times

The cumulative distribution function of packet interarrival times [25] for the superposition of m voice over IP users

$$F_m(t) = \begin{cases} 1 - (1 - \lambda_{vp} t)^{m-1} & 0 \le t \le T_{vp} \\ 1 - \frac{(1-p)^m e^{-\beta m (t - T_{vp})}}{(\beta T_{vp} + 1 - p)^{m-1}} & t \ge T_{vp} \end{cases}, \tag{7.3}$$

where the consecutive packets interarrival times, t, are correlated. In Eq. 1 of [25], the $k-$interval squared coefficient of variation sequence was used as a measure of

cumulative covariances among k consecutive interarrival times. In the multiple user arrival process, as m increases, a greater number of consecutive nearby interarrival times are nearly uncorrelated and also have small negative covariances. For a fixed m, the long term interarrival times covariances become positive (Fig. 4 of [25]) with large values that depicts variability (deviation from a Poisson process) in the superposition process. The k^{th} moment of the interarrival times [25]

$$\begin{aligned} E\left[t^k\right] &= \frac{k!}{\lambda_{vp}^k} \frac{1}{m\,(m+1)\cdots(m+k-1)} \\ &-\frac{k}{\lambda_{vp}^k} \sum_{i=0}^{k-1} (-1)^i \begin{pmatrix} k-1 \\ i \end{pmatrix} \frac{(1-\lambda_{vp}T_{vp})^{m+i}}{m+i} \\ &-\frac{k\,(1-p)^m}{\beta^k m^k\,(\beta T_{vp}+1-p)^{m-1}} \sum_{i=0}^{k-1} \frac{(k-1)!}{i!}\,(\beta m T_{vp})^i \end{aligned} \tag{7.4}$$

where $k \leq 4$ and $\begin{pmatrix} k-1 \\ i \end{pmatrix}$ are binomial coefficients.

7.2.3 G/D/1 Queue and Packet Wait Times

Consider the wait times incurred by voice packets, shown in Figs. 7.2 and 7.3, of a first-in-first-out queuing discipline system. In Fig. 7.2, the $n+1^{th}$ packet, C_{n+1}, arrives at the queue with unlimited waiting room and finds the server busy. After, the n^{th} packet departs from the server, C_{n+1} moves from the queue to the server and incurs a wait time w_{n+1}. In Fig. 7.3, a packet C_{n+1} arrives at the queue and finds the server idle for a time period y_n. The packet C_{n+1} moves from the queue to the server and has incurred no wait time. Thus the $n+1^{th}$ packets wait time

$$w_{n+1} = \begin{cases} w_n + D - t_{n+1} & w_n > t_{n+1} - D \\ 0 & w_n \leq t_{n+1} - D \end{cases} \tag{7.5}$$

where t_{n+1} is the interarrival time between packets C_n and C_{n+1}, and the radio burst or the server transmission interval is D. From [26],

$$w_{n+1} - y_n = w_n + D - t_{n+1} \tag{7.6}$$

where $y_n \geq 0$. When $y_n > 0$, $w_{n+1} = 0$ and when $y_n = 0$, $w_{n+1} > 0$ which means that $w_{n+1}y_n = 0$.

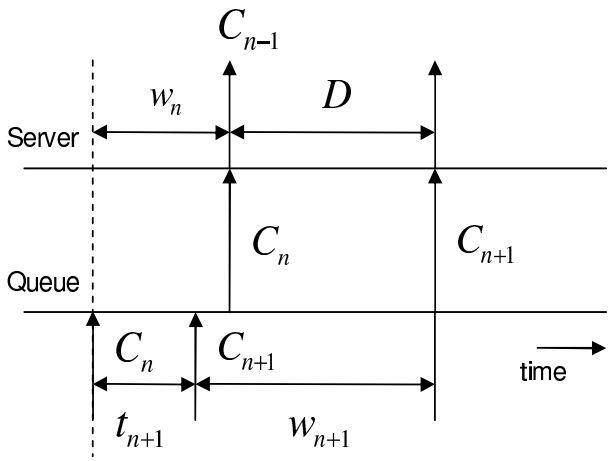

Figure 7.2. Packet arrives and finds server busy..

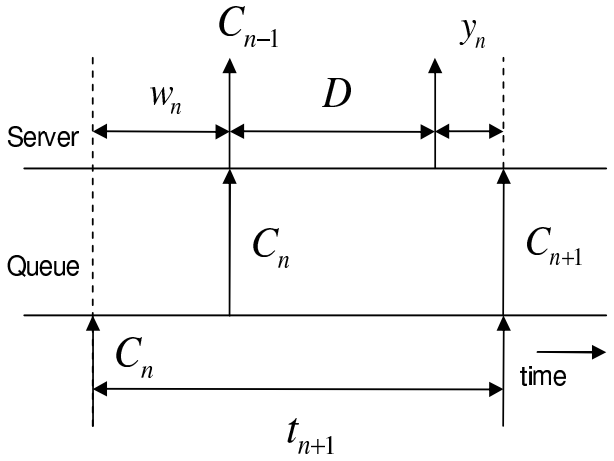

Figure 7.3. Packet arrives and finds server idle..

The utilization factor $\rho_1 = D/E[t]$ and $\Pr[w_n = 0] = 1 - \rho_1$. In our model for multiple voice over IP users, the voice packet interarrival times t_n and t_{n+1} are correlated and assumed to be stationary. The long term positive covariance [25] among interarrival times begin to affect the queue at high values of ρ_1 and have a greater influence on the increase in packet wait times.

7.3 Expected Packet Wait Time

For the wireless reverse links of Sec. 7.2, expected packet wait times, obtained by the modified Little's-multinomial analytical approximation, M/D/1 queue approximation and simulation are compared in Fig. 7.4. Since simulation takes time and resources, in the next sub-section we derive an approximation for the expected packet wait times using Little's theorem and the multinomial distribution. This can be used in design. For large number of users, as shown in Tab. 7.1 and Fig. 7.4, the M/D/1 queue approximation underestimates expected packet wait times, while the modified Little's-multinomial approximation provides a better estimate.

In Fig. 7.4, for $\rho_1 < 0.58$ or $m < 22$ users the M/D/1 queue expected packet wait times approximation can be used as a good estimate. The modified Little's-multinomial analytical expected packet wait times approximation are useful when $0.58 \leq \rho_1 \leq 0.90$ or $22 \leq m \leq 33$ users. In the worst case, the expected packet wait times obtained by the modified Little's-multinomial analytical approximation is 2.2 times that obtained by simulation. For $\rho_1 > 0.90$ or $m > 33$ users, the modified Little's-multinomial analytical approximation underestimates expected packet wait times. In packetized wireless systems, typically the radio queue related expected packet wait times would be on the order of 30 ms in order to meet the overall end-to-end delay budget. Hence obtaining queue delays for the range $22 \leq m \leq 33$ is important for system design.

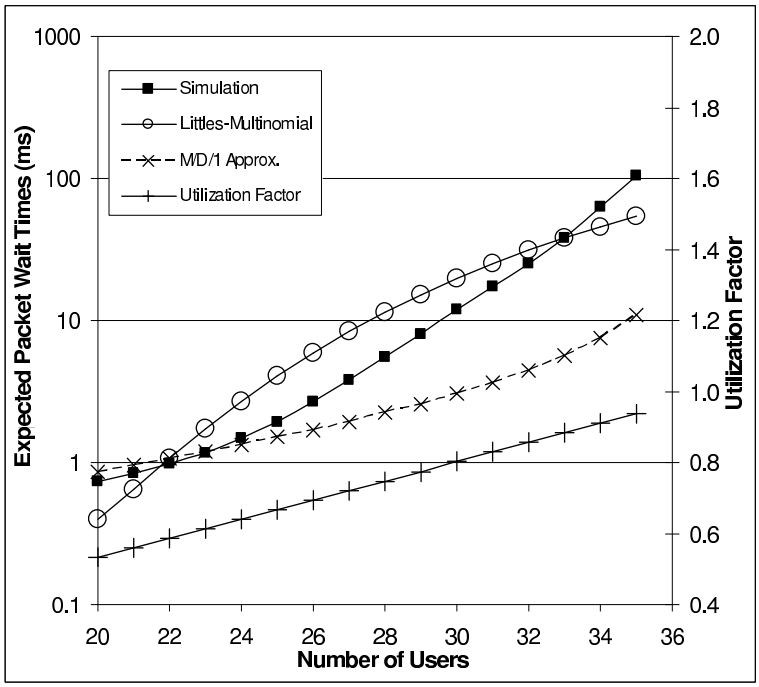

Figure 7.4. Expected packet wait times for a Wireless system.

Table 7.1. Expected packet wait times verses number of users

m	*E[w] (ms) M/D/1 Approx.*	*E[w] (ms) Simulation*	*E[w] (ms) Little's-multinomial*	ρ_1 *Utilization factor*
20	0.86	0.73	0.40	0.54
22	1.07	0.98	1.06	0.59
25	1.51	1.95	4.08	0.67
26	1.71	2.67	5.96	0.69
28	2.23	5.57	11.53	0.75
29	2.59	8.10	15.33	0.78
31	3.63	17.12	25.16	0.83
32	4.44	25.39	31.20	0.86
34	7.48	62.49	45.49	0.90
35	10.90	105.5	53.69	0.94

7.3.1 Modified Little's-Multinomial Approximation

An analytical approximation for the expected packet wait time is derived in the next few sections by applying Little's theorem [26], [36], [37], [38], [39], the multi-

nomial distribution and the total probability theorem. In our model (Fig. 7.1), all users that offer packetized voice traffic to the system are statistically independent. To derive expected packet wait time, a reference users talkspurt-silence duration is divided into three intervals as shown in Fig. 7.5 and during each interval the packet arrivals from other individual users are considered. During each interval the conditional expected packet wait time for a given number of other user talkspurts, that are overlapping (Fig. 7.5) with the reference users interval, is determined using Little's theorem. The per interval carry over delays caused by the previous interval are also determined. The multinomial distribution is used to determine the probability of the number of other user talkspurts that align with the reference users talkspurt and silence intervals. Finally, total probability theorem is used to obtain the unconditional expected packet wait times. The superposition of all users packet arrivals at the virtual queue (Fig. 7.1), assumed to exist at the base station, shall result in correlated interarrival times. By using individual users packet arrivals, our method overcomes the need for mathematical treatment of correlated interarrival times.

7.3.2 Talkspurt Alignment and Busy Period

As shown in Fig. 7.5 the reference users talkspurt-silence duration $0 \leq t \leq T_{TS-S}$ is assumed as the busy period [38]. The queue is recurringly empty since $\rho_1 < 1$, which results in a reset [38] of the arrival and waiting processes. An empty queue marks the end of a busy period while the arrival of the next packet marks the end of this busy cycle and the start of a new busy cycle [38]. The number of packets, the packet interarrival times from the superposition process and wait times in a busy cycle are statistically independent and identical (Assumption II [38]) to those in each busy cycle. However, in one busy cycle the packet interarrival times

from the superposition process are correlated. It is assumed that the busy cycle duration is greater than T_{TS-S}.

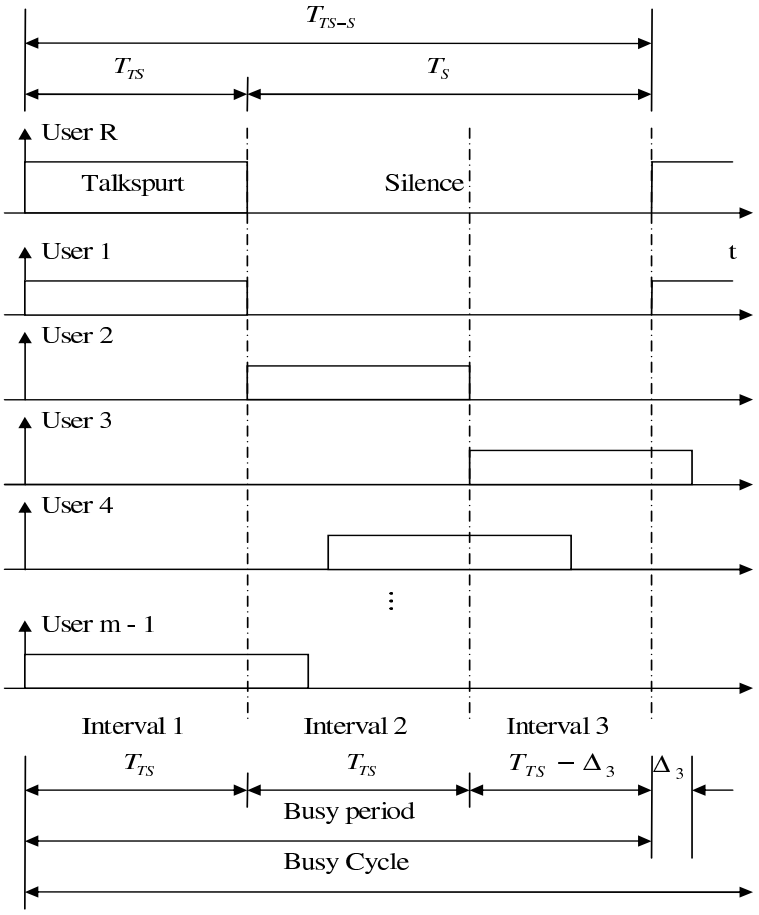

Figure 7.5. The reference users talkspurt-silence interval and alignment of other users talkspurts with the reference user. The busy period is divided into three intervals and the busy cycle extends beyond the talkspurt-silence interval.

We further divide our busy period into 3 intervals $I_1 = \{0 \leq t < T_{TS}\}$, $I_2 = \{T_{TS} \leq t < 2T_{TS}\}$ and $I_3 = \{2T_{TS} \leq t \leq T_{TS-S}\}$ as shown in Fig. 7.5, while the interval $\Delta_3 = 2T_{TS} - T_S$. As described in Sec. 7.2.1, the reference user has a mean talkspurt duration $\alpha^{-1} = 360$ ms and we shall define the reference talkspurt duration $T_{TS} = 360$ ms. Similarly, from Sec. 7.2.1, the reference user has a mean silence

duration $\beta^{-1} = 650$ ms and we shall define the reference silence duration $T_S = 650$ ms. Hence, the reference busy period is $T_{TS-S} = T_{TS} + T_S = 1010$ ms. The next busy cycle starts due to the occurrence of an idle time interval which can occur for $t > T_{TS-S}$.

In Fig. 7.5, user 1, user 2 and user 3's, talkspurt-silence intervals are assumed to depict three basic realizations $r = 1, 2, 3$. Although talkspurt-silence durations for each user is random, for simplicity in analysis it is assumed that these users also have same talkspurt and silence durations of T_{TS} and T_S respectively. To reduce complexity we further assume that the $m-1$ users talkspurt-silence realization shall be one of the three basic realizations $r = 1, 2, 3$. In reality each users talkspurt can start at any instance of time. More than 3 realizations for better accuracy increases complexity of quasi analytical simulation.

During the reference user's talkspurt, talkspurts of other users can line up. In general during interval I_j, the 2^{nd} user, 3^{rd} user or up to the $m-1$ users talkspurts can align. The packet interarrival times during the time interval I_1 depends upon the number of talkspurts that coincide with the reference users talkspurt. If $m - 1 = 34$ talkspurts coincide with the reference talkspurt the interarrival times during I_1 is extremely small. However, if 13 talkspurts coincide with the reference talkspurt the interarrival times during I_1 is larger than the scenario described above. With this simplified model the expected interarrival times during I_1,

$$E[t_n] = \frac{T_{TS}}{mE[N_{vp}]}. \tag{7.7}$$

When a large number of users talkspurts align, many packet interarrival times end up being small (or $t_n < D$) and clustered together resulting in correlated interarrival times. Under such conditions the packet wait times can be extremely large.

7.3.3 Conditional Expected Packet Wait Time per Interval

As shown in Fig. 7.6, during each interval, I_j, the conditional expected packet wait time $E\left[w_{n,j}|k_1, k_2, k_3\right]$ for a given aligned talkspurt count $[k_1, k_2, k_3]$ is determined using Little's theorem. For a given number of aligned talkspurts k_j per interval I_j, the packet arrivals γ_j and packets present L_j are also determined.

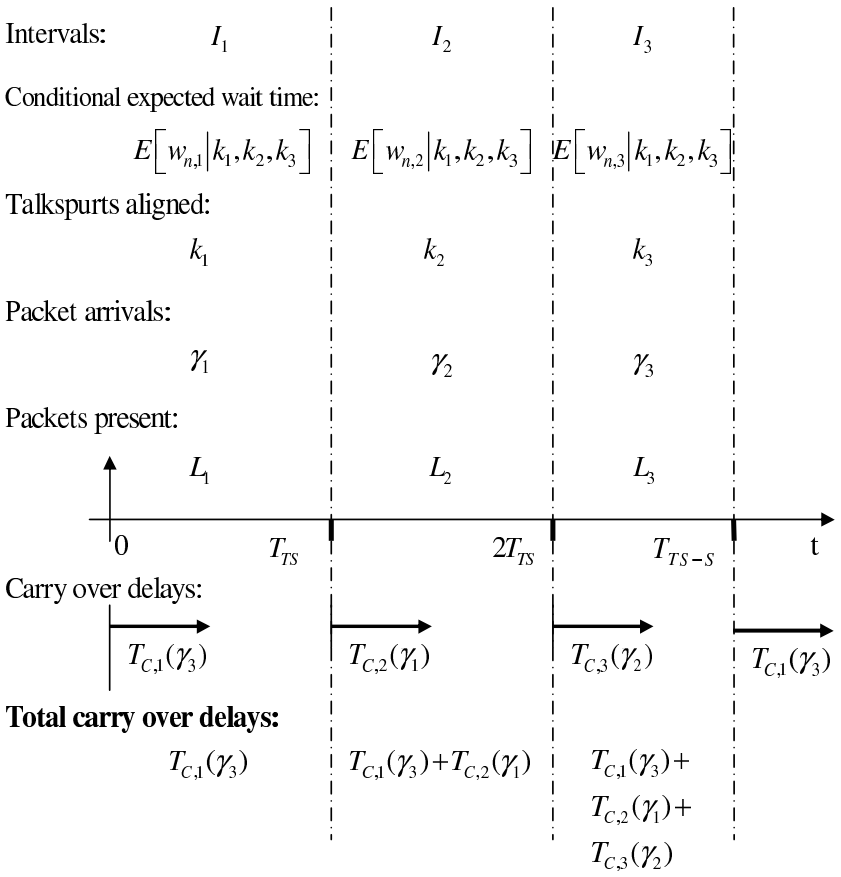

Figure 7.6. One busy periods per interval conditional expected packet wait times, number of talkpurts aligned, number of packet arrivals and number of packets present. Total carry over delays due to cumulative effects of per interval carry over delays.

From Little's Theorem [26], [36], the average number of packets present,

$$L = \xi W, \tag{7.8}$$

where ξ is the average packet arrival rate and W is the average packet wait time in the queue. If the instantaneous packets present in the queue is $L(x)$, Little's theorem can be expressed as [36];

$$\lim_{T_L \to \infty} \frac{1}{T_L} \int_0^{T_L} L\left(x\right) dx = \xi \lim_{N_p \to \infty} \frac{1}{N_p} \sum_{n=0}^{N_p} w_n \tag{7.9}$$

where w_n is the n^{th} packets wait time and N_p is the number of packets processed (arrived, waited and departed). From [26], [38], the instantaneous packets present

$$L\left(x\right) = \gamma\left(x\right) - \psi\left(x\right) \tag{7.10}$$

where $\gamma\left(x\right)$ is the number of packet arrivals to the queue in $(0, x)$ and $\psi\left(x\right)$ is the number of packet departures from the queue in $(0, x)$. The instantaneous packets present (see Fig. 1 of [38]) is the difference between the cumulative number of arrivals and the cumulative number of departures, while $\int_0^{T_L} L\left(x\right) dx$ is the area between the curves for $\gamma\left(x\right)$ and $\psi\left(x\right)$. Or $\int_0^{T_L} L\left(x\right) dx$ is the area under the curve $\gamma\left(x\right)$ minus the area under the curve $\psi\left(x\right)$. In order to apply Little's theorem identification of T_L is crucial. One could assume that T_L is the duration of the the busy period [38] which in this model is T_{TS-S}. However, for this system as the superposition process for arrivals deviates from the Poisson process, in this model Little's theorem is modified by applying it to three intervals of the busy period. In other words in this model T_L is the duration of the interval I_j. The packets present per interval in the queue until the time T_L is used to obtain the conditional waiting time of the packets that arrive during this interval I_j.

The conditional expected packet wait times in I_1,

$$E\left[w_{n,1} | k_1, k_2, k_3\right] = \frac{L_1}{\xi_m}. \tag{7.11}$$

The first moment of the interarrival time $E[t_n]$ for m users is obtained from Eq. 7.4. Hence, the packet arrival rate for m users

$$\xi_m = \frac{1}{E[t_n]} \tag{7.12}$$

The number of packets present in I_1

$$L_1 = \frac{1}{T_{TS}} \int_0^{T_{TS}} \gamma_1(x)\, dx - \frac{1}{T_{TS}} \int_0^{T_{TS}} \psi_1(x)\, dx \tag{7.13}$$

Using geometry for the areas under the curves for $\gamma_1(x)$ and $\psi_1(x)$,

$$L_1 = \frac{\gamma_1(k_1, k_2, k_3)}{2} - \frac{\psi_1}{2} \tag{7.14}$$

where the total arrivals in I_1 or in $(0, T_{TS})$

$$\gamma_1(k_1, k_2, k_3) = E[N_{vp}] + E[N_{vp}]\, k_1 + \frac{\Delta_3}{T_{vp}} k_3. \tag{7.15}$$

For this it is assumed [37] that each packets wait time is charged at the instant of its arrival and an arrival occurs at $t = 0$ and $t \approx T_{TS}$. The packets that depart from the queue, shall be transmitted over the radio channel every D seconds. The total departures in I_1 or in $(0, T_{TS})$

$$\psi_1 = \frac{S_T T_{TS}}{D}, \tag{7.16}$$

where total servers $S_T = 1$ in this system. Finally as $L_j \geq 0$,

$$L_1 = Max\left[\frac{\gamma_1(k_1, k_2, k_3)}{2} - \frac{S_T T_{TS}}{2D}, 0\right]. \tag{7.17}$$

Similarly the conditional expected packet wait time for I_2 and I_3 can be obtained. The conditional expected packet wait times can be determined for a sample point of a space [39] and than averaged over all points of the space as discussed in a later section. In our model, the space is the number of aligned talkspurts per interval.

7.3.4 Conditional Carry Over Delays per Interval

In [39], [38] the residual waiting time for packets present before $t = 0$, is also considered where required. In the model shown in Fig. 7.6, for a given aligned talkspurt count $[k_1, k_2, k_3]$, the carry over effects are considered to be added delays $[T_{C,1}(\gamma_3), T_{C,2}(\gamma_1), T_{C,3}(\gamma_2)]$ to the packets in each interval. During interval I_{j-1} if the number of arrivals is greater than the number of departures, than departures of packets arrived during I_{j-1} continue to occur during I_j. These departures beyond I_{j-1} cause carry over delays to packets in I_j. If the first packet of I_j gets delayed due to carry over delay effects from I_{j-1}, all subsequent packets of I_j also get delayed by the same magnitude of delay. Thus each packet of I_j incurs a delay due to carry over effects from I_{j-1} and wait time due to packets that arrive during I_j.

All packets in I_1 are delayed due to carry over delays $T_{C,1}(\gamma_3)$ from the previous busy cycle. All packets in I_2 are delayed due to $T_{C,1}(\gamma_3) + T_{C,2}(\gamma_1)$, where $T_{C,2}(\gamma_1)$ is the carry over delay due to packets in I_1. Similarly all packets in I_3 get affected by carry over effects. The carry over delays in I_1, due to the packets in I_3,

$$T_{C,1}(\gamma_3) = \frac{1}{S_T}\left\{\gamma_3(k_1, k_2, k_3) - \frac{S_T(T_{TS} - \Delta_3)}{D}\right\} D \tag{7.18}$$

where $S_T(T_{TS} - \Delta_3)/D$ is the number of departures in I_3 and $S_T = 1$ in this system. Since $T_{C,1}(\gamma_3) \geq 0$,

$$T_{C,1}(\gamma_3) = Max\left[\left\{\frac{\gamma_3(k_1, k_2, k_3) D - S_T(T_{TS} - \Delta_3)}{S_T}\right\}, 0\right]. \tag{7.19}$$

Similarly, the carry over delays for I_2 and I_3 can be obtained.

7.3.5 Unconditional Expected Packet Wait Times

The unconditional expected packet wait times is determined by using total probability theorem where the space is partitioned based on the number of aligned

talkspurts. In Sec. 7.3.4 the conditional expected wait time, number of packets present along with number of arrivals and departures is derived for I_1. In Sec. 7.3.3 the conditional carry over delay for I_1 is derived. Extending derivation for I_2 and I_3, the unconditional expected packet wait times at the queue, during the busy period,

$$E[w_n] = \sum_{j=0}^{3} \sum_{k_2=0}^{m-1-k_1} \sum_{k_1=0}^{m-1} \left\{ \sum_{g=1}^{j} T_{C,g}\left(\gamma_{Mod_2[2+g-1]+1}\right) + E[w_{n,j}|k_1,k_2,k_3] \right\} \times \frac{\gamma_j(k_1,k_2,k_3)}{\gamma_T} \times \Pr[k_1,k_2,k_3] \tag{7.20}$$

where $k_3 = m-1-k_1-k_2$. The conditional expected packet wait times in I_j

$$E[w_{n,j}|k_1,k_2,k_3] = \frac{L_j}{\xi_m}. \tag{7.21}$$

The packet arrival rate for m users $\xi_m = \frac{1}{E[t_n]}$ where $E[t_n]$ for m users is from Eq. 7.4. The number of packets present L_j in I_j

$$L_j = \begin{cases} \frac{1}{T_{TS}} \int_{(j-1)T_{TS}}^{jT_{TS}} [\gamma_j(x) - \psi_j(x)]\, dx & j = 1,2 \\ \frac{1}{T_{TS}-\Delta_3} \int_{(j-1)T_{TS}}^{T_{TS}-S} [\gamma_j(x) - \psi_j(x)]\, dx & j = 3 \end{cases}, \tag{7.22}$$

can be shown to be

$$L_j = \begin{cases} Max\left[\frac{\gamma_j(k_1,k_2,k_3)}{2} - \frac{S_T T_{TS}}{2D}, 0\right] & j = 1,2 \\ Max\left[\frac{\gamma_j(k_1,k_2,k_3)}{2} - \frac{S_T(T_{TS}-\Delta_3)}{2D}, 0\right] & j = 3 \end{cases}, \tag{7.23}$$

where $S_T = 1$ in this system and the packet departures during I_3 can be rounded off. Here, during I_j, the number of packet arrivals

$$\gamma_j(k_1,k_2,k_3) = \begin{cases} E[N_{vp}] + E[N_{vp}]\, k_1 + \frac{\Delta_3}{T_{vp}} k_3 & j = 1 \\ E[N_{vp}]\, k_2 & j = 2 \\ Max\left[E[N_{vp}]\, k_3 - \frac{\Delta_3}{T_{vp}} k_3, 0\right] & j = 3 \end{cases}. \tag{7.24}$$

where interval $\Delta_3 = 2T_{TS} - T_S$.

The conditional carry over delays, during I_j,

$$T_{C,g}\left(\gamma_{Mod_2[2+g-1]+1}\right) = \begin{cases} Max\left[\left\{\frac{\gamma_3(k_1,k_2,k_3)D-S_T(T_{TS}-\Delta_3)}{S_T}\right\},0\right] & g=1 \\ Max\left[\left\{\frac{\gamma_{g-1}(k_1,k_2,k_3)D-S_TT_{TS}}{S_T}\right\},0\right] & g=2,3 \end{cases}, \tag{7.25}$$

with $S_T = 1$ for this system.

The total packet arrivals during the busy period,

$$\gamma_T = \sum_{j=1}^{3} \gamma_j\left(k_1,k_2,k_3\right). \tag{7.26}$$

The conditional expected packet wait time across the busy period or the reference talkspurt-silence interval 0 *to* T_{TS-S} is obtained by using a weighted average where the weight for the j^{th} interval is $\frac{\gamma_j(k_1,k_2,k_3)}{\gamma_T}$.

In our simple model (Fig. 7.5) each of the $m-1$ users talkspurt-silence realization end up being one of the three reference realizations depicted by user 1, user 2 and user 3's, talkspurt-silence realizations. For $m-1$ users we now have a sequence of $m-1$ independent trials and at each trial there are three possible outcomes corresponding to the three basic realizations shown in Fig. 7.5. Each realization $r = 1,2,3$ has the respective probabilities of p_1, p_2, p_3. In this sequence of $m-1$ trials , the r^{th} realization occurs k_r time. The joint probability that in the $m-1$ trials the r^{th} outcome occurs k_r times is given by a multinomial distribution

$$\Pr\left[k_1,k_2,k_3\right] = \frac{(m-1)!}{k_1!k_2!k_3!}p_1^{k_1}p_2^{k_2}p_3^{k_3} \tag{7.27}$$

where $p_1 = p_2 = T_{TS}/\left(T_{TS}+T_S\right)$ and $p_3 = 1-p_1-p_2$ to ensure ergodicity of the occurrence of talkspurts in the intervals. Finally, in the limiting case due stationarity $E[w] = E[w_n]$.

7.4 Probability of Outage

The probability of outage, defined as the probability that the wait time exceeds a threshold wait time w_{th} which is considered to be unacceptable to voice quality,

$$P_{outage} = Pr\left[w > w_{th}\right]. \tag{7.28}$$

An upper bound on the probability of outage, derived in the next section using Steffensens inequality, at different thresholds is compared to simulation results in Fig. 7.7, Fig. 7.8 and Table 7.2, for $m = 25$ and 32. As shown in the graphs, Steffensens upper bound is tighter than the simple Markov upper bound. For $m = 25$ (32) in the range of $30 \leq w_{th} \leq 60$, the Steffensens upper bound varies between 7.9 (2.4) to 4 (2.7) times the probability of outage obtained by simulation. This range of w_{th} would be comparable to the latency bound defined in [28]. Similar trends are observed in the probability of outage graphs for other users where $20 \leq m \leq 33$.

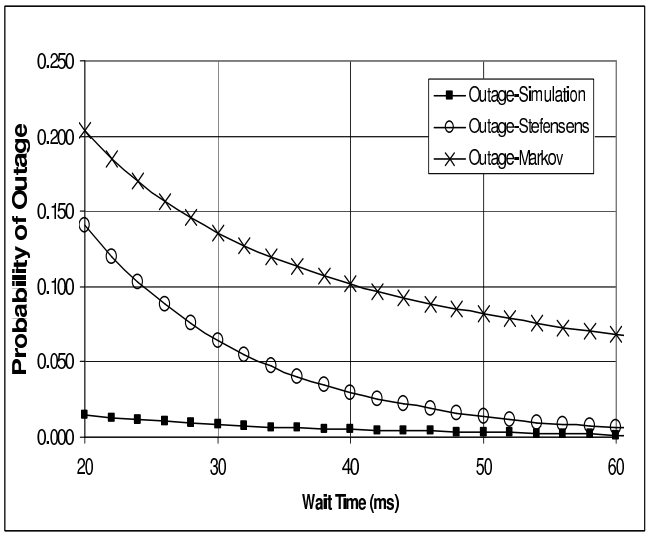

Figure 7.7. P_{outage} for $m = 25$ and $\rho_1 = 0.67$..

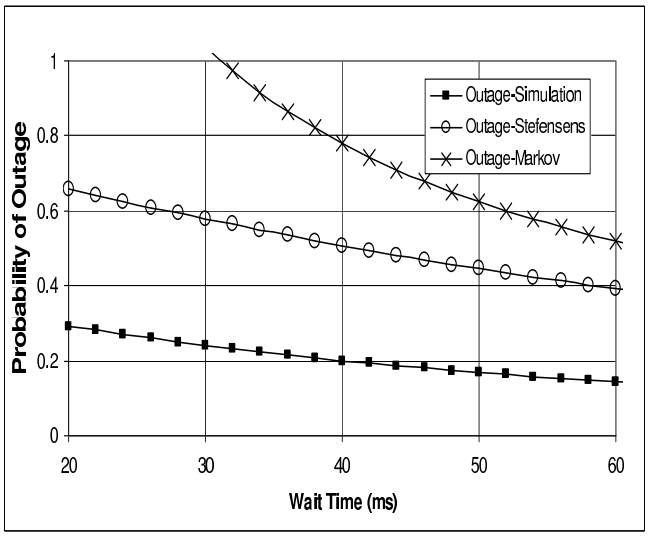

Figure 7.8. P_{outage} for $m = 32$ and $\rho_1 = 0.86$..

Table 7.2. P_{outage} for G/D/1 Queue - Comparison of simulation and Steffensens upper bound

m	$\Pr[w > 30ms]$ *Simulation*	$\Pr[w > 30ms]$ *Steffensens*	$\Pr[w > 60ms]$ *Simulation*	$\Pr[w > 60ms]$ *Steffensens*
25	0.0082	0.0643	0.0015	0.0061
26	0.0162	0.1314	0.0037	0.0248
28	0.0494	0.2960	0.0184	0.1170
29	0.0790	0.3765	0.0330	0.1828
30	0.1188	0.4505	0.0569	0.2531
31	0.1689	0.5176	0.0898	0.3233
32	0.2400	0.5782	0.1430	0.3908

7.4.1 Upper Bound using Steffensen's Inequality

In cases of a large number of users, an analytic approximation for packet wait times and the probability of wait time being zero is known. The Kingman [40] upper bound on the tails of the waiting time distribution cannot be applied as wait times and interarrival times are correlated. To obtain an upper bound on probability of outage, the Chernoff bound cannot be used since the moment generating function

of the wait time is not known. The Chebyshev inequality cannot be used as of the second moment of wait times is not known. While the Markov inequality

$$Pr\left[w > w_{th}\right] \leq E\left[w\right]/w_{th} \tag{7.29}$$

is a weak upper bound.

We derive an upper bound on the probability of outage using Steffensens's inequality [66], [67],

$$\int_a^b g_1(x)v(x)dx \leq \int_a^b g_2(x)v(x)dx \tag{7.30}$$

where $v(x)$ is a monotonically increasing function. The functions $g_1(x)$ and $g_2(x)$ are integrable on the interval $[a, b]$. The inequality in Eq. 7.30 can be proved [67] if the following two conditions hold true:

$$\int_a^x g_1(z)dz \geq \int_a^x g_2(z)dz \qquad\qquad x \in (a, b) \tag{7.31}$$

and

$$\int_a^b g_1(z)dz = \int_a^b g_2(z)dz. \tag{7.32}$$

We shall use the Steffensens inequality by assuming that Eq. 7.31 can be proved if Eq. 7.30 is true. The first density function is the actual probability density function of the wait time, or,

$$g_1(w) = \Pr\left[w = 0\right]\delta\left(w\right) + \Pr\left[w > 0\right]f_c(w) \tag{7.33}$$

where $\rho_S f_c(w)$, the continuous part of the probability density function is not known. Here $S_T = 1$ and hence $\Pr\left[w = 0\right] = (1 - \rho_1)$ and $\Pr\left[w > 0\right] = \rho_1$. The continuous part of the probability density function, obtained from simulation, for $m = 25$ and $m = 32$ are shown in Fig's. 7.9 and 7.10. The graphs show that there is a relatively

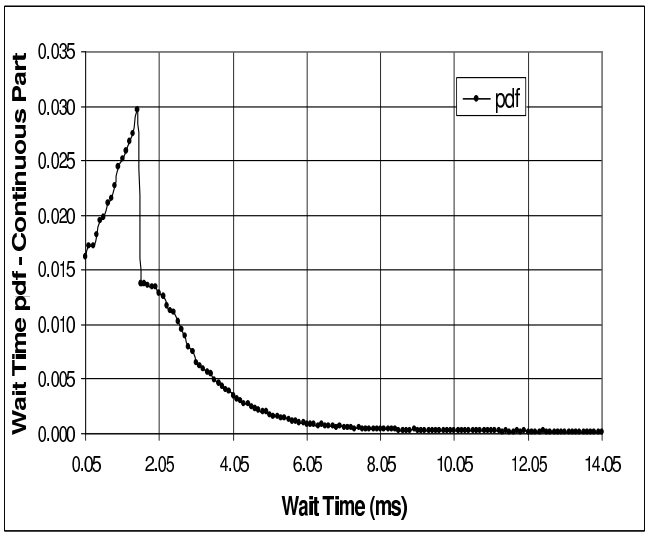

Figure 7.9. $\rho_1 f_c(w)$ for $m = 25$ and $\rho_1 = 0.67$..

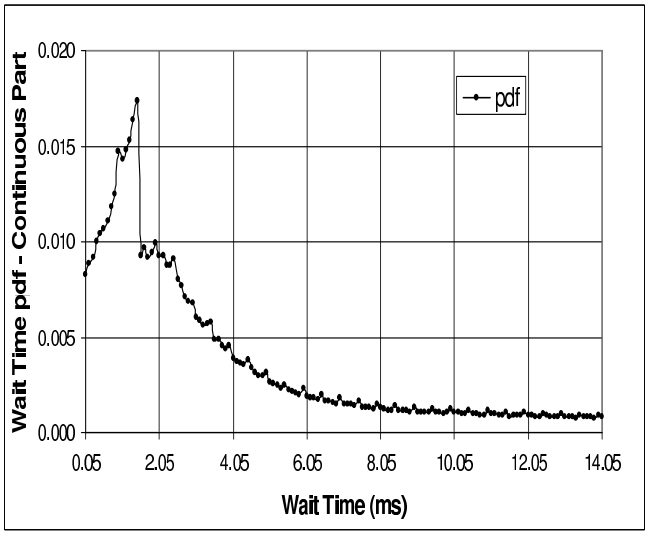

Figure 7.10. $\rho_1 f_c(w)$ for $m = 32$ and $\rho_1 = 0.86$..

high probability of $0 < w \leq D$ which could be explained by the fact that for $t_n \leq D$ the arriving packet would at least have to wait in the queue while the previous packet is being transmitted for the duration D.

The second density assumed to be a modified negative exponential probability density function, or

$$g_2(w) = (1 - \rho_{S_T})\,\delta(w) + \rho_{S_T}\mu_S e^{-\mu_S(w-\Delta_S)}u(w - \Delta_S) \tag{7.34}$$

would enable use of the Steffensens inequality. Here $\mu_S = \rho_{S_T}/(W_U - \Delta_S\rho_{S_T})$ where $W_U = F_U E[w]$ is an upper bound on expected packet wait time and $u(w)$ is the unit step function. The factor F_u of 2.1 was chosen and it was verified that Eq. 7.32 is satisfied by comparisons to simulations. A method to determine this factor, F_u, would be required in the future but for now we use 2.1 as a reasonable assumption. The tails of a cumulative distribution when determined from simulation is never very accurate [68]. In our case, the first condition of Steffensens inequality (Eq. 7.31) requires a much larger W_U, and we use $F_U = 2.1$. A larger F_U can be used at the expense of the bound tightness. The analytical methods to obtain $E[w]$ are shown in the previous section. By applying Eq. 7.30

$$\int_a^b g_1(w)w dw \leq W_U \tag{7.35}$$

if

$$Pr[w \leq w_{th}] \geq \begin{cases} 1 - \rho_{S_T} & w = 0 \\ 1 - \rho_{S_T}e^{-\mu_S(w_{th}-\Delta_S)} & w \geq 0 \end{cases} \tag{7.36}$$

and hence for $w_{th} \geq 0$

$$P_{outage} = Pr[w > w_{th}] \leq \rho_{S_T}e^{-\mu_S(w_{th}-\Delta_S)}. \tag{7.37}$$

There are a few limitations in the direct application of Steffensens inequality. First if Eq. 7.30 is true this does not guarantee that condition 1 or Eq. 7.31 holds true in general for any $g_2(w)$. We choose $g_2(w)$ and F_U by ensuring that condition 1 or Eq. 7.31 is true even at the tails of the distribution of the wait times. Our

choice for $g_2(w)$ was also motivated by the fact that the probability density function for the wait time in an M/M/1 queue is the modified negative exponential ([26], Eq. 5.122). Instead of using a modified negative exponential probability density function for $g_2(w)$ we could also use a Gamma probability density function with a fourth degree of freedom. However, the use of a modified negative exponential density function when compared to the simulation results provided a tighter bound.

7.5 Numerical Results

The expected packet wait times for our wireless system and T1 system [25] are shown in Figs. 7.4 and 7.11 respectively. The probability of outage for our wireless system are shown in Figs. 7.7 and 7.8. For expected packet wait times and probability of outage obtained by simulations, the packet interarrival times for each user is generated independently using Eq. 7.1. Next the aggregate packet interarrival times obtained by monte carlo simulation of the superposition process are applied to a G/D/1 queue. The packet wait times at the queue is obtained from the elementary Eqs. 7.5 and 7.6 for G/D/1 queue. While the probability of outage is obtained from the numerical cumulative distribution function derived from the packet wait time histograms. For the wireless (and T1) system, in the case of $m < 28\,(100)$ and $m \geq 28\,(100)$ users approximately half a million and one million packets are generated respectively. Graphs were not obtained for $\rho_1 \geq 0.95$ since the G/D/1 queue becomes unstable when ρ_1 tends to unity.

7.5.1 Expected Wait Times

The modified Little's-multinomial analytical $E[w_n]$ approximation are obtained using Eq. 7.20 while the M/D/1 queue approximation is obtained from [26] (pp. 191). The first moment of the interarrival times are obtained using Eq. 7.4. Also note that

when using Eq. 7.20, if $L_j = 0$, there are a small number of packets present for the given $[k_1, k_2, k_3]$ and the M/D/1 queue approximation is used for the conditional expected packet wait time.

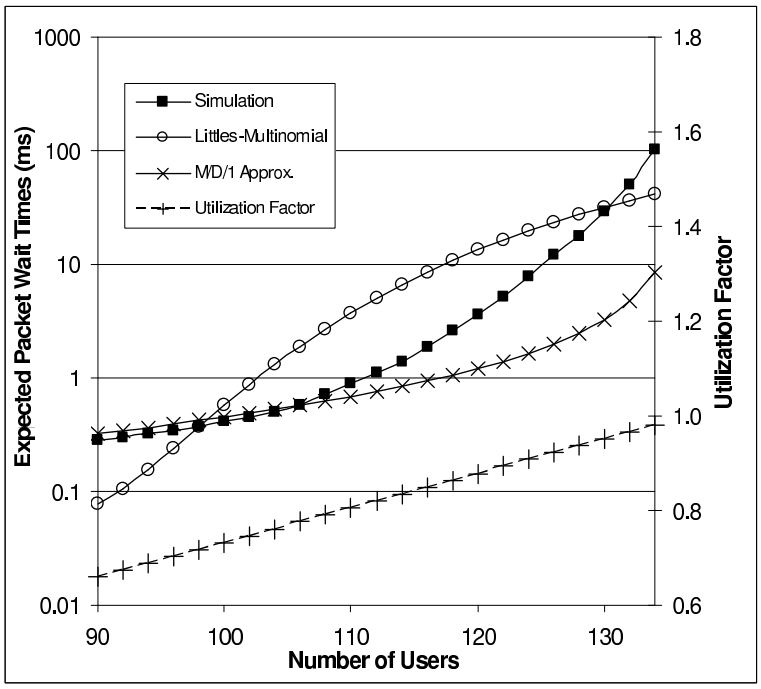

Figure 7.11. Expected packet wait times for a T1 system..

In the case of the T1 system [25], as shown in Fig. 7.11 the expected packet wait times depict a similar trend to those of the wireless system shown in Fig. 7.4. For $\rho_1 < 0.78$ or $m < 106$ users the M/D/1 queues expected packet wait times can be used as an approximation. While for $0.78 \leq \rho_1 \leq 0.95$ or $106 \leq m \leq 130$ the modified Little's-multinomial analytical $E[w_n]$ approximation provides a good estimate of the expected packet wait times for the G/D/1 queue. In the worst case, expected packet wait times obtained by the modified Little's-multinomial analytical approximation is 4.7 times that obtained by simulation. For $\rho_1 > 0.95$ or $m > 130$ users, the modified

Little's-multinomial analytical approximation underestimates expected packet wait times.

7.5.2 Probability of Outage

The Steffensens and Markov upper bounds on probability of outage are obtained by using 7.37 and 7.29 respectively. In the case of the T1 system [25], the Steffensens upper bound on probability of outage and the numerical probability densities depict a similar trend to those of the wireless system.

7.6 Conclusion

For voice over IP wireless reverse links, where the radio channel supports one radio burst (or one server) at any time with acceptable packet error rate, the modified Little's-multinomial analytical approximation for traffic induced expected packet wait times is derived for the first time here. This method provides insight into the physical reasons for correlated interarrival times in the superposition process and queuing wait times. The expected packet wait times are compared to those obtained from the M/D/1 queue approximation and simulation. For utilizations $\rho_1 < 0.58$ or users $m < 22$ the M/D/1 queues expected packet wait times approximation is a good estimate. The modified Little's-multinomial analytical expected packet wait times approximation is a much better estimate when $0.58 \leq \rho_1 \leq 0.90$ or $22 \leq m \leq 33$. Worst case, the modified Little's-multinomial analytical approximation expected packet wait times is 2.2 times that obtained by simulation and it underestimates this first moment for $\rho_1 > 0.90$ or $m > 33$.

The upper bound on the probability of outage, derived for the first time here using Steffensen's inequality, is compared to results obtained by the Markov upper bound and simulation. The Steffensens upper bound is tighter than the simple Markov

upper bound. For $m = 25$ (32) over an outage threshold range of $30 \leq w_{th} \leq 60$, Steffensens upper bound on probability of outage varies between 7.9 (2.4) to 4 (2.7) times that obtained by simulation.

In wireless system design, determination of traffic induced expected packet wait times and probability of outage at high utilization factors is useful in characterizing base stations in reference to end-to-end delay budgets and for Erlang capacity determination. Simulation takes time and resources. Hence, the modified Little's-multinomial analytical approximation for the expected wait times and the Steffensens upper bound on probability of outage can be used for wireless system design. Similarly, these methods can also be used to evaluate real systems where the mean packet interarrival times, talkspurt and silence durations per user are measured and the wireless transmission interval is known. Finally, in a follow up analysis we apply the modified Little's-multinomial analytical approximation and Steffensens upper bound to wireless reverse links that supports two simultaneous radio bursts (or two servers) with acceptable packet error rate.

CHAPTER 8

PACKET WAIT TIMES AND OUTAGE IN VOICE OVER IP DUAL BURST WIRELESS REVERSE LINKS

In voice over IP wireless reverse links with a G/D/2 queue that support simultaneous dual high bit rate bursts at acceptable packet error rate, traffic induced packet expected wait times are determined by the modified Little's-multinomial analytical approximation derived (Chapter 7) for the first time. At high utilization factors, which is the operating point of interest, this analytical approximation provides a much better estimate than the Kingman upper bound approximation. A lower bound on the system being idle is derived for the first time. This is used in the upper bound on the probability of outage, derived for the first time using the Steffensen inequality, which is a better estimate than that obtained by the Markov inequality. The dual burst wireless reverse link provides a capacity gain of 2.16 over the single burst case at a given packet expected wait time threshold. At a 2% probability of outage and 60 ms wait time threshold, the voice over IP users supported is 59. Methods presented here can be used to assess radio packet wait times that can be used for Erlang capacity determination and end-to-end delay budgets in queues. The methods can be extended to G/D/K queues.

8.1 Introduction

In Chapter 7 for voice over IP wireless reverse links which supports only one radio burst (or one server) at any time with acceptable packet error rate, traffic induced expected packet wait times are obtained by deriving the modified Little's-

multinomial analytical approximation. For high utilization factors where correlation between packet interarrival times results in high wait times, this method provides a better estimate of expected packet times than the M/D/1 queues approximation. There is no analytical method to determine expected packet wait times in a G/D/2 queue with correlated interarrival times.

In this Chapter, for voice over IP wireless reverse links which supports two simultaneous radio burst (or two servers) at any time with acceptable packet error rate, traffic induced expected packet wait times are obtained using the modified Little's-multinomial analytical approximation. Two servers increase the number of packets present per interval and reduce the carryover delays from one interval to the next. We compare the expected packet wait times obtained by the dual server modified Little's-multinomial analytical approximation to the Kingman upper bound [40] approximation and simulation. For high utilization factors where correlation between packet interarrival times results in high wait times, the modified Little's-multinomial analytical approximation provides a better estimate of packet expected wait times. Using the modified Little's-multinomial analytical approximation, the dual burst reverse link provides a capacity gain of 2.16 gain over a single burst reverse link.

The modified Little's-multinomial approximation for expected traffic induced packet wait time's in voice over IP wireless reverse links which supports one or two simultaneous radio burst (or servers) at any time with acceptable packet error rate has been derived for the first time. The analytical technique applies queuing theory to the advanced G/D/1 and G/D/2 queues. Furthermore an upper bound for the related probability of outage has been derived for the first time using the Steffensen's inequality. Both these analytical techniques are useful for wireless link capacity determination and can be extended to the G/D/K queue.

8.2 Voice over IP Dual Burst Wireless Reverse Links

In [35] or Chapter 7 we describe our single sector voice over IP wireless reverse link, with the G/D/1 queue, which supported one radio burst at any time with acceptable packet error rate. In this study our radio channel supports two simultaneous radio bursts (or two servers) at any time with acceptable packet error rate. The single voice over IP user interarrival times probability density function, the multiple voice over IP users interarrival times cumulative distribution function and k^{th} moment are described in [35] or Chapter 7.

8.2.1 G/D/2 Queue and Packet Wait Times

Consider the wait times incurred by the voice packets as shown in Figs. 8.1, 8.2 and 8.3 of a first-come-first-served G/D/2 system with total servers $S_T = 2$. In Fig. 8.1, a voice packet C_{n+1} arrives at the queue with unlimited waiting room and finds the servers S_1 and S_2 busy for time periods $w_{n+1,1}$ and $w_{n+1,2}$ respectively. In this case the packet would have a wait time at both servers where $\Delta w_{n+1} = w_{n+1,1} - w_{n+1,2}$ is positive. After, the $n - 1^{th}$ packet departs from the server S_2, the $n + 1$ packet C_{n+1} moves from the queue to server S_2 and incurs a wait time w_{n+1}. In Fig. 8.2, a packet C_{n+1} arrives at the queue and finds the server S_2 idle for a time period $y_{n,2}$ and server S_1 is busy for a time period $w_{n+1,1}$. The packet C_{n+1} moves from the queue to the server S_2 and has incurred no wait time. In Fig. 8.3, a packet C_{n+1} arrives at the queue and finds the servers S_1 and S_2 idle for a time periods $y_{n,1}$ and $y_{n,2}$ respectively. In this case as $y_{n,2} > y_{n,1}$ the packet C_{n+1} moves from the queue to the server S_2 and has incurred no wait time.

The $n + 1^{th}$ packets wait time

$$w_{n+1} = Min\left(w_{n+1,1}, w_{n+1,2}\right) \tag{8.1}$$

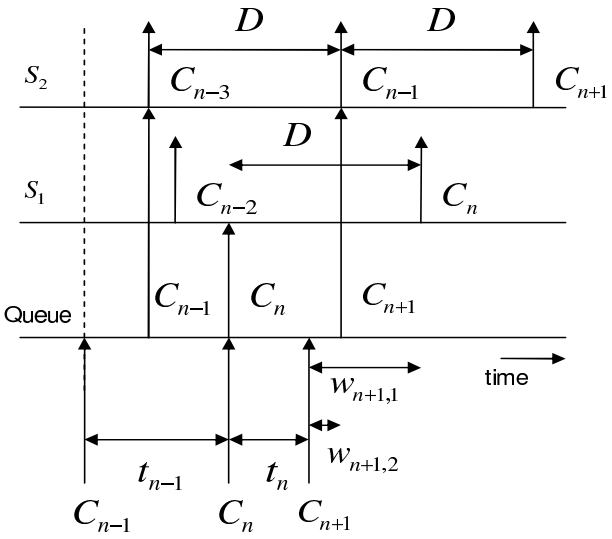

Figure 8.1. Packet C_{n+1} arrives and finds both servers busy ($y_{n,1}, y_{n,2} = 0$).

is the minimum of the wait time periods at each server. The time periods at each server can be expressed as a vector

$$\begin{aligned}&[w_{n+1,1}, w_{n+1,2}]\\ &\quad = [w_{n,1} + s_{n,1}D + y_{n,1} - t_n, w_{n,2} + s_{n,2}D + y_{n,2} - t_n]\end{aligned} \tag{8.2}$$

where, for alternate server selection in case of successive packets, the variables

$$s_{n,1} = \begin{cases} 1 & n = 0, 2, 4, \ldots \\ 0 & n = 1, 3, 5, \ldots \end{cases}$$

$$s_{n,2} = \begin{cases} 0 & n = 0, 2, 4, \ldots \\ 1 & n = 1, 3, 5, \ldots \end{cases} \tag{8.3}$$

are defined. Here t_n is the interarrival time between packets C_n and C_{n+1}. The radio burst or the server transmission interval is D. Even and odd numbered packets are served by S_1 and S_2 respectively. If n is even and $n+1$ is odd, C_n is served by server S_1 and C_{n+1} is served by server S_2. If n is odd and $n+1$ is even, C_n is served by

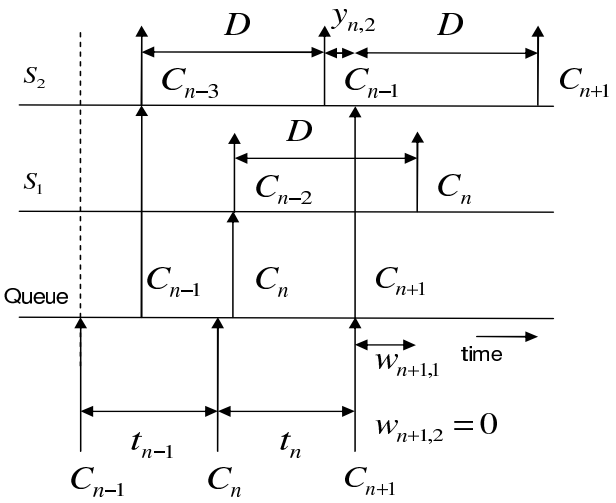

Figure 8.2. Packet C_{n+1} arrives and finds one server idle.

server S_2 and C_{n+1} is served by server S_1. For an odd $n+1^{th}$ packet, using Eq. 8.2, the time periods

$$[w_{n+1,1}, w_{n+1,2}] = [w_{n,1} + D + y_{n,1} - t_n, w_{n,2} + y_{n,2} - t_n] \tag{8.4}$$

The three cases shown in Fig's. 8.1, 8.2 and 8.3, are used to express

$$[w_{n+1,1}, w_{n+1,2}]$$

$$= \begin{cases} [w_{n,1} + D - t_n, w_{n,2} - t_n] & w_{n+1,1} > 0, w_{n+1,2} > 0 \\ [w_{n,1} + D - t_n, w_{n,2} + y_{n,2} - t_n] & w_{n+1,1} > 0, w_{n+1,2} = 0 \\ [w_{n,1} + D + y_{n,1} - t_n, w_{n,2} + y_{n,2} - t_n] & w_{n+1,1} = 0, w_{n+1,2} = 0 \end{cases} \tag{8.5}$$

where $y_{n,S} \geq 0$. For a given server $S = 1$ or 2, when $y_{n,S} > 0$, $w_{n+1,S} = 0$ and when $y_{n,S} = 0$, $w_{n+1,S} > 0$. This means that $w_{n+1,S} y_{n,S} = 0$. This is true for servers $S = 1, 2$. The wait times at each server are related to the idle time. The space $\{w_{n+1,1} > 0, w_{n+1,2} > 0\}$ equals $\{y_{n,1} = 0, y_{n,2} = 0\}$, $\{w_{n+1,1} > 0, w_{n+1,2} = 0\}$ equals $\{y_{n,1} = 0, y_{n,2} > 0\}$ and $\{w_{n+1,1} = 0, w_{n+1,2} = 0\}$ equals $\{y_{n,1} > 0, y_{n,2} > 0\}$.

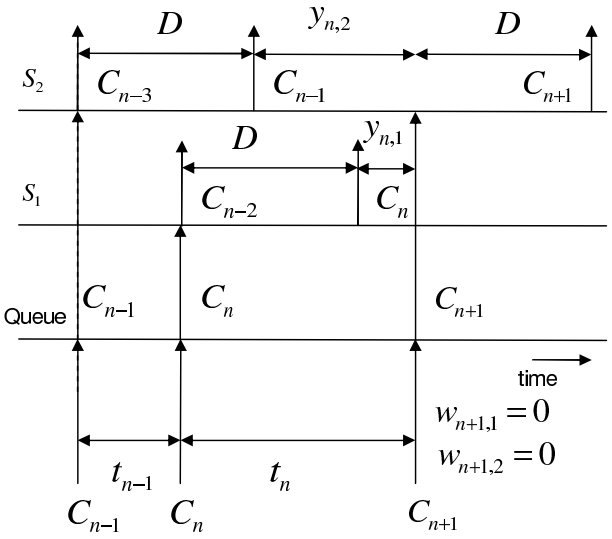

Figure 8.3. Packet C_{n+1} arrives and finds both servers idle.

While the space $\{w_{n+1,1} = 0, w_{n+1,2} > 0\}$ equals $\{y_{n,1} > 0, y_{n,2} = 0\}$ is not possible since the $n+1^{th}$ packet has to be served by S_2. Similarly a set of expression can be shown for an even $n+1^{th}$ packet. While the space $\{w_{n+1,1} >, w_{n+1,2} = 0\}$ equals $\{y_{n,1} = 0, y_{n,2} > 0\}$ is not possible since the $n+1^{th}$ packet has to be served by S_1. The probability of $n+1$ being odd or even,

$$Pr[n+1 = Odd] = Pr[n+1 = Even] = \frac{1}{2} \tag{8.6}$$

or

$$Pr[s_{n+1,1} = 0, s_{n+1,2} = 1] = Pr[s_{n+1,1} = 1, s_{n+1,2} = 0] = \frac{1}{2}. \tag{8.7}$$

In our model for multiple voice over IP users the voice packet interarrival times t_n and t_{n+1} are correlated and assumed to be stationary. The utilization factor [26]

$$\rho_2 = \frac{D}{2E\left[t_n\right]}. \tag{8.8}$$

8.2.2 Bounds on Probability of System being Idle

In this section we derive derive upper and lower bounds on the probability of the system being idle in terms of the utilization factor. These bounds are used later on for the probability of outage. When an odd numbered $n+1$ packet arrives at the queue the dual servers can be in one of three states. The arriving packet can find both servers S_1 and S_2 busy (Fig. 8.1) and the dual server system is considered to be busy. Alternately, it can find S_1 busy and S_2 idle (Fig. 8.2) or it can find S_1 idle and S_2 idle (Fig. 8.3) which means that the dual server system is considered to be idle. Similarly when an even numbered $n+1$ packet arrives at the queue the dual server system can be busy or idle. When a new packet arrives at the queue it finds the dual server system in one of four states, represented by the state space diagram (Fig. 8.4). Each state has an associated probability where

$$\begin{aligned} &Pr[S_1\ Idle, S_2\ Busy] + Pr[S_1\ Busy, S_2\ Idle] \\ &+Pr[S_1\ Idle, S_2\ Idle] + Pr[S_1\ Busy, S_2\ Busy] = 1. \end{aligned} \tag{8.9}$$

The four states of busy and idle pairs can be expressed in terms of idle time $y_{n,1}$ and $y_{n,2}$ at the dual servers and their associated probabilities, where $Pr[y_{n,1} > 0, y_{n,2} = 0] + Pr[y_{n,1} = 0, y_{n,2} > 0] + Pr[y_{n,1} > 0, y_{n,2} > 0] + Pr[y_{n,1} = 0, y_{n,2} = 0] = 1$.

Here we define the probability of a dual server system being idle,

$$\begin{aligned} Pr[System\ Idle] &= Pr[S_1\ Idle, S_2\ Busy] + \\ &Pr[S_1\ Busy, S_2\ Idle] + Pr[S_1\ Idle, S_2\ Idle] \end{aligned} \tag{8.10}$$

and the probability of a dual server system being busy

$$Pr[System\ Busy] = Pr[S_1\ Busy, S_2\ Busy]. \tag{8.11}$$

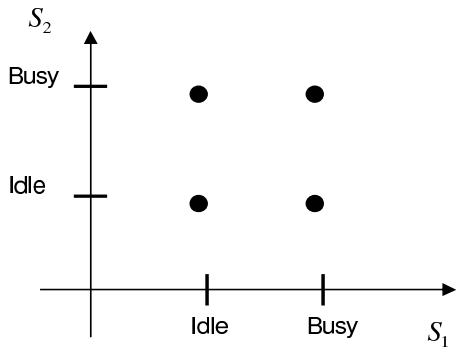

Figure 8.4. The dual server busy and idle state space diagram.

Consider the dual servers over an arbitrarily long interval of time τ. The idle and busy time intervals at server S_1 are $Pr[S_1\ Idle]\tau$ and $\tau - Pr[S_1\ Idle]\tau$ respectively. Similarly the idle and busy time intervals at server S_2 are $Pr[S_2\ Idle]\tau$ and $\tau - Pr[S_2\ Idle]\tau$ respectively. The number of packets served by the dual server,

$$Packets_{Served} = \frac{\tau - Pr[S_1\ Idle]\tau + \tau - Pr[S_2\ Idle]\tau}{D} \tag{8.12}$$

and the number of packets that arrive during the time interval τ,

$$Packets_{Arrived} = \frac{\tau}{E\left[t_n\right]}. \tag{8.13}$$

Over a long interval of time $\tau \to \infty$, $Packets_{Served}$ and $Packets_{Arrived}$ can be equated. Since each server has symmetrical loading $Pr[S_1\ Idle] = Pr[S_2\ Idle]$,

$$Pr[S_1\ Idle] = 1 - \rho_2 \tag{8.14}$$

where utilization factor ρ_2 is given in Eq. 8.8. The probability of the dual server system is idle given in Eq. 8.10 can also be expressed as

$$Pr[System\ Idle] = Pr[S_1\ Idle] + Pr[S_2\ Idle] - Pr[S_1\ Idle, S_2\ Idle]. \tag{8.15}$$

Since $Pr[S_2\ Idle] > Pr[S_1\ Idle, S_2\ Idle]$, or the probability of one server being idle is always greater than the probability of both servers being idle,

$$Pr[System\ Idle] > 1 - \rho_2. \tag{8.16}$$

Finally, as $Pr[S_1\ Idle, S_2\ Idle] \geq 0$,

$$Pr[System\ Idle] < 2\,(1 - \rho_2)\,. \tag{8.17}$$

8.3 Expected Packet Wait Time

For the voice over IP reverse links that support dual bursts, expected packet wait times, obtained by the modified Little's-multinomial analytical approximation, the G/D/2 queue Kingman upper bound approximation and simulation are compared in Fig. 8.5 and Tab. 8.1. Although Kingman's upper bound assumes successive interarrival times are independent, we use it as an approximation. For a large number of voice users or at high utilizations, the G/D/2 queue Kingman upper bound approximation underestimates expected packet wait times, while the modified Little's-multinomial approximation provides a better estimate. At high utilizations the correlation between interarrival times results in higher wait times, hence, the Kingman upper bound underestimates the expected wait times.

Fig. 8.5 shows that for $\rho_2 < 0.83$ or $m < 60$ users the Kingman upper bound approximation on expected packet wait times can be used as a conservative estimate. The modified Little's-multinomial analytical expected packet wait times approximation are useful when $0.80 \leq \rho_2 \leq 0.91$ or $60 \leq m \leq 68$ users where expected packet wait times are underestimated using the the Kingman upper bound approximation. In the worst case, expected packet wait times obtained by the modified Little's-multinomial analytical approximation is 3.8 times that obtained by simulation. In packetized wireless systems, typical radio queue related expected packet wait times

Table 8.1. Expected packet wait times verses number of users

m	*E[w] (ms) Kingman Approx.*	*E[w] (ms) Simulation*	*E[w] (ms) Little's--multinomial*	*E[w] (ms) Utilization Factor*
40	1.86	0.28	1.71	0.53
58	3.37	1.82	7.78	0.78
60	3.80	2.82	10.88	0.80
62	4.37	4.85	14.89	0.83
64	5.16	7.93	19.87	0.86
66	6.31	13.48	25.83	0.88
68	8.14	23.46	32.73	0.91
70	11.50	43.18	40.52	0.94

can be on the order of 10 to 30 ms to meet the overall end-to-end delay budget. Hence, obtaining expected packet wait times for the range $60 \leq m \leq 68$ is important for system design.

8.3.1 Modified Little's-Multinomial Approximation

The modified Little's-multinomial analytical approximation for expected packet wait times is derived in Chapter 7 for the G/D/1 queue or $S_T = 1$ (Eq. 7.20). The approximation holds true for the G/D/2 queue, with two servers $S_T = 2$. In the G/D/2 queue there is an increase in the number of packets present per interval and a reduction in the carryover delays from one interval to the next.

8.4 Probability of Outage

The probability of outage calculated from the Steffensens upper bound and Markov inequality, are compared to simulation results in Fig. 8.6, Fig. 8.7 and Table 8.2. As shown in the graphs, the Steffensens upper bound is tighter than the simple Markov upper bound. For $m = 60$ (68) in the range of $30 \leq w_{th} \leq 60$, the Steffensens

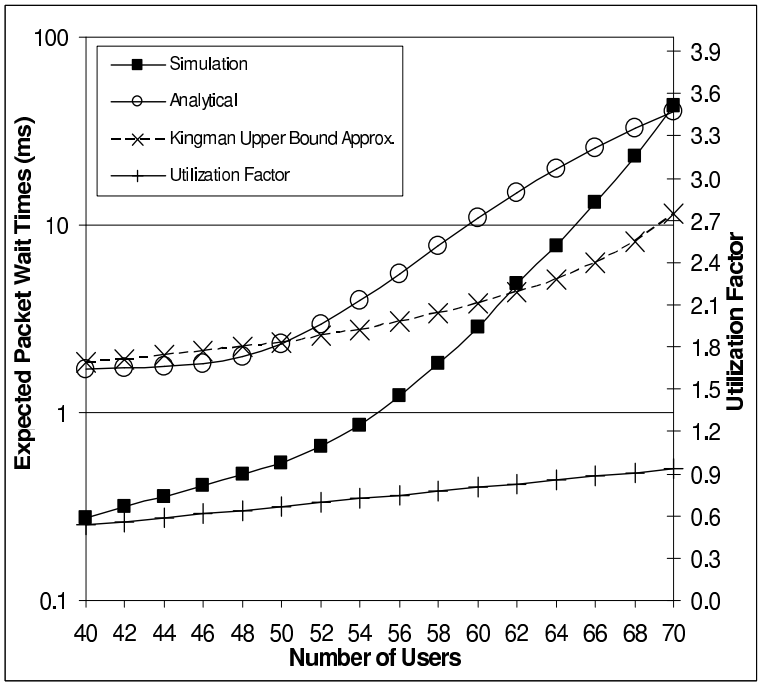

Figure 8.5. Expected packet wait times for wireless reverse links that support two simultaneous radio bursts or dual servers.

upper bound varies between 9.2 (2.1) to 11.9 (2.1) times the probability of outage obtained by simulation. Similar trends are observed in probability of outage graphs for other users where $40 \leq m \leq 58$.

Table 8.2. P_{outage} for G/D/2 Queue - Comparison of simulation and Steffensens upper bound

m	$\Pr[w > 30ms]$ *Simulation*	$\Pr[w > 30ms]$ *Steffensens*	$\Pr[w > 60ms]$ *Simulation*	$\Pr[w > 60ms]$ *Steffensens*
60	0.0200	0.1835	0.0035	0.0419
62	0.0458	0.2722	0.0120	0.0894
64	0.0806	0.3616	0.0302	0.1528
66	0.1427	0.4455	0.0654	0.2249
68	0.2429	0.5215	0.1342	0.2992

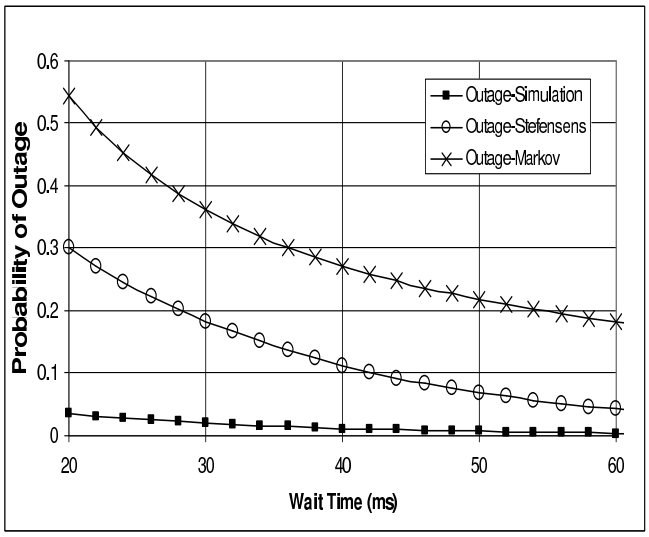

Figure 8.6. P_{outage} for G/D/2 Queue with $m = 60$ and $\rho_2 = 0.80$.

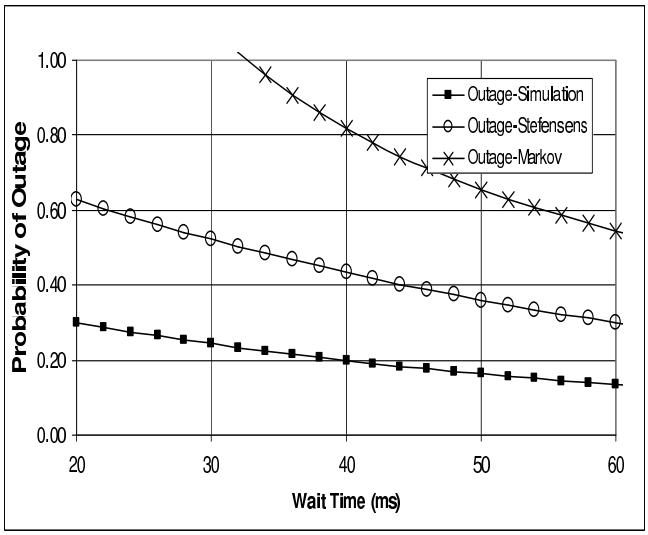

Figure 8.7. P_{outage} for G/D/2 Queue with $m = 68$ and $\rho_2 = 0.90$.

8.4.1 Upper Bound using Steffensen's Inequality

For the G/D/2 queue the Markov upper bound, which is Eq. 7.29 in Chapter 7, is weak. An upper bound (Eq. 7.37) on the probability of outage was derived

in Chapter 7 using Steffensens inequality. Similarly, for the G/D/2 queue the upper bound on probability of outage

$$P_{outage} = Pr\left[w > w_{th}\right] \leq \rho_2 e^{-\mu_S(w_{th}-\Delta_S)}, \tag{8.18}$$

where ρ_2 is the G/D/2 queue utilization factor shown in Eq. 8.8. There are some differences between the upper bound for the G/D/1 queue and that of the G/D/2 queue. For the G/D/2 queue, in the case of $g_2(w)$ (or Eq. 7.34) we use

$$Pr[w = 0] = Pr[System\ Idle] > 1 - \rho_2. \tag{8.19}$$

For this, the lower bound on $Pr[System\ Idle]$ was obtained in Eq. 8.16. Finally, we use $F_u = 1.5$ for the G/D/2 queue.

The continuous part of the probability density function, obtained from simulation, for $m = 60$ and $m = 68$ are shown in Fig.'s. 8.8 and 8.9. The graphs show that there is a relatively high probability of $0 < w \leq D$ which could be explained by the fact that for $t_n \leq D$ the arriving packet would at least have to wait in the queue while the previous packet is being transmitted for the duration D.

8.5 Voice over IP User Capacity Gain

The voice over IP user capacity gain at a given traffic induced expected voice packet wait time is provided in Tab. 8.3 for a G/D/2 wireless reverse link over that of a G/D/1 wireless reverse link. This capacity gain

$$C_{G,a} = \left.\frac{m_{G/D/2}}{m_{G/D/1}}\right|_{E[w]_{th}} \tag{8.20}$$

where $m_{G/D/2}$ and $m_{G/D/1}$ is the number of packetized voice users for the G/D/2 and G/D/1 wireless reverse links respectively at the expected packet wait time threshold $E[w]_{th}$. The average $C_{G,a} = 2.16$. The modified Little's-Multinomial approximation

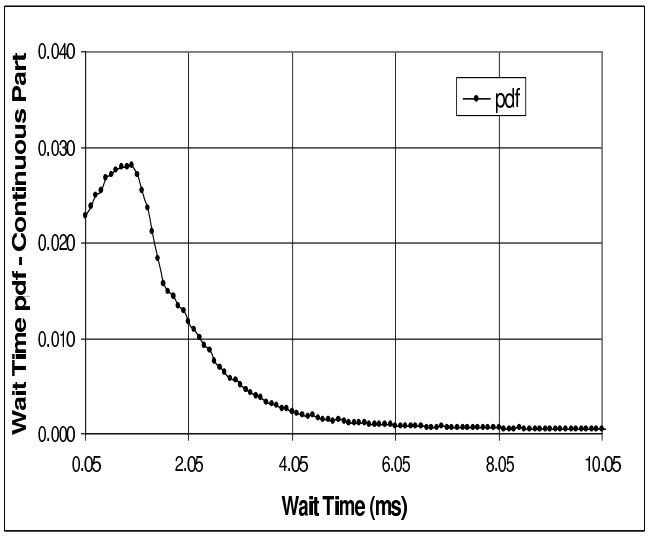

Figure 8.8. $\rho_2 f_c(w)$ for $m = 60$ and $\rho_2 = 0.80$..

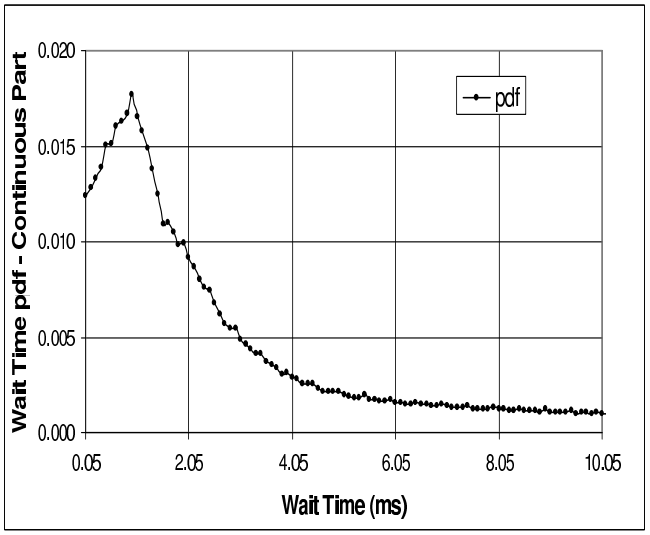

Figure 8.9. $\rho_2 f_c(w)$ for $m = 68$ and $\rho_2 = 0.90$..

is used for $E[w]_{th}$, $m_{G/D/2}$ and $m_{G/D/1}$. In Tab. 8.3, for $E[w]_{th} = 5$ the $m_{G/D/2} = 58$ is obtained from the Kingman upper bound approximation.

Table 8.3. Voice over IP user capacity gains at $E[w]_{th}$

$E[w]_{th}$ (ms)	$m_{G/D/2}$	$m_{G/D/1}$	$C_{G,a}$
5	58	25	2.24
10	60	28	2.14
15	62	29	2.14
20	64	30	2.13
25	66	31	2.13
30	67	32	2.09

In addition, the voice over IP user capacity gain at a given probability of wait time outage is provided in Tab. 8.4 for a G/D/2 wireless reverse link over a G/D/1 wireless reverse link. This capacity gain

$$C_{G,b} = \left. \frac{m_{G/D/2}}{m_{G/D/1}} \right|_{Pr[w>60\text{ms}]=0.02} \tag{8.21}$$

can also be determined for a threshold $w_{th} = 60$ ms and $P_{Outage} = 0.02$. As shown in Tab. 8.4, using simulation results the G/D/2 queue has a $C_{G,b} = 2.2$ while using our upper bound $C_{G,b} = 2.27$. The number of users supported at a given $P_{Outage} = 0.02$ is obtained from Tab's. 8.2 and 7.2 for the G/D/2 and G/D/1 queue respectively. The upper bound on P_{Outage} provides a lower bound on the number of voice over IP users supported. Using the upper bound on P_{Outage} the voice over IP users supported, by the G/D/2 and G/D/1 queue respectively is 4.8% and 7.1 % less than that compared to simulation results.

Table 8.4. Voice over IP user capacity gains at $P_{Outage} = 0.02$

Method	$m_{G/D/2}$	$m_{G/D/1}$	$C_{G,b}$
Simulation	62	28	2.22
Upper Bound	59	26	2.27

8.6 Numerical Results

The expected packet wait times for a G/D/2 wireless systems are shown in Fig 8.5. The single user and aggregate packet interarrival times are generated using the same techniques as in Chapter 7. The packet wait times for simulation curves is obtained from the Eq.'s 8.1 and 8.2 for G/D/2 queue. For $m \geq 56$, users approximately half a million are generated.

8.6.1 Expected Wait Times

The modified Little's-multinomial approximation on the expected packet wait times for dual radio reverse links are obtained using Eqs. 7.20 and $S_T = 2$ as described in Sec. 8.3.1. The moments of the interarrival times are obtained from Chapter 7 Eq. 7.4. The Kingman upper bound on expected packet wait times for a G/D/2 queue [40] is used as an approximation. Ggraphs were not obtained for $\rho_2 \geq 0.95$ since the G/D/2 queue becomes unstable when ρ_2 tends to unity. When using Eq. 7.20, if $L_j = 0$, there are a small number of packets present for the given $[k_1, k_2, k_3]$ and Kingman's upper bound approximation is used for the conditional expected packet wait time. For a T1 system [25] and in the wireless reverse link with the G/D/1 queue (Chapter 7) at high utilization factors the wait time increases due to correlated interarrival times and long queues. Similarly in our wireless reverse link with the G/G/2 queue, at high utilization factors, the expected wait time increases significantly.

8.6.2 Probability of Outage

The Steffensens and Markov upper bounds on probability of outage are obtained by using Eq.'s 7.37 and 7.29 in Chapter 7 and Sections 8.3.1 and 8.4.1. The Steffensens upper bound on probability of outage and the numerical probability densities depict a similar trend to those of the G/G/1 wireless system.

8.7 Conclusion

For voice over IP wireless reverse links, where the radio channel supports two simultaneous radio burst (or two server) at any time with acceptable packet error rate, traffic induced expected packet wait times are obtained from the dual burst modified Little's-multinomial analytical approximation derived for the first time in Chapter 7. The expected packet wait times are compared to those obtained from the G/D/2 queue Kingman upper bound approximation and simulation. For $\rho_2 < 0.80$ or $m < 60$ users the Kingman upper bound approximation on expected packet wait times can be used as a good estimate. At high utilization factors, $0.80 \leq \rho_2 \leq 0.90$ or $60 \leq m \leq 68$ users, the modified Little's-multinomial analytical expected packet wait times approximation provides a better estimate which in the worst case is 3 times that obtained by simulation. The Steffensens upper bound, derived for the first time in Chapter 7, is tighter than the simple Markov upper bound on probability of outage. For $m = 60$ (68) in the range of $30 \leq w_{th} \leq 60$, the Steffensens upper bound varies between 9.2 (2.1) to 11.9 (2.1) times the probability of outage obtained by simulation. The upper bound on probability of outage provides a lower bound on the number of voice over IP users supported. Using our bound at a 2% probability of outage and 60 ms wait time threshold, the voice over IP users supported by the G/D/1 and G/D/2 queue is 26 and 59 respectively, which is 4.8% and 7.1% less than that compared to simulation results. Using the modified Little's-Multinomial approximation for expected wait times, wireless reverse links with dual high bit rate bursts or servers provides an average capacity gain of 2.16 over links with a single burst or server. The modified Littles-Multinomial approximation for expected wait times and Steffensens upper bound on probability of outage can be extended to wireless reverse links with more than two servers.

CHAPTER 9

CONCLUSIONS

Packet wireless cellular systems that support simultaneous voice over IP (VoIP) and packet data services are evolving. The radio channel supports a finite number of simultaneous high bit rate bursts or servers, at an acceptable packet error rate, that are shared by all users whose packet transmission is scheduled. For a given traffic mix, link capacity is the maximum Erlangs and data throughput at a given packet error rate, voice packet expected wait time and probability of wait time outage. Voice packet wait times are traffic induced and due to retransmissions caused by high packet error rate. The following performance and capacity methods, derived in this dissertation, can be used for packetized wireless system design.

9.1 Performance of High Bit Rate DS-SS BPSK Reverse Links

Transmission of a high data rate DS-SS BPSK signal with 7 chip signatures and raised-cosine chip characteristics over a frequency selective channel, results in incoherent intersymbol interference at a dual space diversity four finger RAKE receiver.

9.1.1 Bounds on Error Rate for Dual Space Diversity RAKE

An upper bound on the error rate is derived, using the Prabhu bound, in terms of two intersymbol interference terms and bounds on the marginal distribution of the two smaller terms. A lower bound is derived using Jensen's inequality. For per branch SNR's > 6 dB, the Prabhu bound on error rate is notably better than the standard Gaussian approximation (used for many years) as intersymbol interference

is not Gaussian. At SNR = 8(12) dB, the Prabhu bound and standard Gaussian approximation are respectively 1.8 (1.8) and 3.3 (32) times the results from total probability theorem simulation.

This receiver provides better immunity against intersymbol interference at SNR's $\leq$ 10dB and it provides an 8dB space diversity gain at 10^{-3} error rate. Better error rate estimates predict accurate number of simultaneous bursts supported.

9.1.2 DS-SS BPSK Transmit Power Spectral Density

Reverse link spectral density is derived, for the first time, by expressing the signal as a linear digital modulated waveform. The density is a function of the chip Fourier transform, signature coefficients and information autocorrelation sequence.

This density is used to determine operating SNR by deriving received signal power and averaging it over the channel. The fractional containment bandwidth obtained from the densities for signals with one PN and two Gold sequences shows that a PN sequence results in greater adjacent channel interference.

9.2 Capacity of VoIP Wireless Reverse Links - G/D/S_T Queue

Each voice over IP mobile has its own queue with forward and reverse dedicated control channels that are used to schedule traffic over a high bit rate bursting data channel. We assume a single virtual queue at the base station is equivalent to many physical mobile queues. This virtual queue has correlated interarrival times for the superposition of all links. If the radio channel supports S_T simultaneous high bit rate bursts (or servers) at acceptable[1] packet error rate, then all mobiles share usage of these S_T bursts that are coupled to a G/D/S_T virtual queue at the base station.

[1]In Chapter 6 the radio channel supports at maximum two simultaneous high bit rate bursts at reasonably acceptable packet error rates $\approx$ 2.6% with no coding or retransmission.

9.2.1 Analytical Traffic Induced Expected Packet Wait Times

To obtain traffic induced expected packet wait times, at high utilization factors, the modified Little's-multinomial approximation is derived for the first time. This approximation is in terms of the transmission duration, aggregate packet arrival rate, number of servers, the per voice over IP users expected talkspurt duration, expected silence duration and expected number of packets per talkspurt. This method provides reasons for correlated interarrival times in the superposition process and high queue wait times.

For a G/D/1 queue, our expected packet wait time is a much better estimate at utilizations $0.58 \leq \rho_1 \leq 0.90$ or users $22 \leq m \leq 33$. For $\rho_1 < 0.58$ or $m < 22$, the M/D/1 queues approximation is a good estimate. For $m = 27$ (33), the expected wait times obtained from our method and the M/D/1 approximation is respectively 2.2 (1) and 0.5 (0.1) times that obtained by simulation.

For a G/D/2 queue, our expected packet wait times is a much better estimate at utilizations $0.80 \leq \rho_2 \leq 0.90$ or users $60 \leq m \leq 68$. For $\rho_2 < 0.80$ or $m < 60$, Kingman's upper bound approximation is a good estimate. For $m = 62$ (68), expected wait times obtained from our method and Kingman's bound is respectively 3 (1.4) and 0.9 (0.4) times that obtained by simulation.

Using our method, at an expected packet wait time threshold of 10 ms, the G/D/1 and G/D/2 queues support 28 and 60 voice over IP users respectively. Also the G/D/2 queue provides an **average capacity gain of 2.16** over G/D/1 queue.

9.2.2 Upper Bound on Probability of Wait Time Outage

An upper bound on the probability of outage is derived, for the first time, using Steffensen's inequality and is in terms of the expected packet wait times. Our bound is much tighter than the simple Markov upper bound.

For a G/D/1 queue, with $m = 25$ (32), over an wait time outage threshold range of $30 \leq w_{th} \leq 60$, our bound varies between 7.9 (2.4) to 4 (2.7) times simulation results. For a G/D/2 queue, with $m = 60$ (68), over $30 \leq w_{th} \leq 60$, our bound varies between 9.2 (2.1) to 11.9 (2.1) times simulation results.

The upper bound on probability of outage provides a lower bound on the number of voice over IP users supported. Using our bound at a 2% probability of outage and 60 ms wait time threshold, the voice over IP users supported by the G/D/1 and G/D/2 queue is 26 and 59 respectively, which is 4.8% and 7.1% less than that compared to simulation results.

Simulation takes time and resources, making our methods convenient and attractive for wireless system design. Our methods for wait times statistics, at high utilization factors, is useful in characterizing the S_T burst channel coupled to a base station G/D/S_T queue for end-to-end delay budgets, Erlang capacity evaluation and queue comparisons. It can also be used to evaluate real systems with known transmission intervals and measured packet arrival statistics.

9.3 Future Work

Our methods can be extended to determine:

- Erlang capacity of a DS-SS BPSK high bit rate reverse link system with the G/D/2 queue at a given packet error rate and packet wait times statistics where wait times are traffic and retransmission induced.
- Capacity of a wireless reverse link system with voice over IP and packet data services.
- Capacity of a wireless reverse link system with the G/D/S_T queue.
- Capacity of newer OFDMA wireless systems. Our expected packet wait times and probability of outage methods are independent of the modulation used.

APPENDIX A

RAKE STRUCTURES

In this appendix, we present RAKE structures. To compare the modified and original delayed signature RAKE's, shown in Fig. 4.2, we assume channel delays $\tau_1 = 0$ and $\tau_2 = u_d T_c$ with $u_d = 3$. Here we derive the discrete voltage for $l = 0$,

$$Z_0 = A_S b_0 + \gamma_0 b_0 + \varsigma_1 b_1 + \varsigma_{-1} b_{-1} + n_T. \tag{A.1}$$

In the original structure, amplitude A_S is smaller and intersymbol interference amplitude ς_1 has a coherent component.

A.1 Modified delayed signature RAKE

In this case delay 1 and 2 are equal to τ_2 and 0 respectively. The amplitudes

$$\begin{aligned}
A_S &= \tfrac{\lambda}{\sqrt{2}} \textstyle\sum_{m=1}^{2} r_m^2 \sum_{u=0}^{N-1} a_u^2, \\
\gamma_0 &= \tfrac{\lambda Y}{\sqrt{2}} \times \left[\textstyle\sum_{u=u_d}^{N-1} a_{u-u_d} a_u + \sum_{u=0}^{N-1-u_d} a_{u+u_d} a_u \right], \\
\varsigma_1 &= \tfrac{\lambda Y}{\sqrt{2}} \textstyle\sum_{u=N-u_d}^{N-1} a_{u-(N-u_d)} a_u, \\
\varsigma_{-1} &= \frac{\lambda Y}{\sqrt{2}} \sum_{u=0}^{u_d-1} a_{u+(N-u_d)} a_u,
\end{aligned} \tag{A.2}$$

while $\sigma_n^2 = \sum_{m=1}^{2} r_m^2 \frac{N N_o}{4} + \frac{Y N_o}{2} \sum_{u=u_d}^{N-1} a_{u-u_d} a_u$.

A.2 Original delayed signature RAKE

In this case delay 1 and 2 are equal to 0. The amplitudes are

$$\begin{aligned}
A_S &= \tfrac{\lambda}{\sqrt{2}} \left[r_1^2 \textstyle\sum_{u=u_d}^{N-1} a_u^2 + r_2^2 \sum_{u=0}^{N-1} a_u^2 \right], \\
\gamma_0 &= \tfrac{\lambda}{\sqrt{2}} Y \left[\textstyle\sum_{u=u_d}^{N-1} a_{u-u_d} a_u + \sum_{u=0}^{u_d-1} a_{u+(N-u_d)} a_u + \right. \\
&\qquad \left. \textstyle\sum_{u=0}^{N-1-u_d} a_{u+u_d} a_u \right], \\
\varsigma_1 &= \tfrac{\lambda}{\sqrt{2}} \left[r_1^2 \textstyle\sum_{u=0}^{u_d-1} a_u^2 + Y \sum_{u=N-u_d}^{N-1} a_{u-(N-u_d)} a_u \right], \\
\varsigma_{-1} &= 0.
\end{aligned} \tag{A.3}$$

while $\sigma_n^2 = \sum_{m=1}^{2} r_m^2 \frac{N N_o}{4} + \frac{Y N_o}{2} \left[\sum_{u=u_d}^{N-1} a_u a_{u-u_d} + \sum_{u=0}^{u_d-1} a_u a_{u+(N-u_d)} \right]$.

REFERENCES

[1] R. Price and P. E. Green, "A communication technique for multipath channels," *Proc. IRE*, pp. 555–570, Mar. 1958.

[2] J. G. Proakis, *Digital Communications*, 3rd ed. McGraw-Hill, 1995.

[3] A. J. Viterbi, A. M. Viterbi, and E. Zehavi, "Performance of power-controlled wideband terrestrial digital communications," *IEEE Trans. Commun.*, vol. 41, no. 4, pp. 559–569, Apr. 1993.

[4] J. S. Lee and L. E. Miller, *CDMA Systems Engineering Handbook*. Artech House, 1998.

[5] G. L. Turin, "Introduction to spread-spectrum antimultipath techniques and their application to urban digital radio," *Proc. IEEE*, vol. 68, no. 3, pp. 328–353, Mar. 1980.

[6] M. B. Pursley, "Performance evaluation for phase-coded spread spectrum multiple access phase-coded communications, Part I: System analysis," *IEEE Trans. Commun.*, vol. 25, no. 8, pp. 795–799, Aug. 1977.

[7] E. A. Geraniotis and M. B. Pursley, "Performance of coherent direct-sequence spread-spectrum communications over specular multipath fading channels," *IEEE Trans. Commun.*, vol. COM-33, no. 6, pp. 502–508, June 1985.

[8] T. Eng and L. B. Milstein, "Coherent DS-CDMA performance in nakagami multipath fading," *IEEE Trans. Commun.*, vol. 43, pp. 1134–1143, Apr. 1995.

[9] R. H. Mahadevappa and J. G. Proakis, "Mitigating multiple access interference and intersymbol interference in uncoded CDMA systems with chip level interleaving," *IEEE Trans. Wireless Commun.*, vol. 1, no. 4, pp. 781–792, Oct. 2002.

[10] W. Xu and L. B. Milstein, "On the performance of multicarrier RAKE systems," *IEEE Trans. Commun.*, vol. 49, no. 10, pp. 1812–1823, Oct. 2001.

[11] H. E. Rowe, *Signals and Noise in Communication Systems.* D. Van Nostrand Company, Inc., 1965.

[12] K. Kuchi and V. K. Prabhu, "Power spectral density of GMSK modulation using matrix methods," in *IEEE Military Communications Conference*, Oct. 1999, pp. 45–50.

[13] N. Pronios and A. Polydoros, "On the power spectral density of certain digitally modulated signals with applications to code despreading," *IEEE J. Select. Areas Commun.*, vol. 8, no. 5, pp. 837–852, June 1990.

[14] Z. Ye, A. S. Madhukumar, and F. Chin, "Power spectral density and in-band interference power of UWB signals at narrowband systems," in *IEEE International Conference on Communications*, June 2004, pp. 3561–3565.

[15] K. Pang and D. Keogh, "Direct spread spectrum and its power spectrum," in *IEEE The 8th International Conference on Communication Systems*, Nov. 2002, pp. 1106–1110.

[16] R. Framjee and V. K. Prabhu, "Some considerations of DS-SS BPSK power spectral density and error rate of a high bit rate RAKE," in *IEEE Military Communications Conference*, Oct. 2009, pp. 1–8.

[17] ——, "Error rate considerations for a high bit rate DS-SS BPSK dual space diversity RAKE," in *IEEE Radio and Wireless Symposium (RWS)*, Feb. 2010, pp. 657 – 660.

[18] D. C. Cox, "Delay doppler characeristics of multipath propagation at 910MHz in a suburban mobile radio environment," *IEEE Trans. Antennas Propagat.*, vol. AP-20, pp. 625–635, Sept. 1972.

[19] A. M. D. Turkmani and J. D. Parsons, "Measurement and modelling of wideband mobile radio channels at 900 MHz," *Proc. IEE, Communications, Speech and Vision*, vol. 138, no. 5, pp. 447–457, Oct. 1991.

[20] R. Framjee and V. K. Prabhu, "Zero-forcing equalisation for space-diversity combining in microwave digital radio," *Proc. IEE, Communications*, vol. 144, pp. 107–113, Apr. 1997.

[21] V. K. Prabhu, "Some considerations of error bounds in digital systems," *B.S.T.J*, vol. 50, no. 10, pp. 3127–3151, Dec. 1971.

[22] V. K. Prabhu and H. E. Rowe, "Spectra of digital phase modulation by matrix methods," *B.S.T.J*, vol. 53, no. 5, pp. 899–935, May 1974.

[23] R. C. Dixon, *Spread Spectrum Systems with Commercial Application*, 3rd ed. Wiley Interscience, 1994.

[24] *Application of the E-model: A planning guide*, Telecommunications Standardization Sector of ITU Std., Rev. G.108, 1999.

[25] K. Sriram and W. Whitt, "Characterizing superposition arrival processes in packet multiplexers for voice and data," *IEEE J. Select. Areas Commun.*, vol. SAC-4, no. 6, pp. 833–846, Sept. 1986.

[26] L. Kleinrock, *Queueing Systems, Volume I : Theory*, 1st ed. Wiley Interscience, 1975.

[27] ——, *Queueing Systems, Volume II : Computer Applications*, 1st ed. Wiley Interscience, 1975.

[28] Q. Bi, P. Chen, Y. Yang, and Q. Zhang, "An analysis of VoIP service using 1xEV-DO revision a system," *IEEE J. Select. Areas Commun.*, vol. 24, no. 1, pp. 36–45, Jan. 2006.

[29] A. M. Viterbi and A. J. Viterbi, "Erlang capacity of a power controlled CDMA system," *IEEE J. Select. Areas Commun.*, vol. 11, no. 6, pp. 892–900, Aug. 1993.

[30] C. Heyaime-Duverge, "Bandwidth allocation in multiservice access networks using statistical traffic models," Ph.D. dissertation, Univ. of Texas at Arlington, Arlington, TX, Dec. 2003.

[31] K. O. Stoeckigt and H. L. Vu, "VoIP capacity-analysis, improvement, and limits in IEEE 802.11 wireless LAN," *IEEE Trans. Veh. Technol.*, vol. 59, no. 9, pp. 4553–4563, Nov. 2010.

[32] D. Miao and H. Chen, "A generalised Littles law and its applications for a discrete-time G/D/1 queue with correlated arrivals," *Journal of the Operational Research Society*, pp. 679–689, 2012.

[33] H. Holma and A. Toskala, *WDCMA for UMTS - HSPA Evolution and LTE*. New Jersey: John Wiley and Sons, Ltd., 2007.

[34] D. Minoli and E. Minoli, *Delivering Voice over IP Networks*, 2nd ed. Wiley, 2002.

[35] R. Framjee and J. Bredow, "Packet wait times in voice over IP wireless reverse links," in *IEEE Consumer Communications and Networking Conference (CCNC)*, Jan. 2013, pp. 236–240.

[36] R. B. Cooper, *Introduction to Queueing Theory*, 2nd ed. North Holland, 1981.

[37] S. R. Stidham, "A last word on $L = \lambda W$," *Operations Research*, vol. 22, no. 2, pp. 417–421, 1974.

[38] W. Jewell, "A simple proof of $L = \lambda W$," *Operations Research*, vol. 15, pp. 1109–1116, 1967.

[39] J. Little, "A proof of queueing formula $L = \lambda W$," *Operations Research*, vol. 9, no. 3, pp. 383–387, 1961.

[40] J. F. Kingman, "Inequalities in the theory of queues," *Journal of the Royal Statistical Society*, vol. 32, pp. 102–110, 1970.

[41] M. D. Zoltowski and T. P. Krauss, "Two channel zero forcing equalization on CDMA forward link: Trade offs between multi-user access interference and diversity gains," in *IEEE Conference on Signals, Systems, and Computers*, Feb. 1999, pp. 1541 – 1545.

[42] M. D. Yacoub, *Foundations of Mobile Radio Engineering.* CRC Press, Inc., 1993.

[43] W. C. Jakes, *Microwave Mobile Communications.* New York, NY: IEEE Press, 1974.

[44] P. Balaban and J. Salz, "Optimum diversity combining and equalization in digital data transmission with applications to cellular mobile radio - Part 1: Theoretical considerations," *IEEE Trans. Commun.*, vol. 40, no. 5, pp. 885–894, May 1992.

[45] Y. Yeh and S. C. Schwartz, "Outage probability in mobile telephony due to multile log-normal interferers," *IEEE Trans. Commun.*, vol. 32, no. 4, pp. 380–388, Apr. 1984.

[46] V. K. Garg, *IS-95 CDMA and CDMA 2000: Cellular/PCS Systems Implementation.* Prentice Hall, 1999.

[47] S. H. Tseng and V. K. Prabhu, "Statistical performance estimation of optimum diversity combining and equalization with QAM modulation in cellular and PCS radio channel," in *IEEE Global Telecommunications Conference*, Sept. 1994, pp. 62–68.

[48] *IS-2000*, TIA/EIA Std., 2000.

[49] B. R. Saltzberg, "Intersymbol interference error bounds with application to ideal bandlimited signalling," *IEEE Trans. Inform. Theory*, vol. IT-14, no. 4, pp. 563–568, July 1968.

[50] R. W. Lucky, J. Salz, and E. J. Weldon, Jr., *Principles of Data Communications.* McGraw-Hill Book Co, 1968.

[51] J. Zhang and V. Aalo, "Performance analysis of a multicell DS-CDMA system with base station diversity," *Proc. IEE, Communications*, vol. 148, pp. 112–118, Apr. 2001.

[52] J. Zhang and J. S. Lehnert, "Performance of multicarrier DS/SSMA over fast rayleigh fading channels with doppler diversity," *IEEE Trans. Commun.*, vol. 54, no. 2, pp. 273–283, Feb. 2006.

[53] M. B. Pursley, D. V. Sarwate, and W. E. Stark, "Error probability for direct-sequence spread-spectrum multiple-access communications - part i: Upper and lower bounds," *IEEE Trans. Commun.*, vol. COM-30, no. 5, pp. 975–984, May 1982.

[54] J. S. Lehnert and M. B. Pursley, "Multipath diversity reception of spread-spectrum multiple-access communications," *IEEE Trans. Commun.*, vol. COM-35, no. 11, pp. 1189–1198, Nov. 1987.

[55] D. L. Noneaker and M. B. Pursley, "The effects of sequence selection on DS spread spectrum with selective fading and rake recpetion," *IEEE Trans. Commun.*, vol. 44, no. 2, pp. 229–237, Feb. 1996.

[56] L. Korowajczuk *et al.*, *Designing CDMA2000 Systems*. Wiley, 2004.

[57] J. Davidson, *Voice over IP Fundamentals*. Cisco, 2007.

[58] D. Bertsekas and R. Gallager, *Data Networks*, 2nd ed. Prentice Hall, 1992.

[59] R. F. Rey, Ed., *Engineering and Operations in the Bell System*, 2nd ed. AT&T Bell Laboratories, 1984.

[60] A. J. Viterbi, *Principles of Spread Spectrum Communication*, 3rd ed. Addison-Wesley, 1998.

[61] W. S. Kim and V. K. Prabhu, "Erlang capacity in CDMA systems with alternate frequency planning," in *IEEE International Conference on Communications*, Mar. 1998, pp. 973–978.

[62] D. G. Brennan, "Linear diversity combining techniques," *Proc. IRE*, pp. 1075–1102, June 1959.

[63] A. Papoulis, *Probability, Random Variables and Stochastic Processes*, 2nd ed. McGraw Hill, 1984.

[64] M. Abramowitz and I. A. Stegun, *Handbook of Mathematical Functions with Formulas, Graphs, and Mathematical Tables*. Washington D.C.: US Department of Commerce, 1964.

[65] M. Ju and I. M. Kim, "Closed-form BER results for multiple chip rate CDMA systems based on the simplified improved standard gaussian approximation," *IEEE Trans. Commun.*, vol. 56, no. 1, pp. 14–20, Jan. 2008.

[66] D. S. Mitrinovic, J. E. Pecaric, and A. M. Fink, *Classical and New Inequalities in Analysis*. Kluwer Academic Publishers, 1992.

[67] J. F. Steffensen, "On a generalization of certain inequalities by Tchebychef and Jensen," *Skandinavisk Aktuarietidskrift*, pp. 137–147, 1925.

[68] M. C. Jeruchim, P. Balaban, and K. S. Shanmugan, *Simulation of Communication Systems*. Plenum, 1992.

BIOGRAPHICAL STATEMENT

Richard Framjee received his B.Sc. in Electrical Engineering in 1990 with Honors. He received his MS and Ph.D in Electrical Engineering from The University of Texas at Arlington, in 1994 and 2014 respectively. His interests include Analog and Digital Communications, Modulation Theory, Wireless Communications, Cellular Systems, Queuing theory, Capacity, Random Signals and Noise and Fiber Optic Transmission Systems. He is a Member of Tau Beta Pi, Eta Kappa Nu, Phi Beta Delta. He joined at Nortel Networks, Richardson, TX in 1994 and worked as a GSM RF Systems Engineer and CDMA RF/Network System Performance Architect for product development. As a Solutions Architect with Cerion inc. Frisco, TX he worked on capacity optimization of UMTS networks.